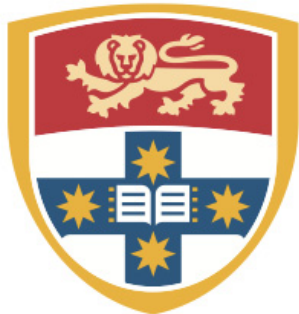


**EXPLORE THE DYNAMIC CHARACTERISTICS OF  
DENTAL STRUCTURES: MODELLING, REMODELLING,  
IMPLANTOLOGY AND OPTIMISATION**

**ZHIPENG LIAO, B.E. (Hon I)**



THE UNIVERSITY OF  
**SYDNEY**

A thesis submitted in fulfilment of the requirements for the degree of  
Doctor of Philosophy

School of Aerospace, Mechanical and Mechatronic Engineering

The University of Sydney, Australia

May 2018

## **CHAPTER 0**


### **FRONT MATTER**

#### **Declaration**

I hereby declare that the work presented in this thesis is solely my own work, and that to the best of my knowledge, the work is original except where otherwise indicated by reference to other authors or works. No part of this work has been submitted for a degree or diploma at any other university or institute.

Name: Zhipeng Liao

SID: 308009525

Signature: 

Date: 11/07/2017

## Preface

For the foreseeable future, I do not anticipate another opportunity to draft a preface of any kind, although I have grown up with the dream of being a novelist. This was when I decided to double the sense of achievement, scribbling away in two languages, with the Chinese version in the next section. Most PhD graduates do not bother to compose a preface due to the lack of readership, which however, is what I suppose quite amusing. What a coincidence would it be, for any random guy in this endless universe, to have a chance of reading this thesis, written by me who is completely irrelevant. It is nothing but feeding a letter into a drift bottle, cleaving the waves and crossing the sea that raves. Seagulls, fishes, sailors, fish men and children on the beach, and whoever brought close by the wind, can be my audience. I just love the possibility that someone unknown to me cares to find out some gibberish in this composition from a forgotten shelf in the library.

Doing research is much less poetic. I used to live in equations, codes, and unintelligible papers. Gradually I got lost in them and finally I lived with them. It was the four years through which I fought to balance between pushing and tolerating myself. I may have changed my mind if given a chance travelling back in time. But at this very moment, I am grateful that I pushed myself to the full potential and that I become younger than yesterday.

In retrospect, I started to understand that people drift in and out of my life, just like the chapters of a book. You place a bookmark only when it is unfinished. I will also remember all those gentle midnights I woke through, and the moonlights I walked through.

Putting sentimentality aside, I would like to deliver something more positive.

I made it.

It is only as significant as its hardship.

## 序

尽管从小立志当一名作家，但在可预见的未来，我应该没机会再写个序。于是我决定抓住机会在这儿写两遍，一版中文，一版英文，以后可以说自己学贯中西。有好心人告诉我，序也得用英文写，这是规定。我说，中文是最美的语言，不信你看看我写的英文。导师一开始便对我说：作为一篇文章的第一作者，不仅要为文章的内容负责，也要成为文章的主人。此话一直铭记在心，我的论文我做主，这就够了。

这个好心人是虚构的。澳大利亚是个自由民主的国度，5%的人说中文<sup>[1]</sup>。导师的话也是虚构的。但这个序应该会留个全尸。

很多同僚并不愿意给自己的博士论文写序，毕竟观者寥寥。这在我看来却是很有趣的地方。茫茫宇宙中，要凑多少次前世的擦身而过，才得以读到一个毫无瓜葛之人的毕业论文呢？就像把信装进漂流瓶，随波逐浪，远济沧海。彼岸沙滩上嬉戏的小孩也可以是我的读者。说不定还会顺带告诉路过的海鸥和渔民。海鸥告诉游鱼，渔民告诉水手。在我看来，这就是人类文明的传播。

而读书科研，就像这部论文的其余部分，远没有这么浪漫主义。我常常活在公式里、代码里、不知所云的论文里，然后迷失于其中。它们是征服不完的，以有涯随无涯，殆矣。于是我学会了如何与它们相处。烦了，就絮叨书中自有颜如玉，乏了，就自嘲愚顽怕读文章。读博这些年，就是在强迫与容忍自己之间找平衡。就算满纸荒唐，落笔无悔。任凭华发渐生，晓镜不愁。有的时候还是烦，就去泳池里劈波斩浪，还是乏，就去商学院看看学妹。每个博士都需要俩水龙头，一个鸡汤不停，一个鸡血不断。

---

<sup>1</sup> 我猜的。

## CHAPTER 0: FRONT MATTER

小学一年级的時候，看到高年級的哥哥，覺得和他們之間隔着無盡的歲月。而現在再回頭看，滄桑皆成須臾。這麼看來，時間就是金錢這句話，簡直是真理，都是貶值的主。於是木心先生說，從前慢，一生只夠愛一個人。不僅是詩，也是啟示。所以，錢要保值，就換成不動產，時間要保值，就換成每時每刻的充實。認真經營到底，便不會有遺憾。

如果時光能倒流，我也許會有不同的人生軌跡。但此刻，我得感謝自己，未負如來卿卿，不昧光陰初心。不妄此生寒窗十載，方度前路春風十里。而我也漸漸明白，生命中過客來去，如書之章節。書籤抽去，便不翻閱。很多年後，若時光真的倒流，我會回去告訴我自己，我還記得機械學院的金屬氣味，記得十一月的藍花楹散落滿地，記得無眠的良夜與伴行的雲月。它們看着曾經的我老去，如今卻風華正茂。

2016年12月16日

午夜，於悉尼家中

## Acknowledgement

My utmost gratitude must go to my supervisor Prof. Qing Li, for his professional and pragmatic guidance throughout the four-year candidature, for his conscientiousness and immense expertise that positively influence me. I could not have imagined having a better supervisor and mentor for my PhD study. Prof. Michael Swain, my auxiliary supervisor, possesses endless academic ideas and he unconditionally delivers them to me. It is a great honour to work with you, with my deepest appreciation. I would also like to thank Dr. Wei Li who is always there to cast the cares.

A very important part of my research was based on collaborations. Therefore I would like to express my sincere thanks towards Prof. M. Ali Darendeliler and his dentistry team for the cooperation which led to several publications. I must thank Dr. Nobuhiro Yoda and Prof. Keiichi Sasaki from Tohoku University, for the clinical data shared, publications co-authored and long-term collaboration and friendship forged.

I would like to extend my thanks to my most frequent co-author (other than supervisors) Dr. Junning Chen. Without your technical support, this thesis would not have been possible. My appreciation also goes to Keke Zheng and Dr. Jianguang Fang who I actively worked and discussed with.

My office buddies, Zhongpu Zhang, Bryant Chang, Andrian Sue, Phillip Tran, Paul Wong, Fangli Jia, Jingxiao Zhong and those who I regularly chat with, thank you for bearing with me and my lame talks, or the other way round, which does not matter. These lovely moments have been unconsciously recorded without replays very likely but altogether, they made my PhD pursuit full of laughter.

## CHAPTER 0: FRONT MATTER

Special thanks to those great minds that reshape me. To Pink Floyd, the origin of my English name and inspiration of all my adolescent imaginations, thank you for accompanying me through all those waking hours. To Bobby Chen (陈升), thank you for unleashing and ushering me into a distant island whenever I need a break from the bothering and find my true self and, to Sergei Rachmaninoff and Pyotr Tchaikovsky, whose Piano Concertos raise my soul.

I am also greatly indebted to Lu Meng whose unconditional love and emotional support simply render me activated and refreshed. Finally, to my parents, words fail me to express my gratitude, when I reminisced about my careless boyhood surrounded by you, when we shared all those silent moments over the phone, when your visages began to fade out of my memory after ten years abroad, and now when I am staring at the old photo of you on the desk. Thank you and I love you all. You are the spiritual underpinning motivating me to keep going.

## CHAPTER 0: FRONT MATTER

### **Authorship attribution statement**

#### *CHAPTER TWO IS BASED ON THE PUBLISHED JOURNAL ARTICLE:*

**Liao, Z.**, Chen, J., Zhang, Z., Li, W., Swain, M., & Li, Q. (2015). Computational modeling of dynamic behaviors of human teeth. *Journal of Biomechanics*, 48(16), 4214-4220.

I, as the first author, made substantial contributions to all of the following:

- (1) The conception and design of the study, or acquisition of data, or analysis and interpretation of data;
- (2) Drafting the article or revising it critically for important intellectual content;
- (3) Final approval of the version to be submitted.

#### *CHAPTER THREE IS BASED ON THE PUBLISHED JOURNAL ARTICLE:*

**Liao, Z.**, Elekdag-Turk, S., Turk, T., Grove, J., Dalci, O., Chen, J., Zheng, K., Darendeliler, M.A., Swain, M., & Li, Q. (2017). Computational and Clinical Investigation on the Role of Mechanical Vibration on Orthodontic Tooth Movement. *Journal of Biomechanics*, 60, 57-64.

I, as the first author, made substantial contributions to all of the following:

- (1) The conception and design of the study, or acquisition of data, or analysis and interpretation of data;
- (2) Drafting the article or revising it critically for important intellectual content;
- (3) Final approval of the version to be submitted.

#### *CHAPTER FOUR IS BASED ON THE PUBLISHED JOURNAL ARTICLE:*

**Liao, Z.**, Chen, J., Li, W., Darendeliler, M. A., Swain, M., & Li, Q. (2016). Biomechanical investigation into the role of the periodontal ligament in optimising orthodontic force: a finite element case study. *Archives of oral biology*, 66, 98-107.

I, as the first author, made substantial contributions to all of the following:



## CHAPTER 0: FRONT MATTER

- (1) The conception and design of the study, or acquisition of data, or analysis and interpretation of data;
- (2) Drafting the article or revising it critically for important intellectual content;
- (3) Final approval of the version to be submitted.

### *CHAPTER FIVE IS BASED ON THE PUBLISHED JOURNAL ARTICLE:*

Yoda, N., **Liao, Z.**, Chen, J., Sasaki, K., Swain, M. and Li, Q. (2016), Role of implant configurations supporting three-unit fixed partial denture on mandibular bone response: biological-data-based finite element study. *J Oral Rehabil*, 43, 692–701.

I, as the second author, made substantial contributions to all of the following:

- (1) The conception and design of the study, or acquisition of data, or analysis and interpretation of data;
- (2) Drafting the article or revising it critically for important intellectual content;
- (3) Final approval of the version to be submitted.

The first and corresponding authors consent to the contexts in this chapter.

### *CHAPTER SIX IS BASED ON THE PUBLISHED JOURNAL ARTICLE:*

**Liao, Z.**, Yoda, N., Chen, J., Zheng, K., Sasaki, K., Swain, M. V., & Li, Q. (2017). Simulation of multi-stage nonlinear bone remodelling induced by fixed partial dentures of different configurations: a comparative clinical and numerical study. *Biomechanics and Modeling in Mechanobiology*, 16(2), 411-423.

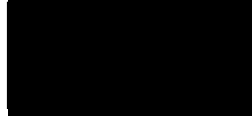
I, as the first author, made substantial contributions to all of the following:

- (1) The conception and design of the study, or acquisition of data, or analysis and interpretation of data;
- (2) Drafting the article or revising it critically for important intellectual content;
- (3) Final approval of the version to be submitted.

## CHAPTER 0: FRONT MATTER

In addition to the statements above, in cases where I am not the corresponding author of a published item, permission to include the published material has been granted by the corresponding author.

Zhipeng Liao



11/07/2017

As supervisor for the candidature upon which this thesis is based, and corresponding author of all above-mentioned publications, I can confirm that the authorship attribution statements above are correct.

Qing Li



11/07/2017

## **Abstract**

The properties of a structure can be both narrowly and broadly described. The mechanical properties, as a narrow sense of property, are those that are quantitative and can be directly measured through experiments. They can be used as a metric to compare the benefits of one material versus another. Examples include Young's modulus, tensile strength, natural frequency, viscosity, etc. Those with a broader definition, can be hardly measured directly. This thesis aims to study the dynamic properties of dental complex through experiments, clinical trials and computational simulations, thereby bridging some gaps between the numerical study and clinical application.

The natural frequency and mode shapes, of human maxilla model with different levels of integrities and properties of the periodontal ligament (PDL), are obtained through the complex modal analysis. It is shown that the comprehensiveness of a computational model significantly affects the characterisation of dynamic behaviours, with decreasing natural frequencies and changed mode shapes as a result of the models with higher extents of integrity and preciseness. It is also found that the PDL plays a very important role in quantifying natural frequencies. Meanwhile, damping properties and the heterogeneity of materials also have an influence on the dynamic properties of dental structures.

The understanding of dynamic properties enables to further investigate how it can influence the response when applying an external stimulus. In a parallel preliminary clinical trial, 13 patients requiring bilateral maxillary premolar extractions were recruited and applied with mechanical vibrations of approximately 20 g and 50 Hz, using a split mouth design. It is found that both the space closure and canine distalisation of the vibration group are significantly faster and higher than those of the control group ( $p < 0.05$ ). The pressure within the PDL is computationally calculated to be higher with the vibration group for maxillary teeth

for both linguo-buccal and mesial-distal directions. A further increased PDL response can be observed if increasing the frequency until reaching a local natural frequency. The vibration of 50 Hz or higher is thus approved to be a potential stimulus accelerating orthodontic treatment.

The pivotal role of soft tissue the PDL is further studied by quantitatively establishing pressure thresholds regulating orthodontic tooth movement (OTM). The centre of resistance and moment to force ratio are also examined via simulation. Distally-directed tipping and translational forces, ranging from 7.5 g to 300 g, are exerted onto maxillary teeth. The hydrostatic stress is quantified from nonlinear finite element analysis (FEA) and compared with normal capillary and systolic blood pressure for driving the tissue remodelling. Localised and volume-averaged hydrostatic stress are introduced to describe OTM. By comparing with clinical results in past literature, the volume average of hydrostatic stress in PDL was proved to describe the process of OTM more indicatively. Global measurement of hydrostatic pressure in the PDL better characterised OTM, implying that OTM occurs only when the majority of PDL volume is critically stressed. The FEA results provide new insights into relevant orthodontic biomechanics and help establish optimal orthodontic force for a specific patient.

Implant-supported fixed partial denture (FPD) with cantilever extension can transfer excessive load to the bone surrounding implants and stress/strain concentration which potentially leads to bone resorption. The immediate biomechanical response and long-term bone remodelling outcomes are examined. It is indicated that during the chewing cycles, the regions near implant necks and apexes experience high von Mises stress (VMS) and equivalent strain (EQS) than the middle regions in all configurations, with or without the cantilever. The patient-specific dynamic loading data and CT based mandibular model allow us to model the biomechanical responses more realistically. The results provide the data for clinical assessment of implant configuration to improve longevity and reliability of the implant-supported FPD restoration. On the other hand, the results show that the three-implant

## CHAPTER 0: FRONT MATTER

supported and distally cantilevered FPDs see noticeable and continuous bone apposition, mainly adjacent to the cervical and apical regions. The bridged and mesially cantilevered FPDs show bone resorption or no visible bone formation in some areas. Caution should be taken when selecting the FPD with cantilever due to the risk of overloading bone resorption. The position of FPD pontics plays a critical role in mechanobiological functionality and bone remodelling.

As an important loading condition of dental biomechanics, the accurate assignment of masticatory loads has long been demanded. Methods involving different principles have been applied to acquire or assess the muscular co-activation during normal or unhealthy stomatognathic functioning. Their accuracy and capability of direct quantification, especially when using alone, are however questioned. We establish a clinically validated Sequential Kriging Optimisation (SKO) model, coupled with the FEM and in vivo occlusal records, to further the understanding of muscular functionality following a fibula free flap (FFF) surgery. The results, within the limitations of the current study, indicates the statistical advantage of agreeing occlusal measurements and hence the reliability of using the SKO model over the traditionally adopted optimality criteria. It is therefore speculated that mastication is not optimally controlled to a definite degree. It is also found that the maximum muscular capacity slightly decreases whereas the actual muscle forces fluctuate over the 28-month period.

## Table of Contents

CHAPTER 0 .....	2
FRONT MATTER .....	2
Declaration .....	2
Preface .....	3
序 .....	4
Acknowledgement .....	6
Authorship attribution statement .....	8
Abstract .....	11
Table of Contents .....	14
CHAPTER 1 .....	20
INTRODUCTION .....	20
1.1 Dissertation Structure .....	20
1.1.1 Chapter 2: Dynamic behaviours of human dental complex .....	20
1.1.2 Chapter 3: Effects of mechanical vibration on orthodontic tooth movement .....	21
1.1.3 Chapter 4: Biomechanical investigation into the role of the periodontal ligament in optimising orthodontic force .....	21
1.1.4 Chapter 5: Role of implant configurations supporting three-unit fixed partial denture on mandibular bone response: a biological data-based finite element study .....	21

## CHAPTER 0: FRONT MATTER

1.1.5 Chapter 6: Simulation of multi-stage nonlinear bone remodeling induced by fixed partial dentures of different configurations: a comparative clinical and numerical study .....	22
1.1.6 Chapter 7: Masticatory muscular functionality following oral reconstruction based on sequential kriging optimisation techniques and medical imaging analysis .....	22
1.2 Publications .....	23
1.2.1 Peer-reviewed journal articles .....	23
1.2.2 Conference papers and presentations .....	24
1.3 Project Aims .....	25
CHAPTER 2 .....	27
DYNAMIC BEHAVIOURS OF HUMAN DENTAL COMPLEX .....	27
2.1 Introduction .....	28
2.1.1 Dental composition .....	28
2.1.2 Mechanical properties of dental structures .....	31
2.1.3 Natural frequency and mode shapes .....	35
2.2 Materials and Methods .....	38
2.2.1 Theory .....	38
2.2.2 Maxilla modelling .....	39
2.2.3 Material properties .....	40
2.3 Results .....	43
2.3.1 Effects of material heterogeneity and non-linearity .....	43

## CHAPTER 0: FRONT MATTER

2.3.2 Damping ratio calculation and damping effects .....	44
2.3.3 Effects of model integrity .....	44
2.4 Discussion .....	47
2.5 Conclusions.....	51
CHAPTER 3 .....	53
VIBRATE TO ENHANCE ORTHODONTICS.....	53
3.1 Introduction.....	54
3.1.1 Mainstream pressure-tension theory .....	54
3.1.2 Other OTM theories.....	56
3.1.3 Types of OTM.....	58
3.1.4 Dynamics in bone metabolism.....	60
3.1.5 Vibration for pain reduction.....	62
3.1.6 Demand for accelerated orthodontic treatment.....	63
3.2 Methods and Materials.....	64
3.2.1 Clinical Study.....	64
3.2.2 Basics of Nonlinear Steady-state Dynamics .....	68
3.2.3 FE Modelling .....	69
3.2.4 Loading and Boundary Conditions .....	71
3.3 Results.....	72
3.3.1 Clinical study .....	72



## CHAPTER 0: FRONT MATTER

3.3.2 Static and mode-based steady-state dynamic FEA .....	73
3.4 Discussion .....	75
CHAPTER 4 .....	80
OPTIMISE ORTHODONTIC FORCE .....	80
4.1 Introduction.....	81
4.2 Methods and Materials.....	83
4.2.1 Finite element modelling .....	83
4.2.2 Loading and boundary conditions.....	85
4.2.3 Material Properties.....	87
4.3 Results.....	88
4.4 Discussion.....	93
4.5 Conclusions.....	100
CHAPTER 5 .....	101
CANTILEVER THE DENTURE .....	101
5.1 Introduction.....	102
5.2 Materials and Methods.....	104
5.2.1 Clinical data acquisition.....	104
5.2.2 Finite element (FE) analysis .....	106
5.3 Results.....	109
5.4 Discussion.....	112
5.4.1 The FE modelling and analysis conditions .....	112

## CHAPTER 0: FRONT MATTER

5.4.2 The influence of implant configuration on mechanical stimuli .....	113
5.4.3 Clinical implication and study limitation.....	114
5.5 Conclusions.....	115
CHAPTER 6 .....	117
MULTI-STAGE BONE REMODELLING INDUCED BY DENTURES .....	117
6.1 Introduction.....	118
6.2 Materials and Methods.....	121
6.2.1 Clinical data acquisition.....	121
6.2.2 Finite element modelling .....	122
6.2.3 Multi-stage bone remodelling algorithm .....	127
6.2.4 Parameter identification via optimisation ... <b>Error! Bookmark not defined.</b>	
6.2.5 Model validation .....	130
6.3 Results.....	131
6.3.1 Model validation .....	131
6.3.2 Effects of FPD configurations .....	133
6.4 Discussion.....	136
6.5 Conclusions.....	142
CHAPTER 7 .....	143
MASTICATION IS NOT OPTIMALLY CONTROLLED .....	143
7.1 Introduction.....	144
7.2 Methods.....	147

## CHAPTER 0: FRONT MATTER

7.2.1 Clinical treatment and medical imaging analysis .....	147
7.2.2 Finite element modelling .....	151
7.2.3 Inverse identification of muscle force.....	152
7.2.4 Linear programming .....	153
7.3 Results.....	154
7.3.1 Optimisation.....	154
7.3.2 Occlusal and medical imaging analysis .....	155
7.3.3 Muscular force identification.....	156
7.4 Discussion.....	159
7.4.1 SKO vs. optimality criteria .....	159
7.4.2 The irrationality of optimality for mastication.....	160
7.4.3 Clinical implications and limitations of this study .....	161
CHAPTER 8 .....	164
CONCLUSIONS.....	164
8.1 Orthodontics.....	165
8.2 Oral Rehabilitation and Bone Remodelling.....	166
8.3 Muscle.....	167
8.4 Closing Remarks.....	168
REFERENCES .....	169

# CHAPTER 1

## INTRODUCTION

### 1.1 Dissertation Structure

There are eight chapters in this thesis, excluding Chapter 0 which covers the front matters. In this thesis, the dynamic properties of dental complex are explored, including those of the periodontal ligament (PDL), cortical and cancellous bone, damping ratio, complex natural frequency and mode shapes, sensitivity to external mechanically-induced stimulus, bone metabolism and remodelling, and time-dependent muscular activity. The relevant applications are also investigated, including orthodontics, implantology and craniofacial surgery. They are summarised below.

#### *1.1.1 Chapter 2: Dynamic behaviours of human dental complex*

In the first chapter, the natural frequency and mode shape, using finite element models of different integrities and PDL properties, are evaluated. The nonlinearity of the PDL and heterogeneity of bony tissues are incorporated. A mode-based Rayleigh damping model is established for the accurate extraction of complex natural frequency and mode shapes. The results will be systematically compared with those of past literature. This chapter provides a foundation for the future study to further advance the modelling of dental complex and understanding the mechanobiology and mechanotransduction involving human dental structures.

### ***1.1.2 Chapter 3: Effects of mechanical vibration on orthodontic tooth movement***

On the basis of Chapter 2, we continue to study the dynamic properties of maxillofacial structures and how it can help enhance orthodontic treatment. In this chapter, a pre-defined mechanical stimulus, in form of vibration, is induced to test the response of tooth movement to the impetus. In collaboration with Sydney Dental Hospital, we are able to recruit 13 patients in the clinical trial with each subject requiring bilateral extraction of premolar. Vibration is applied for the experimental group, using a split-mouth protocol. The parallel computational simulation is conducted, mimicking the same loading and boundary scenarios. The dynamic properties, i.e. local natural frequency is expected to play a very important role. The safety and efficacy of the vibration protocol are investigated both clinically and computationally.

### ***1.1.3 Chapter 4: Biomechanical investigation into the role of the periodontal ligament in optimising orthodontic force***

The focus is still on the key soft tissue, the PDL. We aim to quantify the optimal orthodontic force by introducing the thresholds that regulate the orthodontic tooth movement. The hydrostatic pressure, which quantifies the overall disturbance of the blood circulation within the microvasculature, is adopted as the indicator. This seemingly simple and simplified model may effectively describe and hence predict how the tooth is moved under a certain magnitude of force. The results can shed lights on the selection of a light force or heavy force strategy, or even better, the exact magnitude needed for the optimal orthodontic treatment.

### ***1.1.4 Chapter 5: Role of implant configurations supporting three-unit fixed partial denture on mandibular bone response: a biological data-based finite element study***

In this chapter, we report the collaborative work with Faculty of Dentistry, Tohoku University. A three-unit implanted fixed partial denture (FPD) was installed in a female subject. Real-time dynamic occlusal loads in 3D during the maximum voluntary clenching (MVC)

were measured using a piezoelectric force transducer. Equivalent strain and von Mises stress are obtained as preliminary indicators to assess the response of peri-implant regions of interest. The configurational effects are to be analysed and clinical implications are provided.

### ***1.1.5 Chapter 6: Simulation of multi-stage nonlinear bone remodeling induced by fixed partial dentures of different configurations: a comparative clinical and numerical study***

The same case in the last chapter, together with the same loading and boundary conditions, is studied. The emphasis is on the bone remodelling outcome, which is hypothesised to be dynamic and with a strong time-dependence, contradicting some conventional views. A multi-stage bone remodelling algorithm is formulated, featuring phase-dependent remodelling parameters, including remodelling constants, reference stimulus and bandwidth of lazy zone. This modified algorithm is to be compared with the traditional tri-linear bone remodelling model, via statistical validation against clinical data. In addition, an orthotropic and heterogeneous bone property is introduced to maximise the modelling accuracy. Bone remodelling outcomes induced by different denture designs is also comparatively analysed.

### ***1.1.6 Chapter 7: Masticatory muscular functionality following oral reconstruction based on sequential kriging optimisation techniques and medical imaging analysis***

We believe that the masticatory muscular functionality may change as the time goes by. The change amplifies if involving a major craniofacial surgery. A 66-year old male diagnosed with oral cancer was recruited in our up to now 28-month follow-up after a mandibular reconstruction surgery. Occlusal loads were measured at different time points. Utilising this, in conjunction with the sequential Kriging optimisation (SKO) technique, we are able to know the most possible muscular force magnitude and directions following the jaw resection. It is also highly doubted by us that the muscular co-activation strictly and

unconditionally comply with the optimality criteria, long accepted, with increasing scepticism recently though, by the wider community. It is to compare the results of SKO model with those based on traditional optimality strategy so how muscle is controlled can be comprehended better.

### 1.2 Publications

There have been several publications, including journal papers, conference proceedings, as well as conference posters and presentations raised from or indirectly related to the thesis. They are summarised below.

#### 1.2.1 Peer-reviewed journal articles

1. **Liao, Z.**, Chen, J., Zhang, Z., Li, W., Swain, M., & Li, Q. (2015). Computational modeling of dynamic behaviors of human teeth. *Journal of Biomechanics*, 48(16), 4214-4220.
2. **Liao, Z.**, Chen, J., Li, W., Darendeliler, M. A., Swain, M., & Li, Q. (2016). Biomechanical investigation into the role of the periodontal ligament in optimising orthodontic force: a finite element case study. *Archives of oral biology*, 66, 98-107.
3. **Liao, Z.**, Yoda, N., Chen, J., Zheng, K., Sasaki, K., Swain, M. V., & Li, Q. (2017). Simulation of multi-stage nonlinear bone remodelling induced by fixed partial dentures of different configurations: a comparative clinical and numerical study. *Biomechanics and Modeling in Mechanobiology*, 16(2), 411-423.
4. **Liao, Z.**, Elekdag-Turk, S., Turk, T., Grove, J., Dalci, O., Chen, J., Zheng, K., Darendeliler, M.A., Swain, M., & Li, Q. (2017). Computational and Clinical Investigation on the Role of Mechanical Vibration on Orthodontic Tooth Movement. *Journal of Biomechanics*, 60, 57-64.

## CHAPTER 1: INTRODUCTION

5. Li, W., Lin, D., Chen, J., Zhang, Z., **Liao, Z.**, Swain, M., & Li, Q. (2014). Role of Mechanical Stimuli in Oral Implantation. *Journal of Biosciences and Medicines*, 2(04), 63.
6. Yoda, N., **Liao, Z.**, Chen, J., Sasaki, K., Swain, M. and Li, Q. (2016), Role of implant configurations supporting three-unit fixed partial denture on mandibular bone response: biological-data-based finite element study. *J Oral Rehabil*, 43, 692–701.
7. Zhang, Z., **Liao, Z.**, Yoda, N., Li, W., Sasaki, K., Hong, G., Swain, M.V. and Li, Q. (2016). XFEM fracture modelling for implant-supported fixed partial dentures. *Applied Mechanics & Materials*, 846.
8. Yoda, N., **Liao, Z.**, Chen, J., Sasaki, K., & Li, Q. (2016). The biomechanical responses of mandibular bone installed with fixed partial denture. *Applied Mechanics and Materials*, 846, 276-281.
9. Zheng, K., Yoda, N., Chen, J., **Liao, Z.**, Sasaki, K., Swain, M. and Li, Q. Investigating the Influence of Buccal Bone Thickness on Bone Remodeling around Maxillary Anterior Implantation. Submitted to Biomechanics and Modeling in Mechanobiology.
10. Yoda, N., Zheng, K., Chen, J., **Liao, Z.**, Koyama, S., Peck, C., ... & Li, Q. (2018). Biomechanical analysis of bone remodeling following mandibular reconstruction using fibula free flap. *Medical Engineering & Physics*. 56, 1-8.

### **1.2.2 Conference papers and presentations**

11. **Zhipeng Liao**, Junning Chen, Ali M Darendeliler, Michael Swain, Qing Li. Biomechanical Evaluation of Optimal Orthodontic Forces on Human Maxillary Teeth. The 11th World Congress on Computational Mechanics (2014). Barcelona, Spain.
12. Wei Li, Junning Chen, **Zhipeng Liao**, Rohana Ahmad, Babak Sarrafpour, Hanako Suenaga, Hans Zoellner, Michael Swain, Qing Li. Biomechanical Roles of Soft Tissues



in Bone Remodelling: Case Studies. The 11th World Congress on Computational Mechanics (2014). Barcelona, Spain.

13. **Zhipeng Liao**, Junning Chen, Qing Li. 3D Heterogeneous Finite Element Modeling of Human Maxilla. The 5th Triennial Congress of Advanced Digital Technology in Head and Neck Reconstruction (2014). Beijing, China.
14. **Zhipeng Liao**, Johnathan Grove, Oyku Dalci, Junning Chen, Keke Zheng, Michael Swain, M. Ali Darendeliler, Qing Li. Effects of Vibration on Orthodontic Tooth Movement. 21st Congress of the European Society of Biomechanics (2015). Prague, Czech Republic.
15. **Liao, Z.**, Yoda, N., Zheng, K., Sasaki, K., Swain, M. V. & Li, Q. Simulation of multi-stage nonlinear bone remodelling induced by fixed partial dentures of different configurations. The 12th World Congress on Computational Mechanics (2016). Seoul, Korea.
16. Zheng, K., Chen, J., **Liao, Z.**, Yoda, N., Sasaki, K., Swain, M., Li, Q. Effects of Bone Graft Thickness on Implantation-induced Bone Remodelling in Maxillary Anterior Buccal Bone. The 12th World Congress on Computational Mechanics (2016). Seoul, Korea.

### 1.3 Project Aims

This thesis have the following aims.

- (1) Generate an anatomically accurate and structurally detailed human dental complex, including mandible, maxilla and soft tissues. Patient specific heterogeneous and anisotropic bony properties are studied and adopted.

## CHAPTER 1: INTRODUCTION

- (2) Investigate the dynamic properties of dental structures, including damping ratios, damping coefficients, natural frequency and mode shapes, and the factors contributing to the accuracy.
- (3) Explore whether the concurrent use of vibration together with conventional static orthodontic force, on the basis of dynamic properties of dental structure, would accelerate tooth movement.
- (4) Calculate the optimum orthodontic force by quantifying the pressure within microvasculature of soft tissues.
- (5) Understand the biomechanics of implant-supported fixed partial denture of different configurations.
- (6) Assess the outcomes of bone remodelling with the installation of fixed partial dentures.
- (7) Establish a multi-stage bone remodelling algorithm with the clinical validation using sequential Kriging optimisation technique.
- (8) Propose a more easily validated and mathematically convincing approach to estimate time-dependent masticatory muscular activity.

## CHAPTER 2

### DYNAMIC BEHAVIOURS OF HUMAN DENTAL COMPLEX

Despite the importance of dynamic behaviours of dental and periodontal structures to clinics, the biomechanical roles of anatomic sophistication and material properties in quantification of vibratory characteristics remain under studied. In this chapter it was aimed to generate an anatomically accurate and structurally detailed 3D finite element (FE) maxilla model and explore the dynamic behaviours of human teeth through characterizing natural frequencies (NFs) and mode shapes. The FE models with different levels of structural integrities and material properties were established to quantify the effects of modelling techniques on the computation of vibratory characteristics.

The results showed that the integrity of computational model considerably influences the characterisation of vibratory behaviours, as evidenced by declined NFs and perceptibly altered mode shapes resulting from the models with higher degrees of completeness and accuracy. A primary NF of 889 Hz and the corresponding mode shape featuring linguo-buccal vibration of maxillary right 2<sup>nd</sup> molar were obtained based on the complete maxilla model. It was found that the periodontal ligament (PDL), a connective soft tissue, plays an important role in quantifying NFs. It was also revealed that damping and heterogeneity of materials contribute to the quantification of vibratory characteristics. The study provided important biomechanical insights and clinical references for future studies on dynamic behaviours of dental and periodontal structures.

## 2.1 Introduction

### 2.1.1 Dental composition

#### 2.1.1.1 Periodontal Ligament

Illustrated in Fig. 2.1a is the anatomical configuration of a normal tooth where the periodontal ligament (PDL) and alveolar bone are the major components involved in Orthodontic tooth movement (OTM). The PDL is composed of five principal fibre groups: alveolar crest, horizontal, oblique, periapical and inter-radicular fibre groups (Fig. 2.1b). It is a collagenous connective tissue lying and connecting between the cementum on the root surface and the alveolar bone and especially adapted to be capable of withstanding pressures of mastication and resisting movement in various directions such as twisting, lateral and tipping. Alveolar bone (also called as alveolar process) forms at the base of tooth to accommodate the teeth into the jaws and support and protect the teeth. It is where bone remodelling occurs and allows OTM.

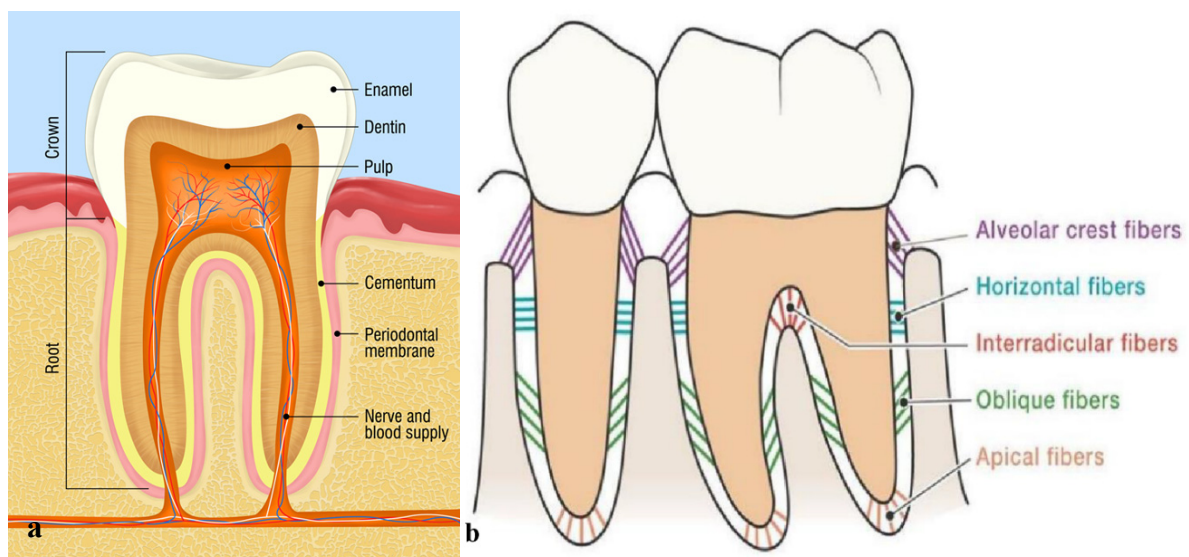


**Fig. 2.1** (a) Tooth anatomy [1]; (b) PDL fibres[2].

## CHAPTER 2: DYNAMIC BEHAVIOURS OF HUMAN DENTAL COMPLEX

### *2.1.1.2 Other Dental Tissues*

Enamel, formed by cells called ameloblasts, forms tooth's outer coating which is the hardest, stiffest, and one of the most durable load-bearing and most highly mineralised tissues in the human body. It structurally consists of millions of enamel rods or prisms which are positioned parallel to each other and perpendicular to the dentin surface beneath and is chemically composed of 95-98% inorganic matter (primarily hydroxylapatite), 1-2% organic contents and 4% water content by weight [3].

Dentin is a creamy white and yellow connective tissue forming the largest portion of tooth structure and covered by enamel in anatomic crown and by cementum in anatomic root. It consists of 45-50% inorganic apatite crystals, 30% organic matrix and around 25% water content. Dentin is formed from odontoblasts that secrete collagen and mineralised tissue that assemble a material that is harder and denser than bone [4].

Dental pulp occupies the pulp cavity in the tooth and contains 75% water and 25% organic content. It is a viscous connective tissue consisting of collagen fibres and ground substance that supports the vital cellular, vascular and nerve structures of teeth [3].

Cementum is the hard dental tissue enveloping the anatomical roots and formed from cells called cementoblasts. It consists of roughly 45-50% inorganic material and 50-55% organic contents and water by weight. Cementum is resorbed in some pathological conditions [3].

### *2.1.1.3 Maxilla*

The maxilla or the upper jaw, one of the major facial bones, is composed of a body and four processes: zygomatic, frontal, alveolar and palatine processes (Fig. 2.2). It forms the orbital cavity, the floor and lateral walls of the nose, part of the cheek. Maxilla also keeps the

maxillary teeth in a non-movable to enable chewing. The upper component of the maxilla is called the orbital surface that forms the lower and inner surface of the orbital cavity. The exterior surface is referred as frontal process. The regions of key importance in mechano-transduction are the body that houses the maxillary air sinuses and the alveolar process that projects downwards and develops in response to the teeth [5]. One of the differences between maxilla and mandible is their bony architecture, for which they have dissimilar pattern of their vascular supply. The maxilla has lighter construction and connects some cranial structures while the mandible has more self-contained structure and is more proximal to other long bones [6].

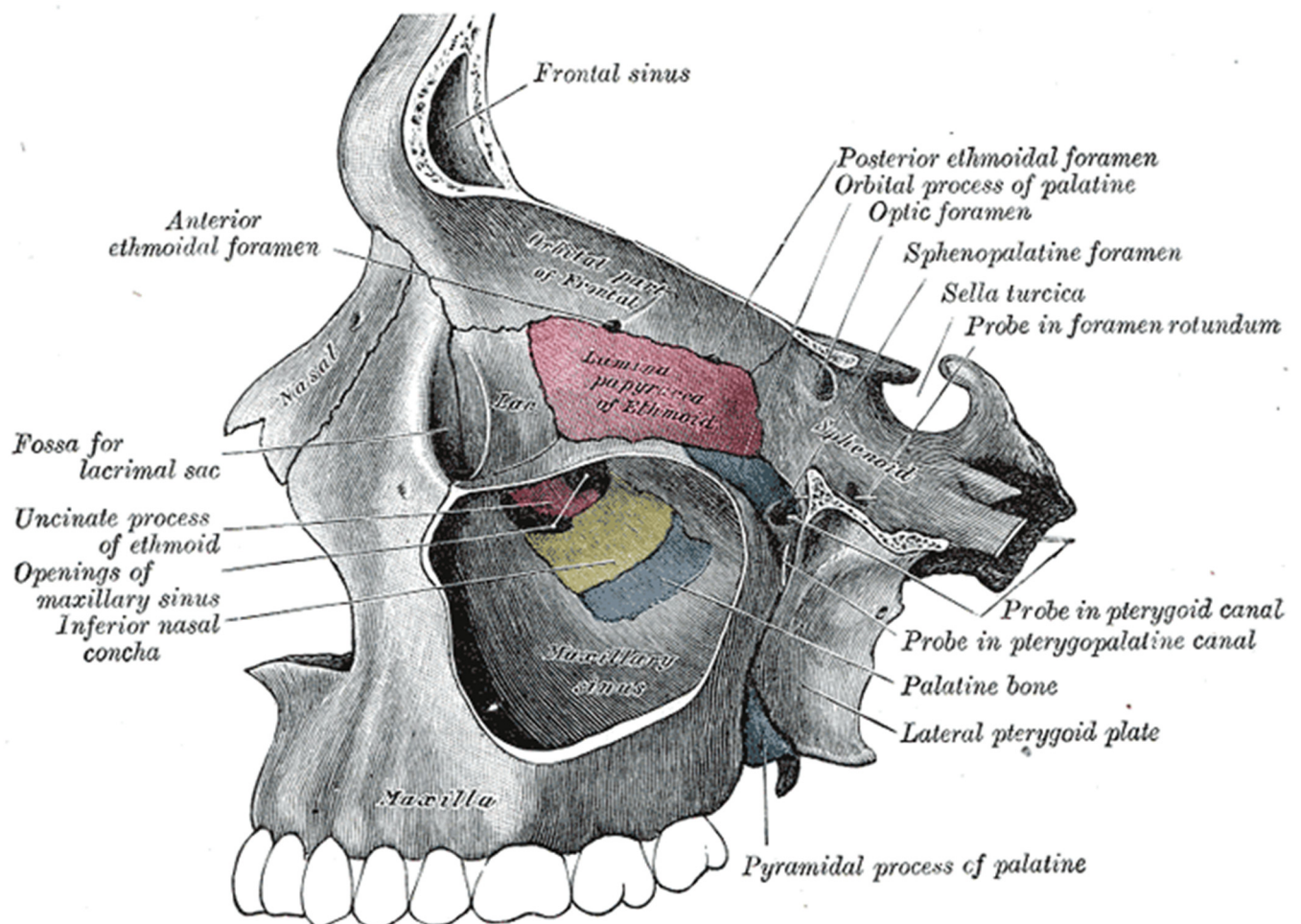


Fig. 2.2 Left maxillary sinus opened from the exterior [7].

### 2.1.2 Mechanical properties of dental structures

The material properties of dental structures are of importance for comprehending how teeth and their supporting structures respond and adapt to external mechanical load and essential for accurate FEA. As this thesis focuses on the FE modelling and analysis, the emphases in terms of structurally mechanical properties are drawn on elastic properties, including Young's moduli, Poisson's ratios, densities as well as linearity and degree of anisotropy of dental components, which are required by modelling and dynamic simulation.

#### 2.1.2.1 Dentin

Shown in Fig. 2.3 is the schematic representation of the measurements of elastic moduli against the year in which they were published. Since 1999 there has appeared to be a four-time difference in measurements of elastic modulus. This uncertainty could probably result from either a viscoelastic response, i.e. stress relaxation or experimental facility, instead of the actual deviation of dentin's Young's modulus [8]. The agreement between indentation and sonic measurement methods, two main approaches employed to determine dentin's properties, allows to allocate the magnitude from 18 to 25 GPa, in comparison to the previously accepted range (13 - 16 GPa).

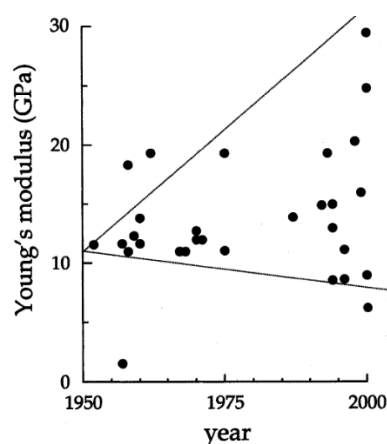


**Fig. 2.3** The Young's moduli of dentin, reported over the past 50 years [8].

There is a slight degree of hexagonal anisotropy (transverse isotropy) due to dentin's anisotropic structure, i.e. the planar organisation of the mineralised collagen fibrils. The stiffest direction is perpendicular to the tubules axis of, i.e.  $E_{33}/E_{11} = 0.92$ , according to Kinney *et al.* 21. In addition, drying the hydrated dentin diminished hexagonal anisotropy of dentin, which was consistent and explained the studies conducted by Wang and Weiner [9]. Similarly, Poisson's ratio of dentin showed a remarkable anisotropy, with  $\nu_{21} = 0.45$  and  $\nu_{31} = 0.29$ ; and  $\nu_{21} = \nu_{31} = 0.29$  when dentin was dry being recorded [9].

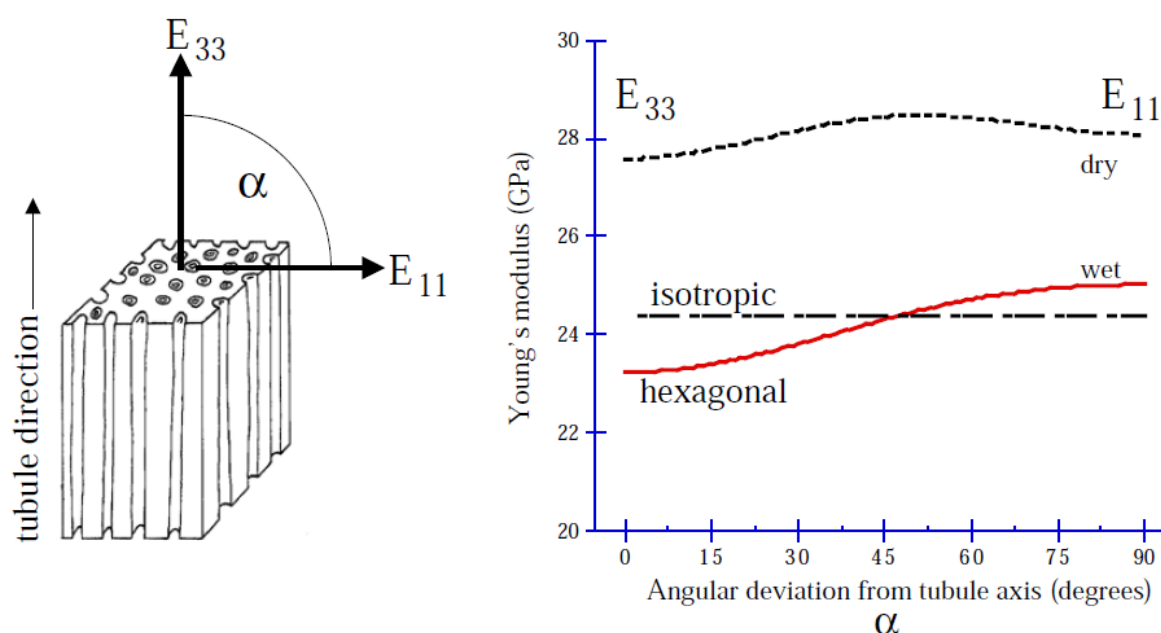


**Fig. 2.4** The angular dependence of elastic modulus of dentin (wet and dry), measured with the angles from the tubule axis [9].

### 2.1.2.2 Enamel

Over the past several decades, extensive researches on mechanical properties and behaviours of human enamel, along with relevant mechanical tests from macro scale to micro and nano-scale, have been performed. A limited number of studies utilising macro-scale tests with a relatively large variation of results can be observed, with from  $46.2 \pm 4.8$  GPa to  $84.1 \pm 6.2$  GPa for Young's modulus of top surface of enamel being the data recorded. This



inconsistency and inaccuracy is a consequence of the anisotropy nature of enamel and the sample size limit of human enamel. The development and employment of indentation techniques and equipment lessens this deviation of results and in general higher Young's moduli of enamel were registered using micro- and nano-scale methods. The other trend that can be seen is that the cross-section of enamel has lower Young's modulus than that of top surface.

### 2.1.2.3 PDL

To date, there have been an enormous number of researches on the crucial role of the PDL in tooth mobility and bone remodelling, including its Young's modulus which is a salient determinant for tooth movement [10]. Nonetheless, a marked variation of the PDL's mechanical properties has been documented in literature. Difficulties lie in directly acquiring the PDL statistics owing to the high dependence of tooth movement on tooth morphology [11] and possibly on strain rate [12]. Elastic modulus of the PDL was evaluated to range between 0.01 MPa and 1.75 GPa and Poisson's ratio range between 0.28 and 0.49 [13].

From biomaterials viewpoints, the PDL is a kind of connective tissue that is vascular and fibre-reinforced. It is majorly composed of collagen fibres and blood vessels. Its nerve endings are sheathed in an amorphous mucopolysaccharide matrix [14, 15]. The collagenous fibres are in the forms of collective bundles. A myriad of studies consistently revealed the nonlinearity and time dependence PDL's mechanical properties [15]. Table 2.1 below recapitulates the reported elastic properties of the PDL along with corresponding method.

**Table 2.1** Young's modulus and Poisson's ratio of the PDL. Adapted from Fill *et al.* [13]. Note that the references relevant to this table are not included in the reference list of this thesis.

## CHAPTER 2: DYNAMIC BEHAVIOURS OF HUMAN DENTAL COMPLEX

Reference	Year	Young's modulus (MPa)	Poisson's ratio	Species	Tooth	Method
Yamanda and Evans [43]	1970	1.4	—	Human	All teeth	Experimental
Atkinson and Ralph [44]	1977	3.8	—	Human	Lower premolar	Experimental
Mandel et al. [45]	1986	3	—	Human	Lower premolar	Experimental
Thresher and Saito [46]	1973	1379	0.45	Human	Upper incisor	2D-FEM
Wright [47]	1975	49	0.45	Human	All teeth	2D-FEM
Wider et al. [48]	1976	68.9	0.45	Human	Molar	2D-FEM
Yettram et al. [49]	1977	0.18	0.49	Human	Upper incisor	2D-FEM
Takahashi et al. [50]	1980	9.8	0.45	Human	Lower teeth	2D-FEM
Atmaram and Mohammed [51]	1981	175–350 <sup>i</sup>	0.45	Human	Molar	2D-FEM
Siegele et al. [52]	1986	0.26, 8.5 <sup>i</sup>	0.28	Human	Upper incisor	2D-FEM
Farah et al. [53]	1988	6.9	0.45	Human	Lower molar	2D-FEM
Ko et al. [54]	1992	68.9	0.45	Human	Upper incisor	2D-FEM
Middleton et al. [55]	1996	0.75–1.5 <sup>i</sup>	0.45	Human	Canine	2D-FEM
Weinstein et al. [56]	1980	68.9	0.45	Human	Lower premolar	3D-FEM
Tanne et al. [57]	1987	0.69	0.49	Human	Lower premolar	3D-FEM
Goel et al. [58]	1992	1750	0.49	Human	Lower premolar	3D-FEM
Korioth and Hannam [59]	1994	2.5–3.2	0.45	Human	Lower teeth	3D-FEM
Pietrzak et al. [6]	2002	0.010–0.031 <sup>ii</sup>	0.45–0.49	Human	Upper incisor	3D-FEM
Rees and Jacobsen [60]	1997	50	0.49	Human	Lower premolar	Exp/2D-FEM
Cook et al. [61]	1982	68.9	0.45	Dog	Upper premolar	Exp/3D-FEM
Andersen et al. [62]	1991	0.08–68.9 <sup>ii</sup>	0.30–0.49	Human	Lower premolar	Exp/3D-FEM
Tanne et al. [41]	1998	0.667	0.49	Human	Upper incisor	Exp/3D-FEM
Siebers [63]	1999	0.05, 0.22 <sup>iii</sup>	0.3	Pig	Canine	Exp/3D-FEM
Jones et al. [64]	2001	1	0.45	Human	Upper incisor	Exp/3D-FEM
Qian et al. [65]	2001	2, 10–90 <sup>iii</sup>	0.3	Dog	Canine	Exp/3D-FEM
Yoshida et al. [66]	2001	0.25–0.96 <sup>ii</sup>	0.45	Human	Upper incisor	Exp/3D-FEM
Poppe et al. [67]	2002	0.05, 0.28 <sup>iii</sup>	0.30	Human	Incisors, canines	Exp/3D-FEM
Cattaneo et al. [68]	2005	0.07, 0.044, 8.5	0.45	Human	Lower teeth	Exp/3D-FEM
Li et al. [69]	2006	6.89	0.45	Human	Incisor	Exp/3D-FEM
Gonzales et al. [70]	2009	0.7	0.49	Rat	Upper molar	Exp/3D-FEM
Meyer et al. [71]	2010	0.5 (matrix), 10 (PDL)	0.47, 0.35	Dog	Central incisor	Exp/3D-FEM

<sup>i</sup>Calculation performed with two types of PDL elements.

<sup>ii</sup>Calculations performed using various values of Young's modulus.

<sup>iii</sup>Calculations performed using a bilinear behaviour of Young's modulus.

### 2.1.2.4 Maxilla

Numerous literatures have quantified the mechanical properties of bone, with the emphasis on long bone. Nevertheless, there are limited studies on the quantitative properties of the mandible and even less measuring properties of the maxilla due to the anatomical and morphological complexity of the maxilla stemming from the great number of sutures between the maxilla and adjacent bones and the sinuses that occupy almost the entire internal region of the maxillary body. This structural intricacy leads to the difficulty to apply techniques and compression testing to obtain credible property data<sup>29</sup>.

Seong *et al.* [16] employed nano-indentation technique to measure the Young's modulus and apparent density of bone species at four anatomical regions, maxillary anterior,

maxillary posterior, mandibular anterior and mandibular posterior. The results divulged that maxillary bone has significantly lower apparent density and elastic modulus compared with mandibular bone despite the tested regions and anterior maxillary bone was found to be less stiff and dense than posterior maxillary bone. The average values of Young's moduli for anterior and posterior maxillary bone were estimated to be 14.5 GPa and 15.3 GPa respectively and the apparent densities for them were calculated to be  $0.79 \text{ g/cm}^3$  and  $0.57 \text{ g/cm}^3$  respectively.

### *2.1.3 Natural frequency and mode shapes*

Natural frequency (NF) analysis has been widely adopted as a non-invasive and effective method to evaluate periodontal condition, teeth stability and implant osseointegration [17-25]. It provides an alternative means to the traditional radiographic evaluation that has limitation on biomechanical quantification [17, 19, 20, 22, 26]. Alveolar bone loss and periodontal attachment decay (Fig. 2.5), as a critical manifesting index of deterioration of periodontal health, can be correlated with noticeable reduction of NF of the periodontal structures [21, 23]. The determination of NF of dental tissues or the tissues in the vicinity of dental implants can also help assess the condition of natural tooth and stability of dental implant through follow-up clinical tests or computational bone remodelling simulation [18, 25, 27-29]. In addition, an on-human trial has clinically proved the efficacy of vibration of high frequency and low magnitude on acceleration of orthodontic tooth movement (OTM) [30, 31]. This further raises the motivation for improving existing understanding of NF and mode shape associated with dental structures which is far from perfect.

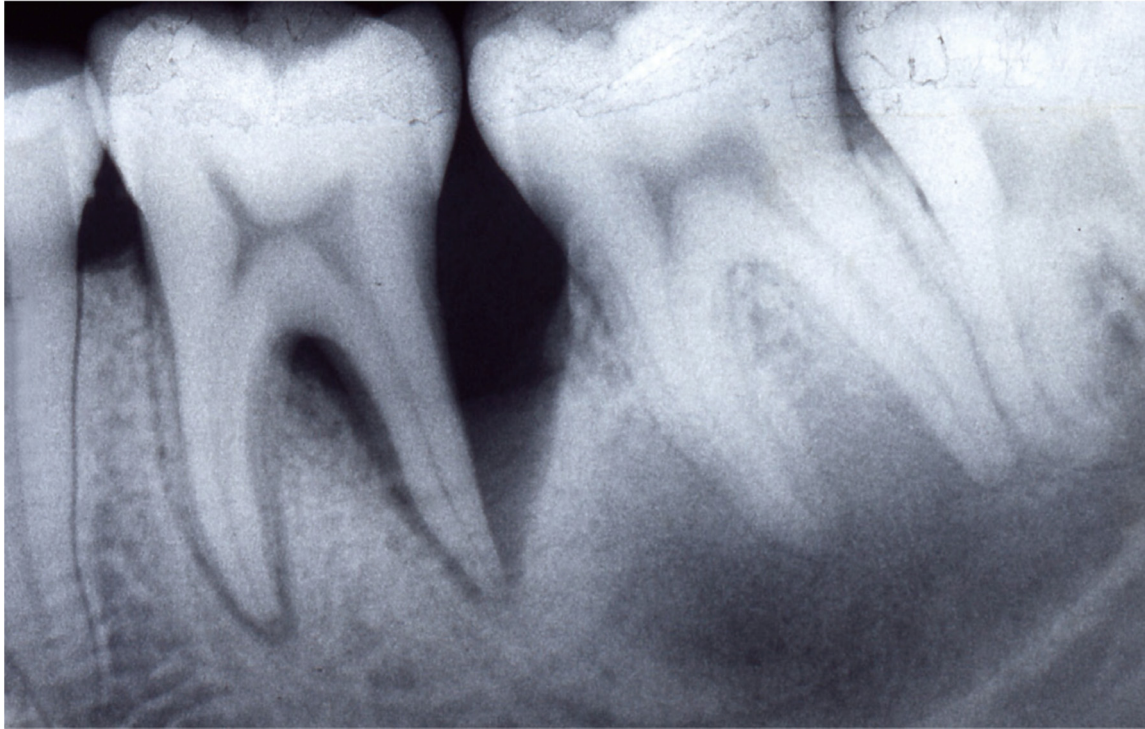


**Fig. 2.5** Severe angular alveolar bone loss [32].

Currently, natural frequencies of teeth, with or without periodontal tissues, are mainly extracted by experiments. Probing methods, conventionally employing impulse hammer, frequency spectrum analyser and acoustic microphone or accelerometer (Fig. 2.6), have been intensively utilized in the research community [17, 20, 33]. However, such approaches may fail to obtain biomechanically accurate vibratory characteristics of tissues of interest even though it contributes towards achieving clinical objectives, e.g. predicting periodontal attachment condition. This is ascribable to the fact that any structure can have multiple natural frequencies and corresponding mode shapes, depending on the material properties, morphology and degree of freedom. The present practical approaches usually target at one particular tooth without comprehending the NFs and mode shapes of the entire structure [21, 22, 33]. The frequency where peak or amplified response occurs is approximated to be, or is close to, the resonant frequency. This normally results from superimposing external vibration on its natural frequency profile, whereby this protocol is, in effect, a forced rather than a free

vibration. Moreover, the frequency scanning interval can be simply too large to capture all natural frequencies experimentally. Despite some clinical data garnered, the characteristics of forced vibration and damping effect can possibly render such experimental approaches incapable of precisely quantifying the dynamic behaviours of dental structures.

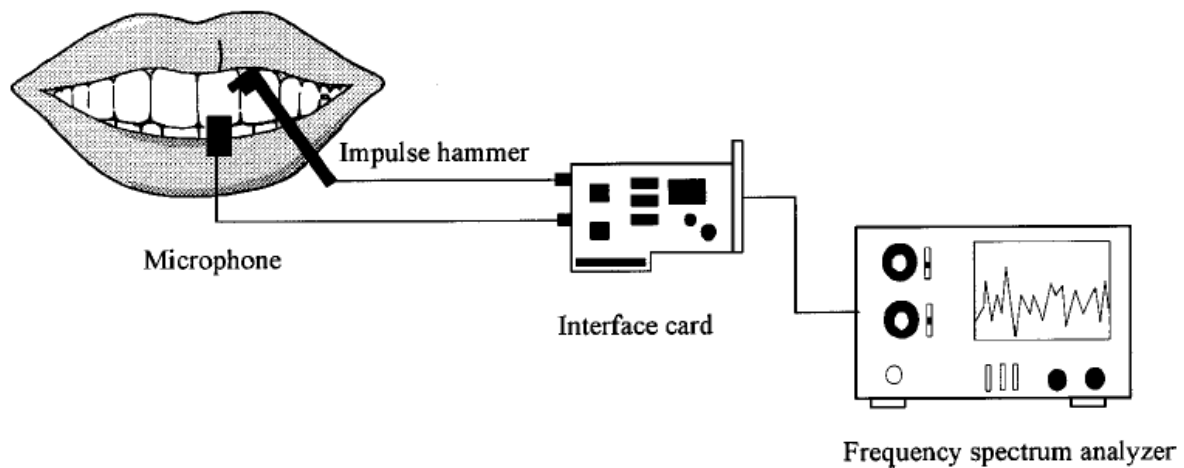


**Fig. 2.6** Instruments and testing methods for NF identification [17].

Computational methods represented by finite element (FE) approaches were therefore introduced to overcome the abovementioned technical difficulties and mimic free vibration of periodontal structures [21-24, 34]. However, some challenges have to be drawn. Firstly, damping effects of most biological materials, if not all, are difficult to be simulated, which can impose significant influence on dynamic analyses. This as a result, contributes to the major omission of damping effects by most theoretical and FE studies regarding NF extraction on dental or periodontal structures to date [18, 20, 21, 24, 34]. It is even more arduous to measure damping coefficients and factors of structures of human bodies. The periodontal ligament (PDL), acknowledged as a visco-elastic material, can potentially act as a damper during dynamic motion, in spite of the significant difficulty of precisely defining relevant damping coefficients from rather limited references. The damping property should be considered during FEA in which its sensitivity on vibratory characteristics needs to be verified. Secondly, the

incorporation of non-linearity of soft tissue, the PDL in this study, can substantially complicate the NF extraction due to the strain/time-dependency of the stiffness. For such non-linear materials, it is theoretically challenging to obtain one or one group of natural frequencies that correspond to one group of mode shapes in the context of different stress states which lead to different extents of deformation and hence varying elastic moduli as the load changes. Thirdly, in most studies, dental bony materials were modelled to be homogeneous while they exhibit site-dependent nature. Accordingly, the effects of incorporation of the heterogeneity need to be examined. Finally, the anatomical inaccuracy of FE models lowered the validity of the results. In literature, most FE studies investigating NF of dental structures used the sectioned models containing single tooth and part of its surrounding tissues [18, 19, 21-23]. It must be pointed out that unlike stress and strain assessments, NF is a global measurement of the dental structure. Such anatomical simplification can considerably alter the overall stiffness, mass and damping characteristics from an intact model. As a result, a collection of natural frequencies and mode shapes of a relatively intact dental model has not been available to date.

This chapter aimed to address these issues by creating an anatomically accurate and structurally detailed maxilla model for identifying the dynamic behaviours. The influence of introduction of damping effects, heterogeneity and non-linearity of materials on the computation of vibratory characteristics will also be elucidated.

## **2.2 Materials and Methods**

### ***2.2.1 Differential equations of motions***

The dynamic model can be physically defined as the summation of a series of mass-spring-damper systems, hence consisting of multiple degrees of freedom. The discretisation of the system into multiple elemental masses leads to a corresponding number of differential equations of motions, as represented in a matrix form as:

$$(\lambda^2 \mathbf{M} + \lambda \mathbf{C} + \mathbf{K})\mathbf{X} = 0 \quad (2.1)$$

where  $\lambda$  denotes the eigenvalue,  $\mathbf{X}$  stands for the complex eigenvector and  $\mathbf{M}$ ,  $\mathbf{C}$  and  $\mathbf{K}$  represent mass matrix, damping matrix and stiffness matrix, respectively. In this work, the subspace projection method, a built-in algorithm in Abaqus/Standard (Dassault Systèmes, Waltham, USA) was employed which allowed rapid convergence to the desired eigenvalues for complex NF analysis and eigenvectors for mode shape analysis.

### ***2.2.2 Maxilla modelling***

A complete human maxilla model was generated based on computerized tomography (CT) images in DICOM format with a resolution of approximately 0.2mm/pixel. ScanIP 4.3 (Simpleware Ltd., Exeter, UK) was employed for image segmentation [35]. The resultant maxilla model comprised a full set of maxillary teeth, their adjacent PDLs with thicknesses varying from 0.2mm to 0.4mm [36], sectioned alveolar bone and surrounding cortical bone, as presented in Fig. 2.7. The surface models, obtained from ScanIP as STL files, were imported into Rhinoceros (Robert McNeel & Associates, Seattle, US) for further processing.

To explore the effect of the integrity of the FE model on NFs and mode shapes, the models with single tooth, five teeth and half-model were also prepared for comparison. The far-field surfaces of the sectioned model were fully clamped as the boundary condition. All the parts were set to be bonded (tied) with their neighbouring parts [37]. The convergence test was conducted in accordance with mesh convergence test similarly to those reported in literature [38].

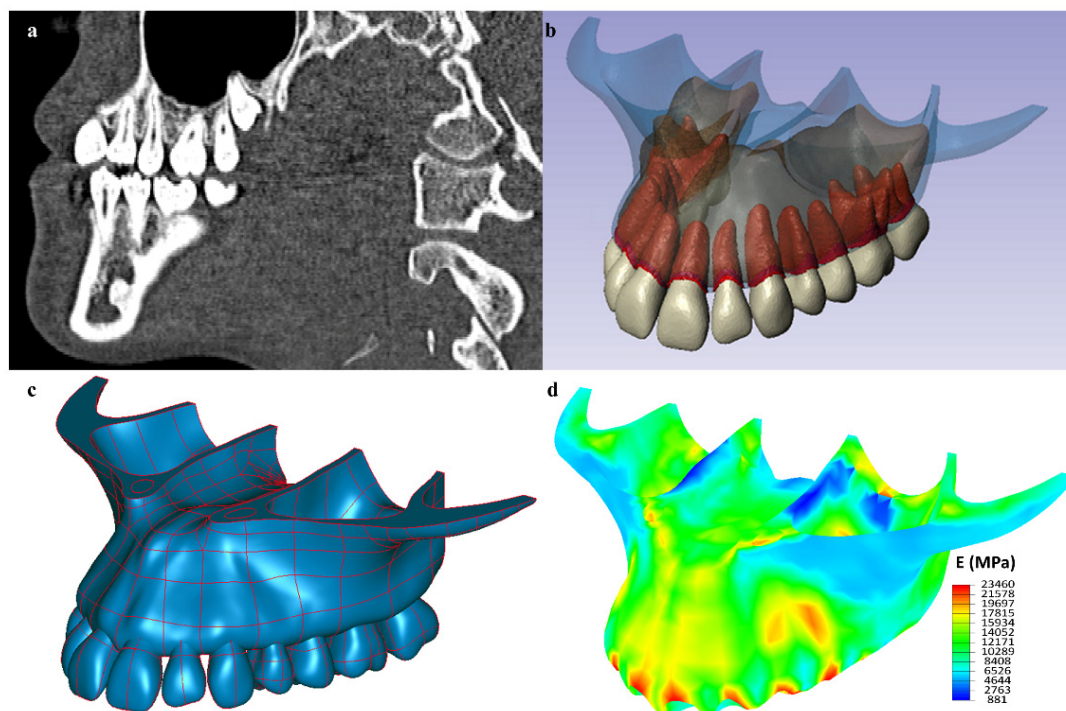


**Fig. 2.7** (a) DICOM images processed in ScanIP; (b) Masks generated for each dental material in ScanIP; (c) NURBS surfaces created in Rhinoceros; (d) Mapping of heterogeneous Young's modulus in Abaqus.

### 2.2.3 Material properties

Heterogeneous material properties were assigned to the cortical and alveolar bone as per the Hounsfield Unit (HU) in CT images. A Python program was employed to extract and process DICOM data [35]. The manipulation among HU values, densities and Young's moduli was conducted in accordance with the study by Field *et al.* [39]. Young's moduli for bony structure, i.e. cortical and alveolar (cancellous) bone, were calculated to be in the range from 881 MPa to 23,460 MPa (Fig. 2.7d), which was consistent with the data adopted in literature [37, 40, 41]. The PDL is a non-linear material and the incorporation of nonlinearity of PDL can visibly alter the FEA results, as acknowledged by a series of studies [41-44]. Nonetheless, while it is not difficult to calculate one NF for a particular mode shape based on linear material whose elastic modulus is constant regardless of deformation, it is computationally demanding



to calculate NFs of a nonlinear material under different loading conditions or stress states since the natural frequencies will change instantaneously with the change in elastic moduli. In other words, if the material is elastically non-linear, one state of stress of this material corresponds to one NF or one group of NFs given Eq. (2.1). Accordingly, there are an infinite number of groups of NFs corresponding to possibly countless number of stress states. ‘‘Piecewise’’ elastic modulus, ranging from 0.01 MPa to 10 MPa, was therefore introduced to investigate the influence of elastic modulus of the PDL on NF and mode shapes based on previously reported elastic moduli of the PDL [13]. Material properties are summarized in Table 2.2 [45-47].

**Table 2.2:** Material properties

Material	Young's Modulus (MPa)	Poisson's Ratio	Density (kg/m <sup>3</sup> )
Cortical Bone	Heterogeneous	0.31	1990
Alveolar Bone	Heterogeneous	0.3	410
Tooth	186,000	0.31	2140
PDL	Variously linear	0.45	1200

Damping effects have been considered to have influence on the vibratory characteristics of a structure [48]. A classic and convenient way of attaining damping properties is to introduce Rayleigh damping matrix which has the form of

$$\mathbf{C} = \alpha\mathbf{M} + \beta\mathbf{K} \quad (2.2)$$

where  $\alpha$  and  $\beta$  represent mass-proportional and stiffness-proportional Rayleigh coefficients, damping low and high frequency modes, respectively. Orthogonality and relations between the modal equations allow Eq. (2.2) to be rewritten as [49]:

$$\zeta_i = \frac{\alpha}{2\omega_i} + \frac{\beta\omega_i}{2} \quad (2.3)$$

## CHAPTER 2: DYNAMIC BEHAVIOURS OF HUMAN DENTAL COMPLEX

where  $\zeta_i$  and  $\omega_i$  are the modal damping factor and the undamped circular natural frequency for the  $i^{\text{th}}$  mode, respectively. Undamped circular natural frequencies were extracted first. The number of modes extracted was based on the accumulated effective masses of modes added in any global translational direction. The number of modes was estimated to be sufficient when the sum of effective mass of each mode indicates more than 90% of the total mass, whereby it can be suggested that the current mode number presents significant participation in a specific exciting direction [49, 50].

The damping ratios of maxillary dental structure can range from 0.091 to 0.24 [19], which was approximated as the range of damping ratios for the 1<sup>st</sup> to the  $n^{\text{th}}$  modes, where the  $n^{\text{th}}$  was the last mode extracted rendering at least 90% mass participation. Damping ratios for the modes other than the 1<sup>st</sup> and the  $n^{\text{th}}$  modes were estimated through the interpolation method similar to the literature by Chowdhury and Dasgupta [50]. To determine the Rayleigh coefficients, a function  $S(\alpha, \beta)$  can be formulated using the least square technique as:

$$S = \sum_{i=1}^n \left[ \left( \frac{\alpha}{2\omega_i} + \frac{\beta\omega_i}{2} \right) - \zeta_i \right]^2 \quad (2.4)$$

Partial differentiating  $S$  with respect to both  $\alpha$  and  $\beta$  and let the first partial derivatives be zeroes, yielding:

$$\alpha = \frac{2 \left( \sum_{i=1}^n \omega_i^2 \sum_{i=1}^n \frac{\zeta_i}{\omega_i} - n \sum_{i=1}^n \omega_i \zeta_i \right)}{\left( \sum_{i=1}^n \omega_i^2 \sum_{i=1}^n \frac{1}{\omega_i^2} \right) - n^2} \quad (2.5)$$

$$\beta = \frac{2 \left( \sum_{i=1}^n \omega_i \zeta_i \sum_{i=1}^n \frac{1}{\omega_i} - n \sum_{i=1}^n \frac{\zeta_i}{\omega_i} \right)}{\left( \sum_{i=1}^n \omega_i^2 \sum_{i=1}^n \frac{1}{\omega_i^2} \right) - n^2} \quad (2.6)$$

## 2.3 Results

### 2.3.1 Effects of material heterogeneity and non-linearity

It can be observed from Fig. 2.7d that the highest Young's modulus was found to be in the vicinity of teeth sockets and it decreased towards the superior part of maxilla. In addition, a symmetric pattern with respect to the sagittal plane can also be seen. It was found that the introduction of heterogeneous properties of bony tissues slightly increased the NFs of the first 20 modes, compared with the NFs of homogeneous model in which 14,700 MPa and 490 MPa were used as Young's moduli of cortical bone and cancellous bone respectively [37] (Fig. 2.8). It should be noted that the Young's modulus of the PDL was assumed to be 1 MPa throughout the study, when investigating the factors other than Young's modulus [51]. The effects of variation in Young's modulus of PDL can also be seen on the dynamic behaviours, as presented in Fig. 2.9. It was found that a higher stiffness of the PDL generated higher NFs in the first 10 modes.

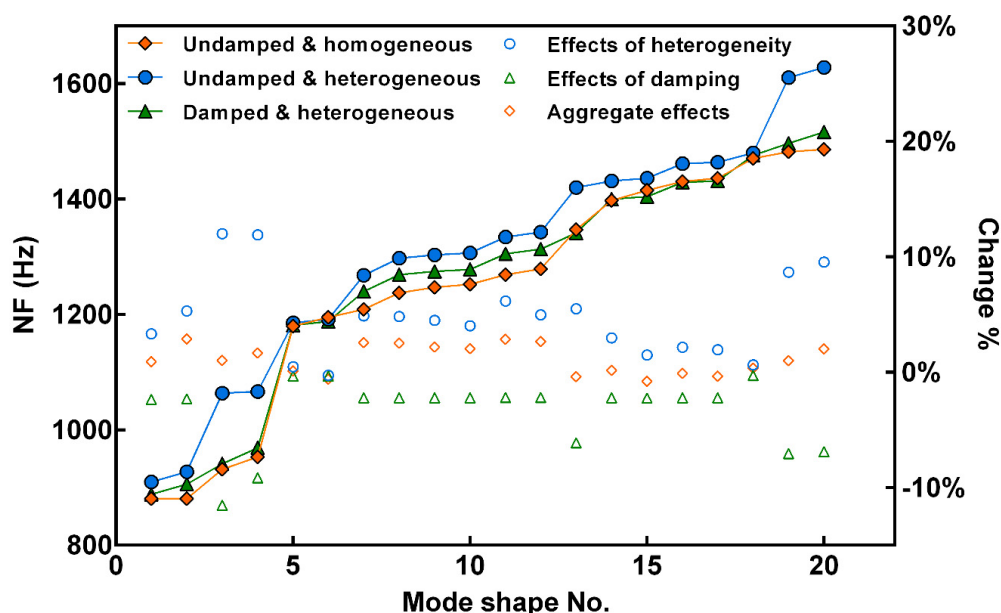


**Fig. 2.8** Effects of damping and heterogeneity of this study. The aggregate effects were the averaged-out effects considering both damping and heterogeneity.

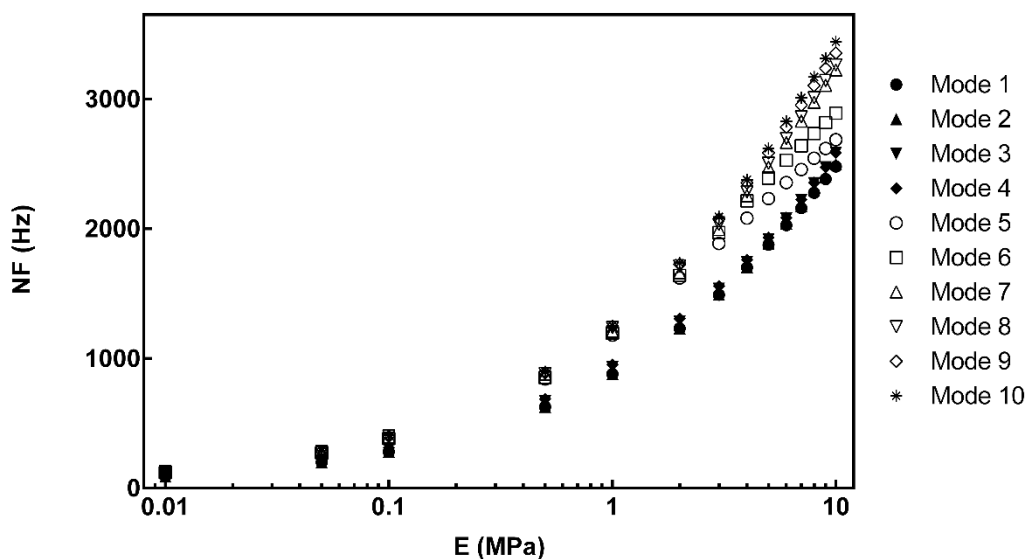


**Fig. 2.9** Effects of PDL's Young's modulus on NFs for the first 10 modes.

### 2.3.2 Damping ratio calculation and damping effects

It was calculated that the first 20 modes were sufficient to contribute more than 90% of total mass in each direction. A spectrum of damping ratios ranging from 0.091 to 0.24 were subsequently assigned to the first 20 modes interpolatively, with the first mode featuring a damping ratio of 0.091 and the 20<sup>th</sup> featuring 0.24. The Rayleigh coefficients were determined to be  $5.684 \times 10^{-3}$  for  $\alpha$  and  $4.5366 \times 10^{-5}$  for  $\beta$ , according to Eqs. 2.5 and 2.6. The first 20 natural frequencies, without and with damping properties, were presented in Fig. 2.8. It can be observed that the damped NFs were marginally lower than their undamped counterparts with the differences averaging at 3.40%. On the other hand, damped and undamped models shared almost the same mode shapes for the first 20 modes.

### 2.3.3 Effects of model integrity

The first 20 mode shapes of these four models (i.e. single-tooth, five-teeth, half model and complete model) with different anatomical completeness were tabulated (Table 2.3) and the corresponding NFs were schematically presented (Fig. 2.10). The first NFs of single-tooth, 5-

teeth, half and complete models were calculated to be 1546 Hz, 1193 Hz, 1024 Hz and 889 Hz, respectively (Fig. 2.10). As the completeness of the models increased, from single to complete maxilla, the NFs of the same order decreased and the position of the primary vibrating tooth tended to shift from anterior to posterior. It should be noted that the vibration herein refers to a mode shape of vibration which is not a realistically occurring motion but virtual pattern or configuration describing inherent vibratory characteristics of a structure. The 1<sup>st</sup> mode shape of single-tooth model featured a linguo-buccal vibration of the canine while the 1<sup>st</sup> mode shape of 5-teeth model could be characterized by linguo-buccal vibration of the 2<sup>nd</sup> premolar (Fig. 2.11). The similar vibratory patterns were recorded for the 1<sup>st</sup> NFs of the half model and complete model but with different vibrating tooth, i.e. the 2<sup>nd</sup> molar. The NFs of higher orders exhibited similar trend to the 1<sup>st</sup> NFs, as plotted in Fig. 2.11. The NF curve of single-tooth model deviated significantly from the other models with better integrity in which the single-tooth model presented dramatically higher increments as NF order increased. By comparison, similar trends of NF curves of the other three models (than the single tooth model) were observed.

**Table 2.3** Mode shapes of different models

	<b>Mode No.</b>	<b>Mode shape</b>	<b>Primary vibrating teeth</b>
<b>Single-tooth</b>	<b>1st</b>	Linguo-buccal	Canine
	<b>2nd</b>	Mesio-distal	Canine
	<b>3rd</b>	Superior-inferior	Canine
<b>5-teeth</b>	<b>1st</b>	Linguo-buccal	2nd premolar
	<b>2nd</b>	Linguo-buccal	1st premolar
	<b>3rd</b>	Linguo-buccal	1st incisor
<b>Half model</b>	<b>1st</b>	Linguo-buccal	2nd molar
	<b>2nd</b>	Mesio-distal	2nd molar
	<b>3rd</b>	Linguo-buccal	2nd premolar
	<b>1st</b>	Linguo-buccal	Right 2nd molar
	<b>2nd</b>	Linguo-buccal	Left 2nd molar
	<b>3rd</b>	Mesio-distal	Right 2nd molar
	<b>4th</b>	Mesio-distal	Left 2nd molar
	<b>5th</b>	Linguo-buccal	Left 2nd premolar

<b>Complete model</b>	<b>6th</b>	Linguo-buccal	Right 2nd premolar
	<b>7th</b>	Linguo-buccal	Left 1st premolar, central incisor
	<b>8th</b>	Linguo-buccal	Left and right central incisor, left and right 1st premolars
	<b>9th</b>	Linguo-buccal	Right 1st premolar, left central incisor
	<b>10th</b>	Linguo-buccal	Left and right central incisors
	<b>11th</b>	Linguo-buccal	Right 1st molar
	<b>12th</b>	Linguo-buccal	Left 1st molar
	<b>13th</b>	Mesio-distal	Left and right central incisor
	<b>14th</b>	Mesio-distal	Left and right central incisor, right lateral incisor
	<b>15th</b>	Mesio-distal & Linguo-buccal	Left and right central incisor (MD), right lateral incisor (LB)
	<b>16th</b>	Linguo-buccal	Left canine, right lateral incisor
	<b>17th</b>	Linguo-buccal	Left canine, right lateral incisor
	<b>18th</b>	Mesio-distal	Right 1st premolar
	<b>19th</b>	Mesio-distal	Left 1st premolar
	<b>20th</b>	Linguo-buccal	Left canine

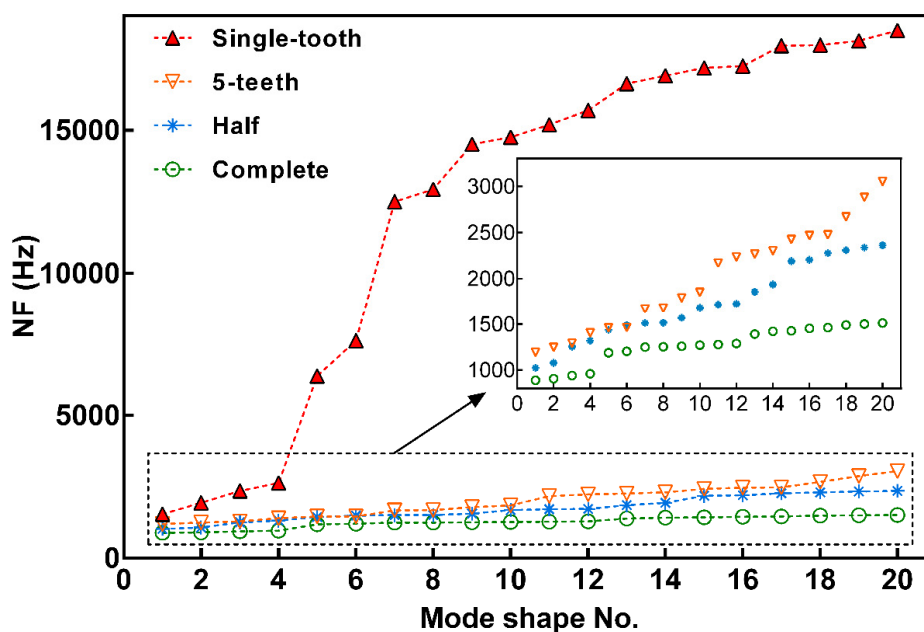


**Fig. 2.10** Comparison of natural frequencies for different levels of model simplification.

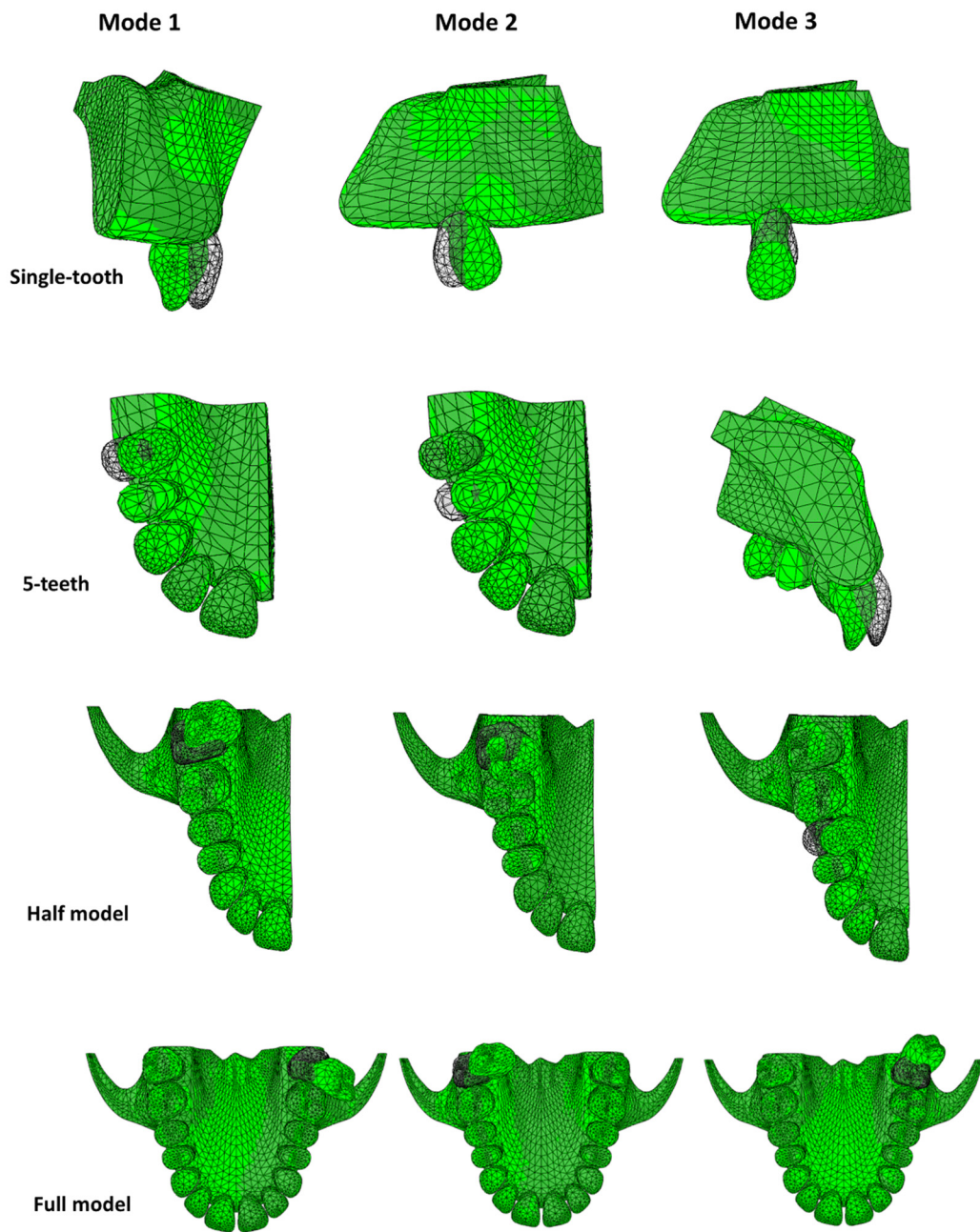


**Fig. 2.11** Mode shapes of models with various integrities.

## 2.4 Discussion

The vibratory characteristics, i.e. NFs and mode shapes of human maxillary model as well as the effects of modelling on vibratory characteristics were explored in this study. There has been no other computational study available that adopted a realistic heterogeneous and

damped maxillary model to analyse their effects on dynamic behaviours. Our study showed that it is more accurate to adopt heterogeneous model to determine NFs and mode shapes of dental structures, as a maximum 14.28% increase at Mode 3 stemming from the heterogeneous properties was recorded when compared with the NFs of its homogeneous counterpart (Fig. 2.8). All other NFs for the first 20 modes were also visibly raised from the heterogeneity of material properties of dental bony tissues. It can be speculated that compared with a homogeneous mapping of elasticity, the variation of Young's modulus in the vicinity of maxillary teeth sockets can possibly change the local gradients and distribution of Young's modulus of the alveolar bone-PDL-tooth complex which have appreciably contributed to its NFs. Nevertheless, no significant change in mode shapes was observed with introduction of material heterogeneity.

Conversely, the incorporation of damping properties lowered NFs by 0.28% to 11.54%, marginally at some modes while moderately at others. This was consistent with the theoretical study by Caughey and O'Kelly [48] who concluded that despite the presence of damping matrix, the damped NFs are always less than or equal to the corresponding undamped NFs. Based on Eq. 2.3, it can also be observed by calculation, with the Rayleigh coefficients determined, that the stiffness-proportional Rayleigh coefficient ( $\beta$ ) contributes significantly more to the damping effects, compared with the mass-proportional Rayleigh coefficient ( $\alpha$ ). This is attributable to the second term in Eq. 2.3 containing  $\beta$  weighing more than 99% of total damping ratio, as a result of high NFs of the model in this study. As the first computational study investigating the damping effects on dynamic characteristics of human dental structures, we presented a procedure that can establish a mode-dependent Rayleigh damping matrix for a model with large degrees of freedom by calculating Rayleigh damping coefficients using least-square fitting method. The results indicated that the PDL can act as a damper in the dental structure, thus effecting a change on NFs. Therefore, it would be more prudent to integrate the



damping properties of a dental or periodontal structure into the examination of its dynamic characteristics.

The effects of both damping and heterogeneous properties were presented in Fig. 2.8, in which the NFs of the first 20 modes in the damped and heterogeneous models were mostly in between the curves featuring undamped-homogeneous model and undamped-heterogeneous model. Consideration of these two factors collectively led to a slight -0.61% to 2.87% change of the NFs of undamped and homogeneous model. However, it may not be rigorous to presumably exclude damping and heterogeneous properties when analyzing dynamic or vibratory characteristics.

In this study, the Young's modulus of the PDL was varied in a piecewise linear manner. As the Young's modulus increased, the NF of the same mode increased in a polynomial manner, for the first ten mode shapes (Fig. 2.9). This study was based on the assumption that either all the PDLs were undeformed or all the PDLs were deformed uniformly, which allowed homogeneous stiffness of the PDLs. The stiffness of PDLs can change if an external load, e.g. orthodontic force, is introduced or varies, whereby the non-linearity of the PDL should be considered. It is therefore important to take into account the effects of PDL's Young's modulus when extracting dynamic characteristics of dental structures. The computational characterisation of NFs and mode shapes of any dental structure, in other words, should be conducted in a context of a presumed or predetermined range of stiffness of the PDL.

As unfolded by Fig. 2.11, the NFs of single-tooth model deviated clearly from those of more integral and complete models. This revealed that frequency analysis using single tooth complex alone may not be appropriate particularly in high frequency range. A more comprehensive insight into NFs and mode shapes of an intact dental structure is crucial to obtaining an exhaustive dynamic biomechanics of the dental structure. The results of the

single-tooth model obtained in this study were nevertheless in good agreement with past clinical measurements, which validated the accuracy of the current model (Fig. 2.12). The 1<sup>st</sup> NF of current single-tooth model (1,546 Hz) fell between the values documented using a probing method (1,350 Hz) and modal test (1,701 Hz) [17, 20]. The results of other past FEA studies seemed to be more biased compared with such clinical data. The factors involved, such as insufficient modelling of surrounding bony structures, could have caused the inaccuracy of these models [22, 24].

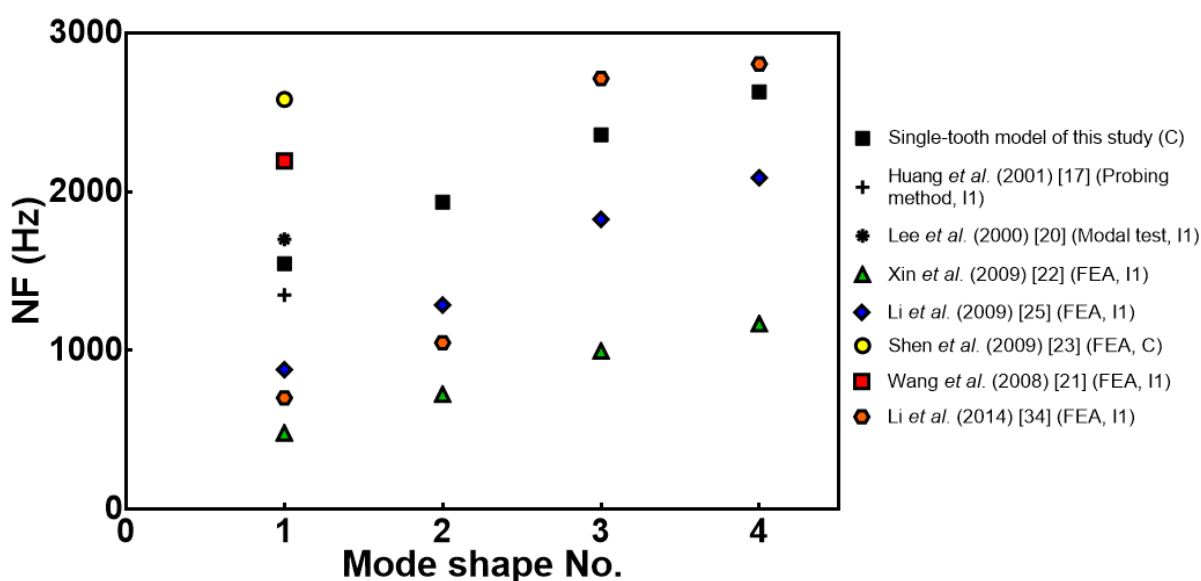


**Fig. 2.12** Comparison of current study with past studies; C and I1 stand for maxillary canine and central incisor respectively.

The morphological extension of the single-tooth model all the way to an intact maxilla model allows one to better accommodate the anatomical sophistication of the dental and periodontal structures which can to a certain extent alter the overall stiffness, mass and degrees of freedom and hence considerably contributes to the preciseness of NF analysis. This has been evidenced in our present study where more integral models exhibited lower NFs of the same mode. Moreover, the greater integrity of the model better illuminates the vibratory characteristics of complex dental and periodontal structure because a theoretically precise

mode shape can hardly be extracted from experiments. The dominant vibrating tooth/teeth and its/their mode shapes of the first few modes showed that energy transfer tended to be through vibrating or impacting posterior teeth instead of anterior teeth. The linguo-buccal direction also dominates other directions such as predominant mechano-transductive pathway (Table 2.3).

The extraction of vibratory characteristics via the FE free vibrational analysis can serve to provide a preliminary reference for further studies involving forced vibrational analysis that requires the comprehension of vibratory characteristics. With the increasing knowledge of dominant vibratory patterns and natural frequencies, clinicians can be better assisted when applying dynamic or cyclic loads. One example can be the use of vibration in conjunction with orthodontic appliances to accelerate OTM, where the selection of more beneficial form, direction and amplitude of vibration should be based on precise free vibration analysis [30, 31]. This study also verified the past experiments investigating NF and mode shapes of dental structure from a biomechanical perspective and set a benchmark for dental modelling, especially pertaining to dynamic analysis or vibrational loading.

### **2.5 Conclusions**

The results obtained in this chapter demonstrated the significance of accurate modelling of dental and periodontal structures in analysing dynamic behaviours, as evidenced by the discrepancies of resultant NFs and mode shapes among the models of differing integrity and different material properties. The NF of the same order increased with the Young's modulus of the PDL. The incorporation of damping effects could reduce the NFs while the introduction of heterogeneity of bony tissue could raise the NFs. Nevertheless, it was found that both of these material properties have insignificant effects on the mode shapes. The results of the current study were validated by comparing the single-tooth model with those clinical

## CHAPTER 2: DYNAMIC BEHAVIOURS OF HUMAN DENTAL COMPLEX

experiments and past FEA studies. It was also found that the primary (1<sup>st</sup>) and high-order NFs of the maxillary structure declined as the completeness of models improved. From the complete maxillary model, the primary NF was obtained to be 889 Hz; and the corresponding mode shape featured predominant linguo-buccal vibration of maxillary right second molar and was symmetric to the 2<sup>nd</sup> mode shape that had a close resultant NF of 906 Hz. Linguo-buccal vibration was found to be more dominant over other vibratory configurations; and posterior teeth were examined to be the main teeth, through which the external energy tends to be transferred.

This study provided key biomechanical insights into the vibratory characteristics of human maxilla and maxillary teeth as well as an important reference for future dental dynamic analysis, especially the studies on periodontal evaluation through vibration and effects of vibration on tooth movement.

## CHAPTER 3

### VIBRATE TO ENHANCE ORTHODONTICS

This chapter aims to explore biomechanics for orthodontic tooth movement (OTM) subjected to concurrent single-tooth vibration (50Hz) with conventional orthodontic force application via a clinical study and computational simulation. Thirteen patients were recruited in the clinical study, which involved distal retraction of maxillary canines with 150 g force for 12 weeks. In a split mouth study vibration and non-vibration side were randomly assigned to each subject. Buccally-directed vibration of 50 Hz, of approximately 20 g of magnitude, was applied on the maxillary canine for the vibration group. A mode-based steady-state dynamic finite element analysis (FEA) was conducted based on an anatomically detailed model, complying with the clinical protocol. Both the extent of space closure and canine distalisation of the vibration group were significantly higher than those of the control group, as measured intra-orally or on models ( $p < 0.05$ ). The volume-average hydrostatic stress (VHS) in the periodontal ligament (PDL) was computationally calculated to be higher with vibration compared with the control group for maxillary teeth and for both linguo-buccal and mesial-distal directions. An increase in vibratory frequency further amplified the PDL response before reaching a local natural frequency. 50 Hz and 20 g single-tooth vibration accelerated maxillary canine retraction. An amplification of PDL response was also shown to be induced by vibration based on computational simulation. The vibration-enhanced OTM can be described by mild, vigorous and diminishing zones among which the mild zone is considered to be clinically beneficial.

### **3.1 Introduction**

#### ***3.1.1 Mainstream pressure-tension theory***

Orthodontics is desired to achieve proper masticatory functionality and aesthetics by moving the teeth to more ideal positions through applying mechanical forces sequentially. Orthodontic tooth movement (OTM) is regarded as a process of a mechaobiologically induced response to external force application to rebalance the physiological and biochemical equilibrium in the dento-facial complex. A tooth can be moved in the periodontal “gap” by establishing a compression side, where the periodontal ligament (PDL) exhibits disorganisation and diminution of fibre production seemingly resulting from vascular constriction, and a tension side, where a growth in cell replication of PDL occurs by stretching PDL fibre bundles (Fig. 3.1a) [52, 53].

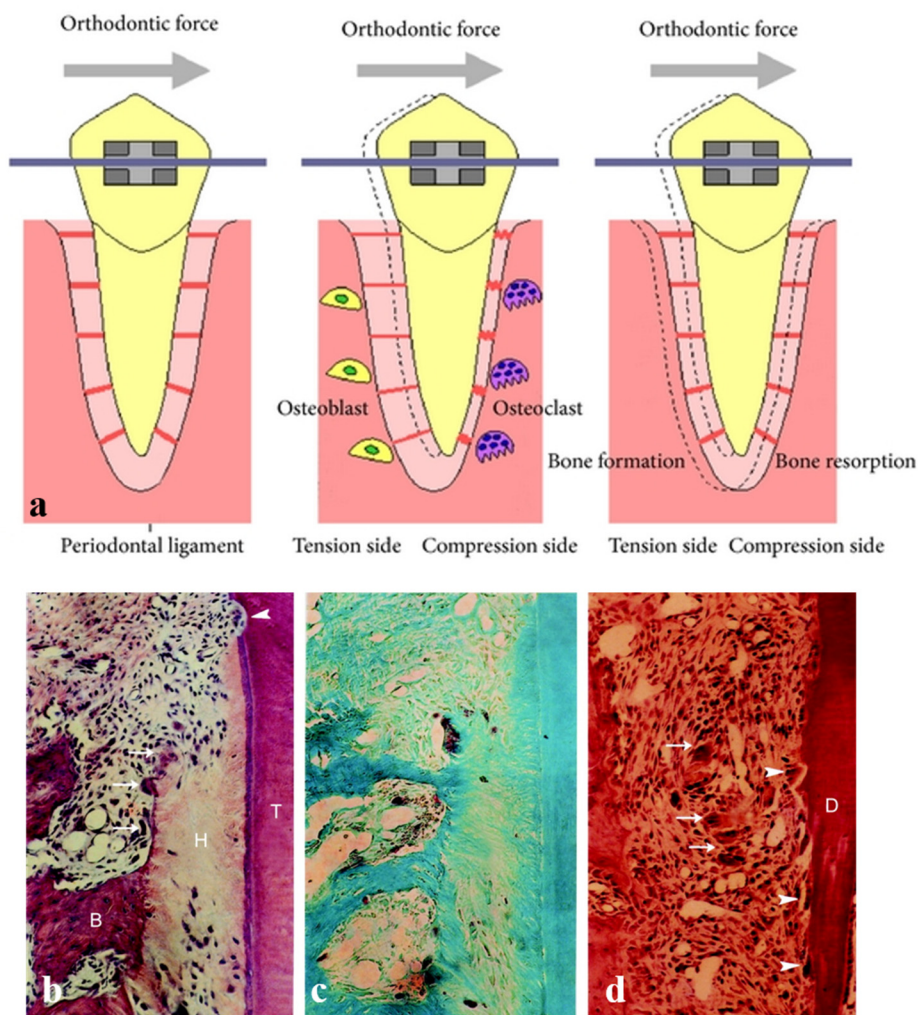


**Fig. 3.1** (a) Orthodontic force generates compression and tension sides on the PDL [54]; Sections of a rat maxillary first molar: in the vicinity of the compression site of the mesio-lingual root 7 days since tooth movement begins; (b) Use haematoxylin and eosin stain; (c) Tartrate-resistant acid phosphatase (TRAP) stain indicates TRAP-positive cells near narrow spaces and hyalinisation zone; (d) Compression region after 10 days. Hyalinised tissues virtually diminished and resorption lacunae became visible on both the dentine and bone surfaces [55].

Contemporary perspectives of abovementioned pressure-tension theory indicate that sustained force application to the tooth produces an alteration and adjustment in bloodstream inside the PDL tissues. The transformation in blood flow subsequently changes the biochemical environment of PDL and stimulates the release of chemical mediators of OTM

that are recognised by and interacted with osteoclasts and osteoblasts such as RANKL, TGF- $\beta$  and OPG. On the compression site, the bony tissues immediately adjacent to the place where PDL necrosis occurs or the hyalinised tissues were absorbed by macrophages, foreign body giant cells and osteoclasts. On the tension site, fibroblasts and osteoblasts are upregulated, followed shortly by osteoid deposition and calcification (Fig. 3.1b-d) [56-58].

### **3.1.2 Other OTM theories**

The physiological fundamentals of tooth movement induced by force and some mechanisms relevant, have been largely studied since the nineteenth century. This quest led to the proposals of three main theories widely accepted and cited to explain bone remodelling process regarding (orthodontic) tooth movement, i.e. the foregoing pressure-tension theory [52, 53, 59], the blood flow theory [60] and the bioelectric theory [61], essentially involving two themes, the PDL and alveolar bone.

The bioelectric or bone bending theory was firstly proposed by Bassett and Becker [60] in 1962. It hypothesises that electric potentials in the stressed tissue will be generated in response to mechanical loadings thereby controlling the tooth movement associated with bone metabolism. When the load is exerted on a tooth, the adjacent alveolar bone bends. Concave bone surfaces featuring activity of osteoblasts are electro-negative while convex bone surfaces featuring activity of osteoclasts are electro-positive or electro-neutral (Fig. 3.2). Experiments in which exogenous electrical currents were used have indicated that PDL and alveolar bone cellular activities were strengthened, as well as rapid tooth movement. In summary, bone bending in conjunction with orthodontic force is possible to trigger bioelectric responses. This may act as an important cellular first messengers.



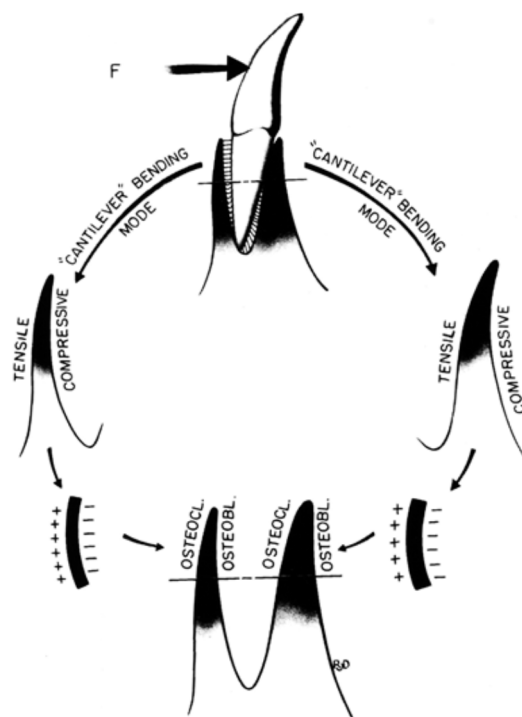


**Fig. 3.2** Areas of concavity and convexity generated on bone bending [62].

According to the theory proposed by Bien [61], “tooth movement occurs as a result of alterations in fluid dynamics in the PDL”, documented as the fluid dynamic or blood flow theory. The application of a force to a tooth with short period would squeeze out the interstitial fluid from the PDL via micro vascular channels. When the force is removed, the recirculation of the interstitial fluid and diffusion from capillary walls would replenish the fluid. However, a heavier force with longer lasting time can cause the escape of interstitial fluid within the PDL toward the apex and cervical areas, which leads to the “squeeze film” effect which slows down the tooth movement. When an applied orthodontic force compresses the PDL, the blood vessels in the compression site also get compressed and this may give rise to stenosis, resulting in aneurysms. Gases in bloodstream can move into the local interstitial fluid and hence establish a favourable surrounding to resorb bone.

### ***3.1.3 Types of OTM***

There are generally five types of tooth movement categorised in orthodontic treatment: tipping movement, bodily movement (translation), rotation, extrusion and intrusion. In these five paths a tooth can be moved up and down, forward and back or rotated.

#### ***3.1.3.1 Tipping***

Tipping is the simplest form of OTM which occurs when the loading is exerted onto a tooth crown and the force does not pass through its centre of resistance (Fig. 3.3a). It is a result of combination of translation and rotation as the applied load creates a moment about the centre of resistance.

#### ***3.1.3.2 Bodily Movement***

Bodily movement or translation implies that all the points on the object are displaced an equal distance in the same direction (Fig. 3.3b). It occurs when the direction line of the force application goes through the centre of resistance of a tooth. As a result, the tooth responds with a pure translating movement the same direction as the line of action of the force application. Bodily movement can be observed during orthodontic extrusion or intrusion or during retraction or protraction of teeth.

#### ***3.1.3.3 Extrusion and Intrusion***

Extrusion of a tooth involves the application of force that vertically moves the tooth away from its bony socket toward opposing teeth, as in closing down an open bite (Fig. 3.3c). It needs to produce tension in PDL fibres.

Intrusion is a common procedure in orthodontic treatment which involves alveolar bone remodelling fulfilled by slowly moving the tooth further into the alveolus (Fig. 3.3d), during which, forces are concentrated at root apex.

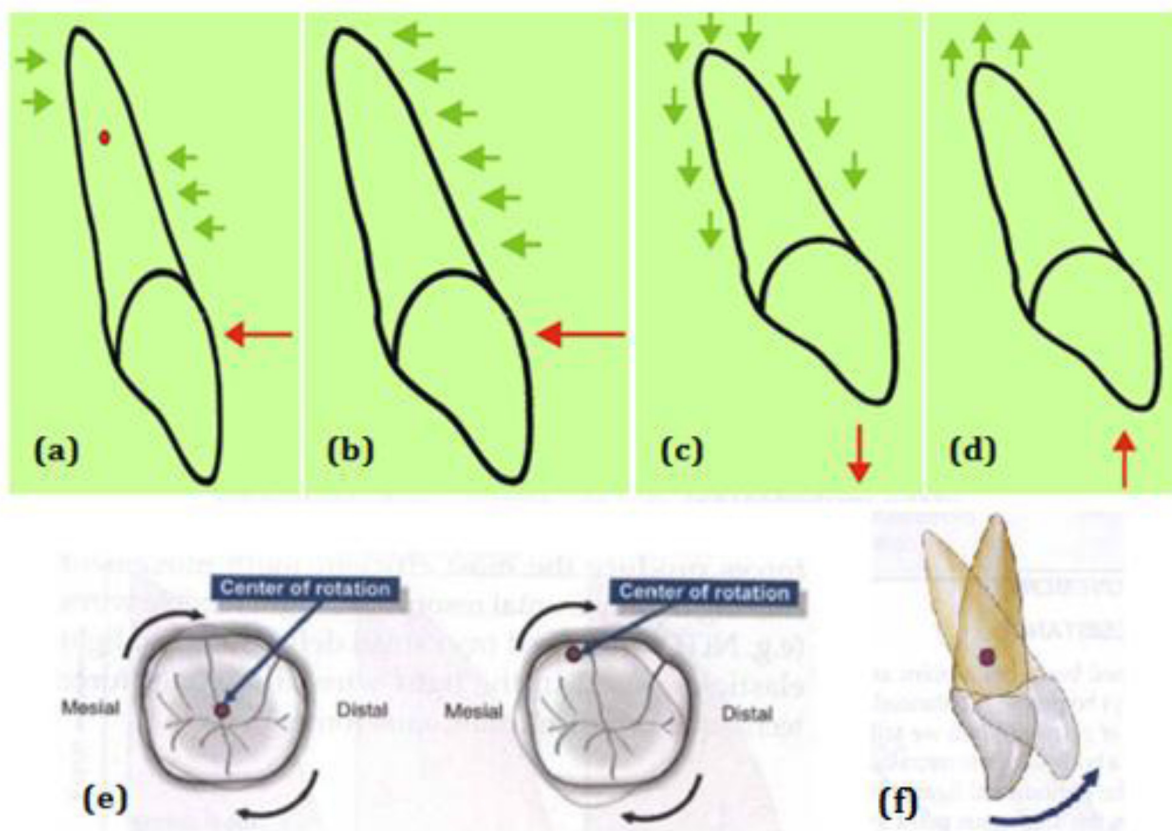


**Fig. 3.3** Forms of tooth movement. (a) Tipping, (b) Translation, (c) Extrusion, (d) Intrusion, (e) Long-axis rotation, (f) Transverse rotation.

#### 3.1.3.4 Rotation

Rotation of a tooth occurs when there is movement of points along the arc of a circle, and the centre of resistance becomes the centre of rotation. It is further categorised into two forms: long-axis rotation (Fig. 3.3e) and transverse rotation (Fig. 3.3f). Long-axis rotation occurs on the long axis of the tooth with the angulation of the axis remaining unchanged while transverse rotation is the rotation in which the angulation of the long axis of the tooth alters.

Rotation/derotation of a tooth on its axis is usually required to straighten a tooth that is rotated inappropriately. Bicuspid are frequently rotated and their correction is difficult to be

maintained unless there is a circumferential incision made around the tooth root to section the elastic fibres.

### ***3.1.4 Dynamics in bone metabolism***

Orthodontic force systems in most orthodontic treatments are static in nature. Dynamic loading and the corresponding biologic and mechanical responses are largely unknown despite its strong relevance to bone remodelling. The frequency of dynamic component of the orthodontic force has not been investigated in research until recently. The fundamentals associated with dynamic loading are that the vibratory or cyclic forces are considered to expedite the bone remodelling process at the cellular level at a far greater rate than static forces [33, 63-68].

The biomechanical roles of dynamic loading on promoting bone's remodelling have been well recognized in orthopaedics. Rubin *et al.* [63, 64] suggested that low-magnitude and high-frequency (LMHF) mechanically-induced signals are anabolic to the skeleton. Accordingly, they may provide a feasible instrument to regulate the sensitivity of bone to mechanically-induced signalling and build a non-pharmacological remedy for osteoporosis based on the fact that these cyclic mechanical impacts could be three orders of magnitude below the extent capable of damaging bone, and strengthen both quality and quantity of bone. Through a randomised and controlled pilot study, Ward *et al.* [67] preliminarily concluded that LMHF mechanical stimulus has the potential to provide a non-invasive and non-pharmacological treatment for children with insufficient bone mineral contents due to disabilities by whole body vibration.

In an animal study, Kopher and Mao [68] compared the effects of oscillatory forces of 5N and 1Hz with the static loads on the growth responses of premaxillomaxillary suture (PMS) and nasofrontal suture (NFS). It was ascertained that cyclic mechanical strain triggered potent

### CHAPTER 3: VIBRATE TO ENHANCE ORTHODONTICS

stimulus for sutural growth. It has also been shown that the LMHF mechanical stimuli assist adaptive bone remodelling of condylar cartilage, evidenced from the fact that the endochondral bone is considerably replaced by the hypertrophic cartilage, according to the study by Sriram *et al.* [69].

However, the *in vivo* studies directly evidencing the efficacy of vibratory forces locally applied to periodontal tissues to promote OTM are fairly scarce, particularly for the trials on humans. It is observed by Nishimura *et al.* [33] that the application of vibration significantly enhanced receptor activator of nuclear factor kappa-B ligand (RANKL) expression of fibroblasts and osteoclasts in the PDL of rats without excessive damage to periodontal tissues. Pulsed electromagnetic field (PEMF) coupled with magnets and/or conventional mechanical force was also demonstrably believed to generate more prominent OTM in rats compared with the scenario without PEMF [65, 66]. Likewise, it was reviewed and summarized by Tanaka *et al.* [70] that low-intensity pulsed ultrasound (LIPUS), a therapeutic technique featuring 1.5 MHz frequency pulses, can be applied to enhance orthodontic treatments. The results of several human trials favoured the adoption of vibration in conjunction with orthodontic treatment with faster OTM being recorded while conflicting results were also reported [30, 71-74]. A convincing mechanism for this vibration-oriented mechanical modulation remains however undetermined.

Compared with experimental studies on the consequence of vibratory loads, there has been a lack of computational dynamic analyses on the biomechanical role of cyclic force. In contrast, exhaustive finite element analysis (FEA) studies on OTM are available however focused on static analyses of the biomechanical responses of the sectioned mandible/maxilla and single or discrete multiple teeth.

### ***3.1.5 Vibration for pain reduction***

The advantages of mechanically induced vibratory stimulation also include the potential capacity to relieve pain induced by the orthodontic treatment. This is particularly important inasmuch as pain is an all-too-common side-effect suffered by patients receiving orthodontic treatments, with approximately 77% of the patients receiving orthodontic therapy reported pain in various extents [75]. In addition, the compliance rate with orthodontic treatment can often be forecasted based on the level of pain initially reported and discomfort suffered [76]. Analgesics are frequently prescribed to reduce the pain, in most cases however, they do not completely eliminate it [77, 78]. Furthermore, it was suggested by Kehoe *et al.* [79] that non-steroidal anti-inflammatory drugs may decelerate the OTM. Proffit *et al.* [80] stated that light force levels tend to induce less pain; on the contrary, Lim *et al.* [81] suggested that most patients still suffered from orthodontic pain despite physiologic and light forces were utilised.

Marie *et al.* [82] sought to evaluate the pain-alleviating effect of vibration as a method to manage pain after orthodontic treatment associated with periodic adjustment of appliances. The study was sized of 21 male and 27 female adult and adolescent patients receiving comprehensive orthodontic treatments, excluding those who had reported any dental pain before orthodontic treatment. The active group received the vibratory stimulation through devices (Fig. 3.4a) for 15 minutes after archwire installation while the control group received no pain relief therapy. Results obtained by repeated measurement analysis of variance suggested significant difference between the pain scores of the two groups with the active group showing a significant lower level of pain scores (Visual analog scores) than the control group over the various time intervals (Fig. 3.4b).

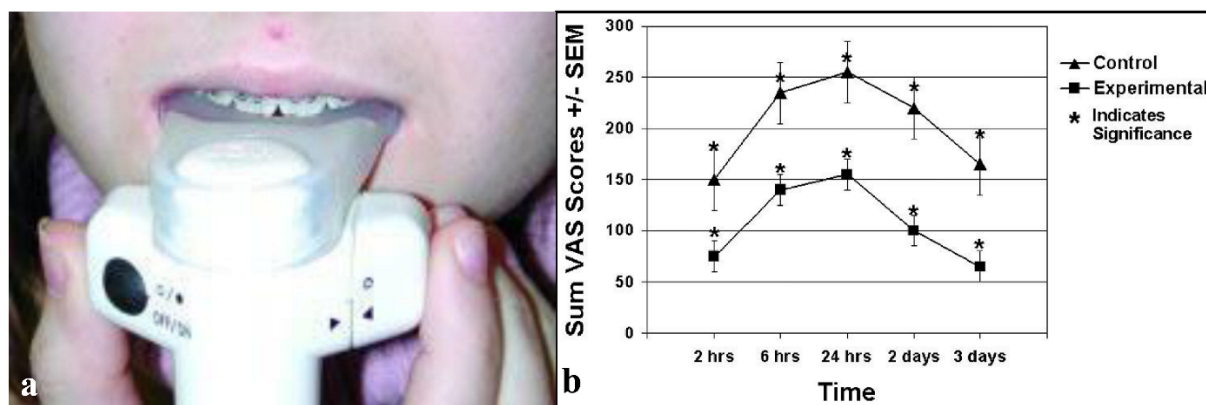


**Fig. 3.4** (a) Vibratory device to induce vibratory stimulation directly onto teeth; it consists of a soft plastic wafer for biting and a battery-powered motor; (b) Visual analog scores for control and experimental groups [82].

Ottoson *et al.* [83] conducted similar investigation in which the 100 Hz vibratory simulation were exerted onto the various sites of the skull of 36 patients suffering from apical periodontitis in the region of the first molar in maxilla or postoperative pain due to the extraction of impacted wisdom teeth for over two days. All subjects except three reported a pain relief by 75% - 100% and out of 12 patients claimed a total pain ease.

Other significant developments in the pain management include the mild laser treatment which was proved to create analgesic effects in some clinical practices, including orthodontics<sup>45</sup>, and the transcutaneous electrical nerve stimulation (TENS) system that offers an alternative to lessen post-orthodontic adjustment pain<sup>48</sup>.

### ***3.1.6 Demand for accelerated orthodontic treatment***

Orthodontics is desired for proper masticatory functionality and aesthetics. Over four million patients under age of 18 received orthodontic treatment in North America in 2006, according to the statistics from American Association of Orthodontists, almost doubling the same figure in 1989 [84]. Nonetheless, the surgery to implant the orthodontic appliances often takes hours in the dental chair and it is a laborious and iterative procedure for both the

## CHAPTER 3: VIBRATE TO ENHANCE ORTHODONTICS

orthodontist and the patient and existing designs of orthodontic appliances such as braces and aligners are far from perfect. Therefore, orthodontic practitioners and patients who receive orthodontic treatments are constantly searching for novel or improved methods to treat malocclusion. An orthodontic acceleration technique which features the introduction of mechanically induced vibration, has been of high interest to dental professionals thanks to its exceptional clinical efficacy to reduce the duration of orthodontic treatment which can normally last 13 months to 31 months, subject to the occurrence of extractions, age of patients and the class of malocclusion [30]. The technology involves the device that complementarily works with all existing orthodontic treatments and accelerates bone remodelling and hence orthodontic tooth movement (OTM). However, loading configurations in most orthodontic courses still remain inconclusive and biologic and biomechanical response to orthodontic dynamic force (especially effect of resonance on OTM) is largely unknown<sup>3</sup>.

This chapter aimed to explore whether the concurrent use of single-tooth vibration combined with conventional static orthodontic force application would have an influence on tooth movement. The first part of this investigation involved an *in vivo* human study employing 50 Hz vibration; and the second part involved *in silico* non-linear dynamic simulation exploring the effects of vibration over a wider range of frequencies through an anatomically detailed FE model. The former enabled the efficacy of vibration and safety of the current regime to be examined, while the latter established a basis to further advance the associated biomechanical understanding.

### **3.2 Methods and Materials**

#### ***3.2.1 Clinical Study***

Thirteen patients, aged between 12 and 16 years with the mean being 14 years, were recruited for orthodontic purposes. The selection criteria, described previously [85], include



### CHAPTER 3: VIBRATE TO ENHANCE ORTHODONTICS

(1) no previous dental or orthodontic treatment, (2) no previous trauma, (3) no past or present signs or symptoms of periodontal condition, (4) no past or present signs or symptoms of bruxism, (5) no significant medical history affecting dentition, (6) no anatomical abnormality of craniofacial or dentoalveolar complex, (7) completed apexification and (8) residence in fluoridated regions. The ethics approvals were collected from The University of Sydney and Ondokuz Mayıs University (2010/135 and 11-0016/1119). The orthodontic protocol for force application and measurement of tooth movement rate were described previously (Fig. 3.5a) [86]. The coil springs were attached to the auxiliary tubes of the maxillary first molar and canine brackets with a 6-mm power arm constructed from 0.016" stainless steel (Dentaurum, Ispringen, Germany) to deliver the force close to the centres of resistance (Fig. 3.6b).

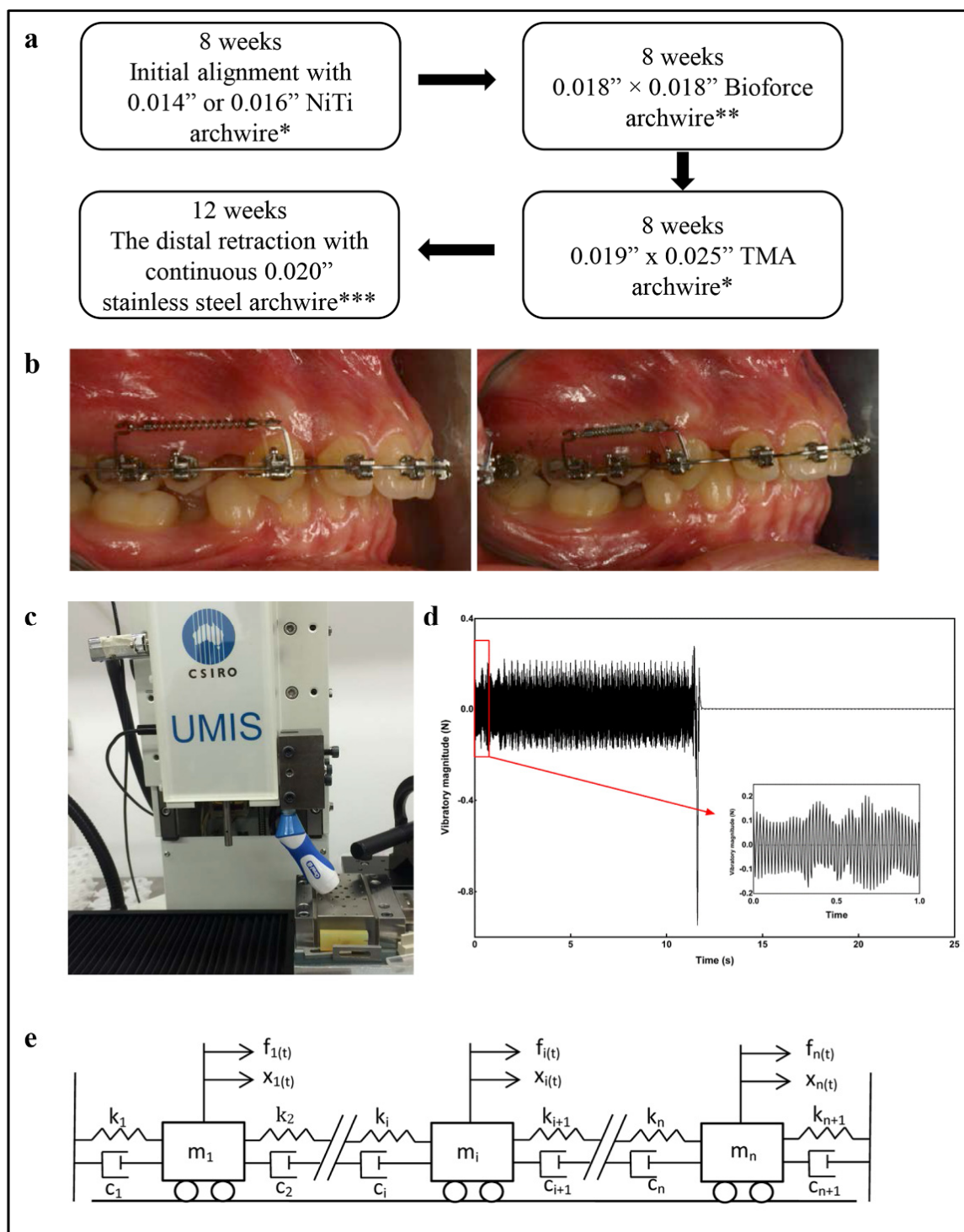


**Fig. 3.5** (a) The stages of orthodontic treatment. \*3M Unitek, Monrovia, California, US, \*\*GAC, Bohemia, NY, US, \*\*\*Dentaurm, Ispringen, Germany. (b) 12-week maxillary canine space closure process. (c) Experimental set-up for vibration measurement. (d) The oscillatory force profile of the vibrator. (e) Free body diagram of spring-mass-damper system.

## CHAPTER 3: VIBRATE TO ENHANCE ORTHODONTICS

Intraoral clinical measurements were made with digital dental callipers (Masel, Bristol, UK), and a baseline maxillary impression (Imprint II, light and heavy, 3M ESPE, St Paul, Minn) was taken before the start of canine retraction (time point T0). The clinical measurements to evaluate total space closure and canine retraction were made every 28 days (T0, T1, T2 and T3) from the beginning of canine retraction, both from the circular spring opening holes on SPEED bracket (Strite Industries Cambridge, Ontario, Canada) clips and from the canine and molar mesio-buccal cusp tips. The total evaluation duration was 12 weeks.

At the end of the evaluation period, another maxillary impression was taken and the specified tooth movements were also assessed from T0 and T4 casts. Stable palatal reference points and the tips of the canines and the first molars were marked with a 0.3 mm lead pencil on both casts [87, 88]. The models were then scanned and measurements were made with CorelDraw X5 (Corel Corporation, Ottawa, Canada). Statistical analysis was performed using SPSS (IBM Corporation, USA). The extent of total space closure and canine distalisation on the vibration and non-vibration sides were compared with Wilcoxon signed rank test.

Each subject was randomly allocated a vibration and sham side, using a split-mouth study design. All the patients were visited each day to ensure full compliance with vibration application. The buccally directed vibration was applied on the canine of vibration side for 10 min/day for 28 days, using an Oral B (USA) Hamming Bird Vibrating Unit and the magnitude of vibratory force was measured to be approximately 0.2 N, equivalently 20 g by using a Kistler (Winterthur, Switzerland) 9256C1 dynamometer (Figs. 3.5c and d). The results were calibrated by the measurement of the loads after the vibration mode was switched off. The measuring time interval was 0.005 s which was shorter than its prescribed maximum period (0.00885 s corresponding to 6800 RPM or 113 Hz of the motor). The vibrating frequency of the terminal tip was measured to be 50 Hz (Fig. 3.5d).

### 3.2.2 Basics of Nonlinear Steady-state Dynamics

The vibration induced force can be considered a steady-state dynamic loading as the frequency and amplitude remain almost unchanged. The dynamic model can be defined as the summation of mass-spring-damper sub-systems and hence consists of multiple degrees of freedom, as represented in a matrix form:

$$\mathbf{M}\{\ddot{x}\} + \mathbf{C}\{\dot{x}\} + \mathbf{K}\{x\} = \{f\} \quad (3.1)$$

where  $\mathbf{M}$ ,  $\mathbf{C}$  and  $\mathbf{K}$  are the mass, damping and stiffness matrices respectively (Fig. 3.5e).  $\{x\}$  and  $\{f\}$  are the displacement and external force vectors, respectively. The vibratory characteristics of a structure can be evaluated by calculating the natural frequencies (NFs) and mode shapes. The responses of a structure subjected to harmonic excitation, an external vibratory force in this instance, can be predicted based on the predetermined eigenvalues and eigenmodes and the solution to the projection of motion equations onto the modes, which gives

$$\ddot{q}_j + c_j \dot{q}_j + \omega_j^2 = \frac{1}{m_j} (f_{1j} + i f_{2j}) e^{i\Omega t} = X_j^N (F_1^N + i F_2^N) \quad (3.2)$$

where  $q_j$  is the amplitude mode  $j$ ,  $c_j$  is Rayleigh damping factor of mode  $j$ ,  $\omega_j$  is the undamped frequency of mode  $j$ ,  $m_j$  is the generalized mass and  $(f_{1j} + i f_{2j}) e^{i\Omega t}$  is the load of mode  $j$  defined by the frequency and can be projected onto the eigenmode  $X_j^N$  as nodal equivalent forces  $F_1^N$  and  $i F_2^N$ .

A Rayleigh damping model was adopted herein to obtain the mode-based damping matrix (Eq. 3.3) and factor (Eq. 3.4), calculated through orthogonality and relations between the modal equations [48, 89].

$$\mathbf{C} = \alpha \mathbf{M} + \beta \mathbf{K} \quad (3.3)$$

$$\zeta_i = \frac{\alpha}{2\omega_i} + \frac{\beta\omega_i}{2} \quad (3.4)$$

where  $\alpha$ ,  $\beta$ ,  $\zeta_i$  and  $\omega_i$  denote mass-proportional, stiffness-proportional Rayleigh coefficients, modal damping factor and undamped circular natural frequency for the  $i$ th mode, respectively. In a previous study, the Rayleigh coefficients were determined to be  $5.684 \times 10^{-3}$  for  $\alpha$  and  $4.537 \times 10^{-3}$  for  $\beta$  through the same model, which were used in this study [89].

### 3.2.3 FE Modelling

An anatomically accurate maxilla model was constructed based on computer tomography (CT) images with resolution of 0.2 mm/pixel. ScanIP 4.3 (Simpleware Ltd., Exeter, UK) was utilized to conduct image segmentation. The post-processing and refinement was performed using Rhinoceros (Robert McNeel & Associates, Seattle, US). The model is comprised of a full set of maxillary teeth, their adjacent PDLs with thicknesses ranging from 0.2 to 0.4 mm [36], sectioned alveolar bone and surrounding cortical bone, as presented in Fig. 3.6. Abaqus/Standard 6.11 was employed for FEA. The model consisted of 893,154 nodes and 525,664 quadratic tetrahedral mesh elements in accordance with a convergence test. All the parts were considered bonded with their neighbouring parts. The brackets, power arm and archwire were modelled based on Dentaurm Discovery brackets (Dentaurm, Ispringen, Germany) (Fig. 3.6e).

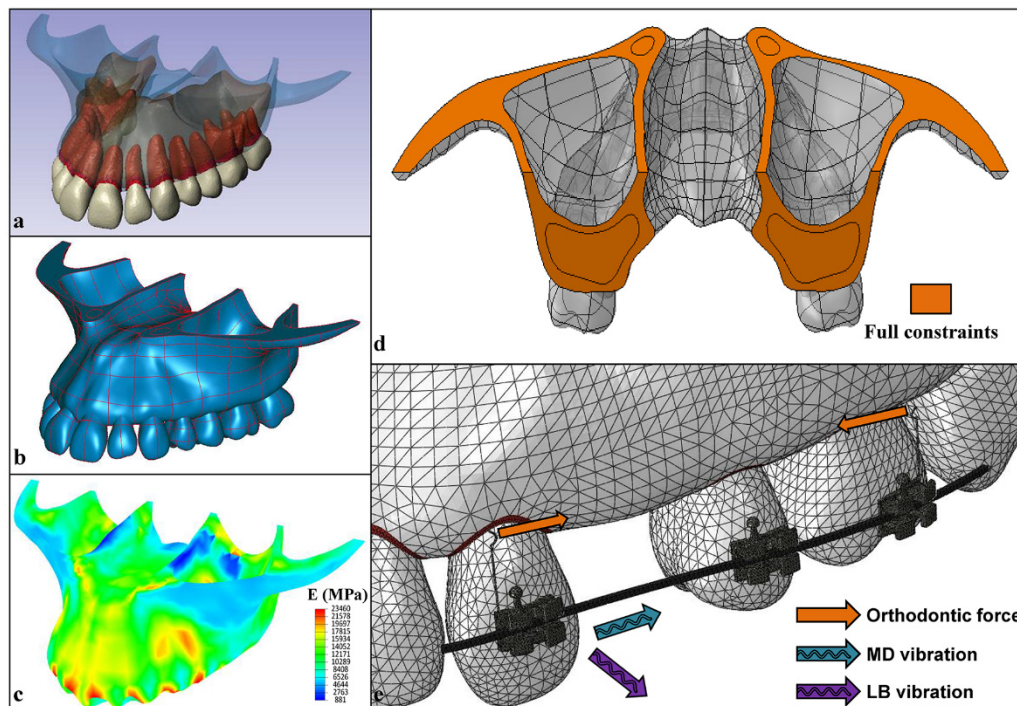


**Fig 3.6** (a) Segmentation of a CT scan using Simpleware ScanIP. (b) Non-uniform rational basis spline (NURBS) in Rhinoceros. (c) Heterogeneous Young's modulus from CT scan grey level values of maxillary bone. (d) Boundary conditions. (e) Loading conditions (for vibration group). Mesio-distal (MD) and linguo-buccal (LB) vibrations were not applied simultaneously.

All the materials involved were modelled as isotropic and elastic (Table 3.1) [90]. It is acknowledged that the PDL is a non-linear material and the incorporation of PDL nonlinearity can visibly alter the FEA results [42, 43, 91]. Therefore, the PDL was modelled as a hyperelastic material, in accordance with a least squares curve fitting on the basis of the stress-strain curve [41, 92]. It has also been suggested that damping effects and heterogeneity of the dental structure can influence its vibratory characteristics [89]. In this case, heterogeneous properties were assigned to the bone as per Hounsfield Unit (HU), based on which the Young's modulus was calculated on an elemental basis (Eq. 3.5) [39].  $\rho_{\min}$  and  $\rho_{\max}$  stand for the minimum and maximum bone densities which were assigned as  $0.69 \text{ g/cm}^3$  and  $1.90 \text{ g/cm}^3$  respectively [39].  $HU_{\max}$  and  $HU_{\min}$  are the maximum and minimum HUs of the scans. The

Young's modulus was determined to range from 884 to 23,460 MPa, which is consistent with the properties found or adopted in other literature [40, 41].

$$\rho_{\text{element}} = \rho_{\text{min}} + \frac{(\rho_{\text{max}} - \rho_{\text{min}})(HU - HU_{\text{min}})}{(HU_{\text{max}} - HU_{\text{min}})} \quad (3.5)$$

**Table 3.1** Material properties

Material	Young's Modulus (MPa)	Poisson's Ratio	Density (kg/m <sup>3</sup> )
Cortical Bone	Heterogeneous	0.33	1990
Alveolar Bone	Heterogeneous	0.33	410
Tooth (Dentin)	20,000	0.20	2140
PDL	Hyperelastic	0.45	1200
Brackets	113,800	0.34	4430
Archwire	200,000	0.3	8000

### 3.2.4 Loading and Boundary Conditions

The loads consisted of both static and dynamic forces, imitating the orthodontic force and vibration respectively (Fig. 3.6e). The orthodontic force was introduced by exerting 150 g forces onto the hooks of 6-mm power arms on the brackets installed on the left maxillary canine and first molar, followed by the application of steady-state dynamic force in the linguo-buccal (LB) and mesio-distal (MD) directions. The frequency of dynamic force ranged from 10 Hz to 2000 Hz, including the 50 Hz that was used in the clinical study. The same computational protocol was applied to the maxillary first and second premolars, central and

lateral incisors. For the control group, a static force, of the same magnitude of vibration, was applied as a supplement to the static orthodontic force.

The volume average hydrostatic stress (VHS), defined by Eqs. 3.6 and 3.7, were evaluated. The quantified results provide an insight into the effects of overall vibratory characteristics of the maxillary periodontal structure and ultimately, its response to cyclical excitation and thus the link to OTM. The hydrostatic stress was recognized as a mechanical indicator to OTM or PDL activity, which correlates with fluid or capillary blood pressure, as also employed by several previous studies [41, 93-95].

$$\sigma_H = \frac{1}{3}(\sigma_{11} + \sigma_{22} + \sigma_{33}) \quad (3.6)$$

$$\bar{\sigma}_H = VHS = \frac{\sum_i^n |\sigma_{H,ele}^i| V_{ele}^i}{\sum_i^n V_{ele}^i} \quad (3.7)$$

where  $\sigma_{11}$ ,  $\sigma_{22}$  and  $\sigma_{33}$  are the principal stresses,  $\sigma_{H,ele}$  and  $V_{ele}$  are the elemental hydrostatic stress and elemental volume and  $\sigma_H$  is the hydrostatic stress respectively.

### 3.3 Results

#### 3.3.1 Clinical study

The extent of teeth total space closure was visibly higher with vibration compared to non-vibration, measured from study models and intra-oral measurements (P=0.022 and P=0.026, respectively; Fig. 3.7 and Table 3.2). Furthermore, the amount of canine distalisation on the vibration side was significantly higher (P=0.009 as measured from the cusp tips). In addition, Pearson's correlation revealed no association between the amount of root resorption (RR), from a previous clinical study, and the amount of canine distalisation [96].



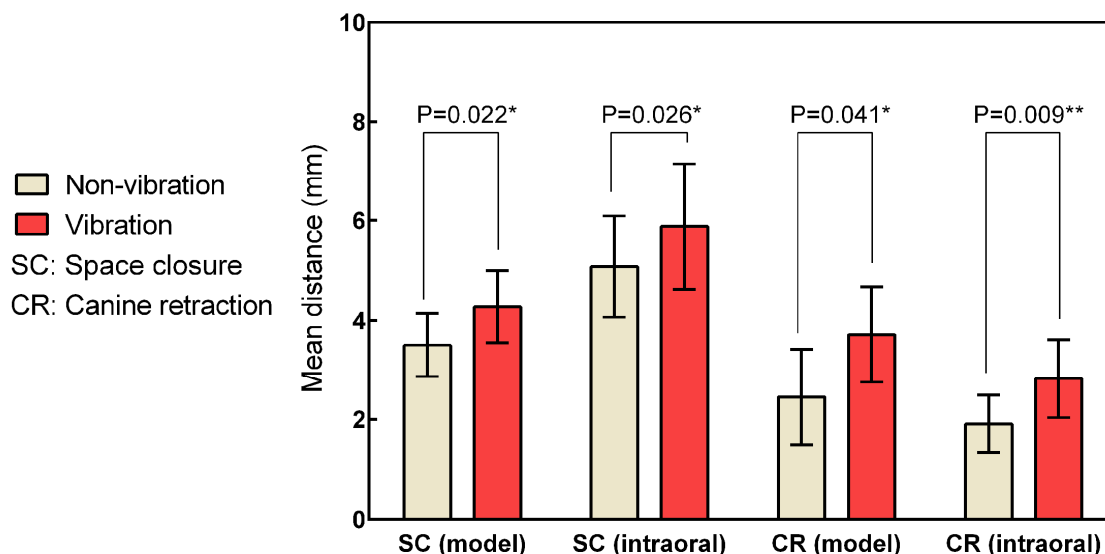


Fig. 3.7 Amounts of teeth movements with standard error.

Table 3.2 Statistical analysis of intra-individual differences between vibration and non-vibration sides

	Vibration			Non-vibration			
	Mean	SE	SD	Mean	SE	SD	
Total space closure (measured via cusp tip on model)	4.270	0.228	0.721	3.500	0.202	0.638	0.022*
Total space closure (measured via cusp tip intra-orally)	5.882	0.367	1.270	5.074	0.293	1.013	0.026*
Canine retraction (measured via bracket on model)	3.710	0.304	0.960	2.450	0.304	0.961	0.041*
Canine retraction (measured via cusp tip intra-orally)	2.820	0.249	0.787	1.910	0.182	0.576	0.009**

(\*P < 0.05, \*\*P < 0.01)

### 3.3.2 Static and mode-based steady-state dynamic FEA

Steady-state vibration in conjunction with existing orthodontic force was computationally proved to amplify the VHS of the PDL regardless of vibration direction and tooth investigated, compared with the control group. The 50 Hz vibration increased the VHS

## CHAPTER 3: VIBRATE TO ENHANCE ORTHODONTICS

of canine PDL by 9.17% and 10.79% for the mesio-distally and linguo-bucally directed vibration, respectively. The influences of the 50 Hz vibration for central incisor, lateral incisor, first premolar and second premolar are also presented schematically (Fig. 3.8a and b). It can be observed that the highest amplification induced by 50 Hz vibration, approximately the same frequency applied in the clinical study, was recorded with lateral incisor vibrated mesio-distally and first premolar vibrated linguo-bucally. Nonetheless, the general enlargements of tissue responses were statistically similar, ranging from 7.28% to 13.53%.

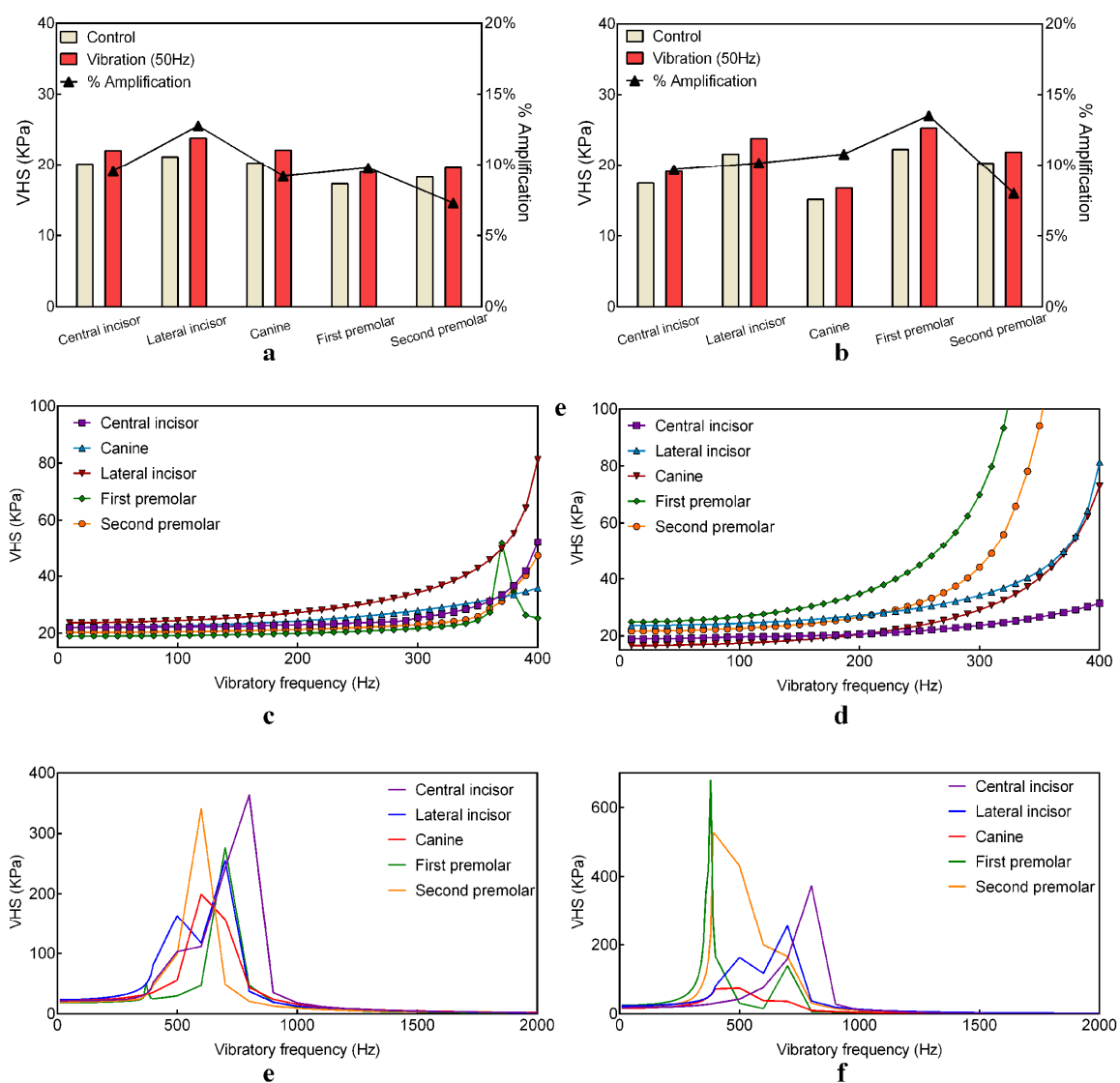


**Fig. 3.8** The vibration-induced amplification of pressure in maxillary teeth's PDL for (a) mesio-distal and (b) linguo-buccal vibration during tooth distalisation. PDL responses versus different vibratory frequencies: (c) low-medium frequencies directed in the mesio-distal direction. (d) low-medium frequencies directed in the lingual-buccal direction. (e) low-high frequencies in the mesio-distal direction. (f) low-high frequencies in the lingual-buccal direction.

The augmentations of PDL response from the vibration also varied in different directions. No significant difference of VHS for central incisor and lateral incisor was observed. First and second premolars and canine, by comparison, saw observable discrepancies when comparing the effects of vibrations in linguo-buccal and mesio-distal directions. Figs. 3.8a and b showed that higher amplifications of the first and second premolars and canine were found for linguo-buccal vibration.

The effects of variation of vibratory frequencies are plotted in Figs. 3.8c-f. Generally comparable trends of tissue response can be seen irrespective of the type of teeth and vibratory direction. The average hydrostatic pressures gradually increased with the exciting frequencies until the medium frequencies (approximately in the range of 200 Hz to 400 Hz) were reached after which the rates of increase climbed exponentially. The responses peaked and exponentially decreased without plateauing with further increase of frequencies up to 2000 Hz. Even higher loading frequencies retarded the decrease and progressively led to a pressure level lower than that of the control group and eventually fully counteracted the existing stress. It can also be recognized that the first premolar and lateral incisor exhibited multiple local resonance frequencies in a short interval while others showed only one response peaks (Figs. 3.8e and f).

### 3.4 Discussion

In the present study, using 50 Hz of vibration for only 10 min/day, it was found in a split mouth model that the amount of space closure and canine distalisation was significantly

higher on the vibration side. A generic vibratory response of the PDL can be schematically illustrated in Fig. 3.9. When the frequency is within the mild zone, there is a gentle amplification of PDL response, e.g. VHS. The response of the PDL at this zone is thought to be benign. As the exciting frequency approaches the first local natural frequency, the response was exponentially aggregated, being categorized as the vigorous zone where a small frequency increase can result in a leap in response level. The diminishing zone follows where the tension-compression nature was transformed and counteracts the existing orthodontic force. However, the vigorous zone is clinically irrelevant due to the unfeasibility of introducing ultra-high frequency up to thousands of Hz.

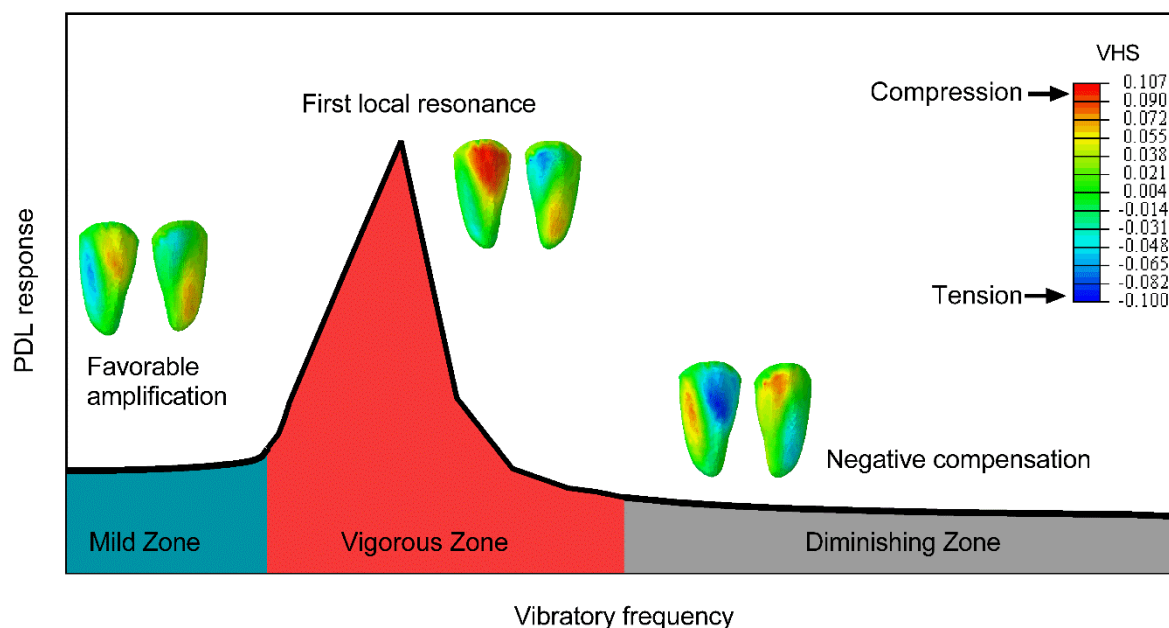


**Fig. 3.9** Schematic illustration of correlation between vibratory frequency and PDL response. The boundaries defining different zones are not definite.

It has been shown that an inordinate magnitude of orthodontic force may lead to several inter-correlated adverse effects, including hyalinisation, orthodontic root resorption (ORR), OTM deceleration and PDL necrosis [97-99]. The amplification of stress level induced by vibration needs to be restricted to an acceptable level without undesirable outcomes. It was

proposed and verified via experiments and FEA that tissue necrosis may occur if the hydrostatic pressure exceeds certain threshold, e.g. systolic pressure of 16 kPa (120 mmHg) [90, 94, 100]. The present *in-silico* study indicates that the frequency applied (50 Hz), either in the mesio-distal or linguo-buccal directions, was significantly lower than the first local resonance frequencies of maxillary teeth calculated to be in the range from 300 Hz to 800 Hz (Figs. 3.8e and f). Therefore, it can be expected that the vibratory frequency currently applied, e.g. through 50 Hz single-tooth vibration in this study, 30 Hz AcceleDent device, is biomechanically safe as it is significantly lower than the first natural frequencies.

An antecedent parallel study has suggested the potential of vibration in preventing or reducing orthodontic RR in human, a major side-effect resulted from excessive orthodontic force [96]. The current on-human study further affirmed the safety, if not the capacity of inhibiting RR, of vibration application with orthodontic treatment, with no correlation between the amount of RR and space closure being identified. This is also agreed by a recent animal study where it was concluded that there is no statistically significant influence of vibratory loads on orthodontic root resorption [101].

The results of the current study have shed additional light on the mechanism of vibration-enhanced OTM. It is suggested that mild amplification of the PDL pressure, while being insufficiently high to cause necrosis of the structures, may actuate the relevant cells and biological mediators such as RANKL, TGF- $\beta$  and OPG and hence enhances the biological events responsible for OTM. The vibration oriented in line with the OTM direction, i.e. MD direction in this case, did not visibly enhance the PDL response, compared with the LB group (Figs. 3.8a and b). In the clinical study, vibration was also applied in a different direction to that of OTM. Both computational and clinical studies indicated that random vibration could facilitate OTM. The mild response zone, under a low-medium frequency vibration, is proposed to be favoured clinically. No extremely excessive pressure, additional to the pressure induced

## CHAPTER 3: VIBRATE TO ENHANCE ORTHODONTICS

by static orthodontic force, is generated within this range where relevant cells and factors may however respond and take effect.

It is also suggested that the mechanism for OTM acceleration may be more biologically based than mechanically based. The dynamic vibration was only introduced 10 min/day in our study. The application of vibration was not lasting and hence the amplification of the PDL response. In other words, the short duration of vibration application, along with its potential to accelerate OTM, implies that vibration stimulates OTM-related cells and factors through this temporarily sustained and dynamic amplification of pressure level within the PDL. It is also speculated that the transformation of forcing nature and the fluctuation of hydrostatic pressure within the PDL may contribute to the activation at a cellular level. Microcirculatory condition transformation, e.g. increase of bloodstream velocity in the PDL possibly introduced by the vibration [33, 102] and hence the activity level of bone remodelling, may be another salient contributor to OTM acceleration.

The results of this study echoed several previous studies, including two animal studies by Darendeliler *et al.* [66] and Nishimura *et al.* [33], in which it was claimed that vibration enhances OTM, and several clinical studies by Kau *et al.* [30], Bowman [71], Leethanakul *et al.* [73] and Pavlin *et al.* [74], in which the AcceleDent vibrator (30 Hz, all-teeth vibration) or electric toothbrush were also found to accelerate OTM. Likewise, several *in vitro* studies have shown that low magnitude high frequency (LMHF) vibration or cyclic tensile loading can promote human PDL stem cells (PDLSCs) or PDL cells (PDLs) proliferation [103, 104] or osteogenic differentiation without detriment to the vitality of the PDL cells [105]. However, conflicting results were obtained from the studies by Woodhouse *et al.* [72] and Miles *et al.* [106] when using AcceleDent devices and Tooth Masseur vibrator respectively, as they found no evidence supporting the beneficial effects of supplemental vibrational force on OTM. This discrepancy may arise from two different reasons. Firstly, all-teeth vibration can be less

## CHAPTER 3: VIBRATE TO ENHANCE ORTHODONTICS

controllable than single-tooth vibration. The vibration received by the target tooth for the former is likely to be of much lower frequency or amplitude due to unfavourable tooth positioning and morphology, which may lead to insufficient contact between tooth and vibrating medium. Secondly, the energy loss during vibration delivery has been largely ignored in most studies. Energy dissipation is a consequence of many mechanical related factors such as damping and friction. As a consequence the amplitude of force and frequency received by the target dental structure can be considerably lower than the motor vibrating frequency which was sometimes labelled as the tooth vibrating frequency. In this study, the rotor frequency was measured to be 113 Hz using an optical tachometer. This was over 50% higher than what was eventually transmitted to the vibrator terminal or maxillary canine (50 Hz). Therefore, it is suggested that single-tooth vibration and accurate measurement of vibrating frequency should be necessitated to investigate the vibratory effects.

One limitation of the present study was the potential non-compliance of participants in terms of duration of usage despite the daily check-up by the examiners. In addition, when applying the vibration directly onto the tooth, it was possible to introduce extra force magnitude by hand and biting and hence the vibratory force magnitude could be higher than 20 g. The current FE model also generalizes the dental structure of a large population, which may not include the discrepancies of material properties and morphologies. Future clinical study are suggested to vibrate the tooth of relevance at higher frequency within the mild zone for reasonably higher PDL response with larger sample size if possible.

## CHAPTER 4

### OPTIMISE ORTHODONTIC FORCE

This chapter aimed to precisely locate centres of resistance (CRe) of maxillary teeth and investigate optimal orthodontic force by identifying the effective zones of orthodontic tooth movement (OTM) from hydrostatic stress thresholds in the periodontal ligament (PDL).

We applied distally-directed tipping and bodily forces ranging from 0.075 N to 3 N (7.5 g to 300 g) onto human maxillary teeth. The hydrostatic stress was quantified from nonlinear finite element analysis (FEA) and compared with normal capillary and systolic blood pressure for driving the tissue remodelling. Two biomechanical stimuli featuring localised and volume-averaged hydrostatic stresses were introduced to describe OTM. Locations of CRe were determined through iterative FEA simulation.

Accurate locations of CRes of teeth and ranges of optimal orthodontic forces were obtained. By comparing with clinical results in literature, the volume average of hydrostatic stress in PDL was proved to describe the process of OTM more indicatively. The optimal orthodontic forces obtained from the *in-silico* modelling study echoed with the clinical results *in vivo*. A universal moment to force (M/F) ratio is not recommended due to the variation in patients and loading points. Accurate computational determination of CRe location can be applied in practice to facilitate orthodontic treatment. Global measurement of hydrostatic pressure in the PDL better characterised OTM, implying that OTM occurs only when the majority of PDL volume is critically stressed. The FEA results provide new insights into relevant orthodontic biomechanics and help establish optimal orthodontic force for a specific patient.



## 4.1 Introduction

Orthodontic tooth movement (OTM) has been widely thought to occur due to compression and tension within the surrounding tissues generated by orthodontic appliances, which was traditionally documented as the classic “pressure-tension” theory (Fig. 3.1a) [59]. In this physiological process, the periodontal ligament (PDL) plays a crucial role in regulating OTM as the microvasculature and blood flow contained within the PDL may be partially or completely occluded due to its exposure to certain level of pressure, hence adjusting the periodontal interstitial fluid [107, 108]. This can cause the dysfunction or necrosis of PDL tissue, followed by a cascade of events directing OTM via recruitment of osteoclasts and osteoblasts and release of RANKL, TGF- $\beta$  and OPG (Fig. 4.1) [56, 58]. There have been a number of clinical studies addressing the challenges of obtaining the “ideal” orthodontic forces for OTM [109, 110]. However, no general consensus has been available to date, particularly with the associated fundamental biomechanics.

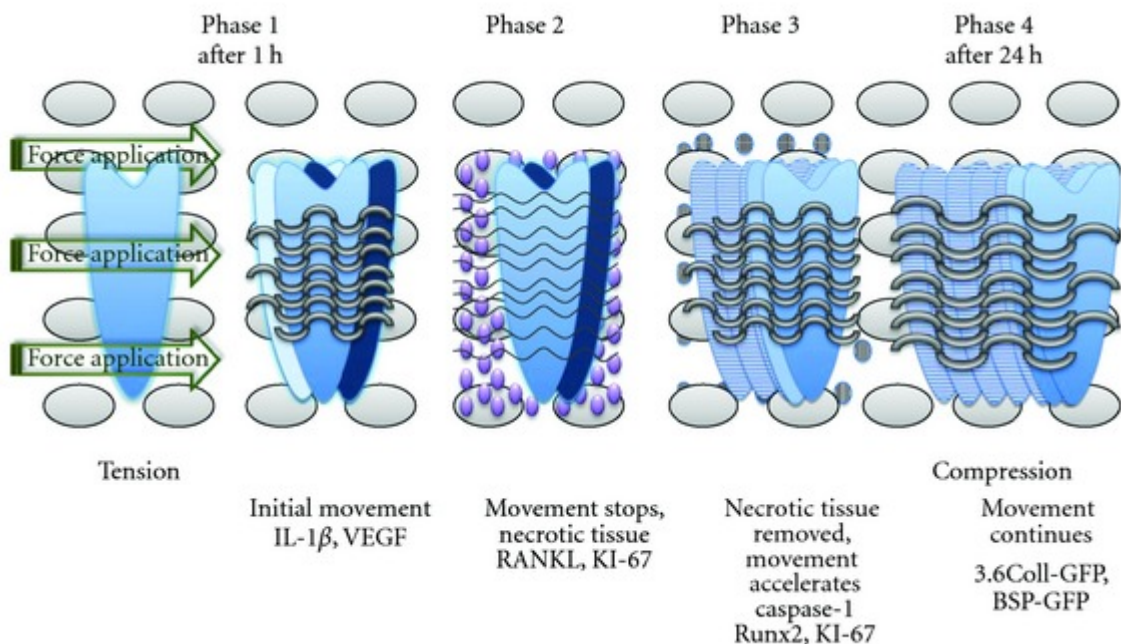


**Fig. 4.1** Schematic illustration of OTM phases [111].

## CHAPTER 4: OPTIMISE ORTHODONTIC FORCE

It has been proposed on the basis of several clinical experiments and biomechanical studies that external pressure comparable to capillary blood pressure of 4.7 kPa (35 mm Hg) can be a stimulus to initiate OTM and root resorption [93, 94, 112, 113], while other studies adopted a higher pressure of 16 kPa (120 mmHg), namely the human systolic pressure, as an indicator for predicting PDL tissue necrosis and hyalinisation [100, 114]. It has also been hypothesised that hydrostatic stress higher than the capillary blood pressure may start to induce PDL occlusion and dysfunction to some degree [37, 94, 113]. Nevertheless, the capillary blood vessels may not collapse completely under this pressure. When the pressure rises to the systolic pressure, it exceeds the physiological upper limit and can lead to complete occlusion [93, 114, 115]. When the pressure rises to a certain level, the rate of OTM can possibly be plateaued or even decreased [100, 110, 114].

However, there has been no exact quantitative linkage and correlation between the turning point of OTM deceleration and the stress or pressure state in the PDL. It is therefore imperative to introduce such a quantitative reference for orthodontic therapies. The abovementioned thresholds, i.e. 4.7 kPa (capillary blood pressure) and 16 kPa (human systolic pressure) were adopted herein as the hypothesised simulative quantities that act as the lower and upper thresholds for suggesting an optimal level of orthodontic force.

The incorporation of 3D finite element (FE) method enables to quantify important biomechanical data for more accurate analysis of dental structure and manipulation of OTM that may be hardly achieved from clinical studies [29, 37, 107, 108, 116-118]. For example, precise localisation of the centre of resistance (CRe) and the centre of rotation (CRot) for a required tooth movement may not be easy due to considerable variation in individual tooth and bony anatomy. A CRe is an important reference point through which a force is applied so that the tooth moves without rotation (i.e. pure translation). A CRot is the point with respect to which the rotation occurs. Simulation and clinical conduct of a pure translation of tooth

## CHAPTER 4: OPTIMISE ORTHODONTIC FORCE

without tipping remain a demanding task in orthodontics and largely rely on clinical experience or the estimation of CRe by approximating 40% from the alveolar crest to the length of tooth root [119, 120]. For this reason, several computational modelling methodologies have been introduced to estimate the locations of CRe and CRot, thereby helping achieve desirable OTM in an effective way [119-121].

Although it has been educated and reported that the estimation of CRe and hence moment to force (M/F) ratio should be based on tooth movement type and morphological variation of teeth [114, 122], very few systematic and widely-used method of accurate CRe estimation was provided. To date, no general agreement in terms of accurate or universal CRe for each tooth has been made owing to the variation of the teeth morphology from patient to patient. As a result, it is challenging to provide a universal or general range of optimal orthodontic forces determined by considering detailed biomechanical responses in the PDL and alveolar region. Therefore, from biomechanical perspective, precise localisation of CRe in a patient-specific manner is considered critical to estimating the optimal orthodontic forces.

This chapter aims to construct an anatomically accurate 3D human maxilla model based on clinical CT images and computationally investigate the optimum orthodontic forces in mesio-distal tipping and translational directions on maxillary teeth, via introducing an active spectrum of orthodontic force in relation to the mechanical stimulus namely hydrostatic stresses for OTM.

### **4.2 Methods and Materials**

#### ***4.2.1 Finite element modelling***

An anatomically accurate maxilla model was constructed based on CT images of an average subject with a resolution of approximately 0.2 mm/pixel. ScanIP 4.3 (Simpleware Ltd.,

## CHAPTER 4: OPTIMISE ORTHODONTIC FORCE

Exeter, UK) was utilised to process the CT images. The CT images were segmented by defining thresholds for different tissues in terms of the greyscale values, and then refined and contrasted by applying filters. The resultant maxilla model comprised a full set of maxillary teeth, adjacent PDLs with thicknesses ranging from 0.2 mm to 0.4 mm [36], sectioned alveolar bone and surrounding cortical bone, as displayed in Fig. 4.2a. Two unerupted wisdom teeth of the subject were not included in this model for simplicity [123].

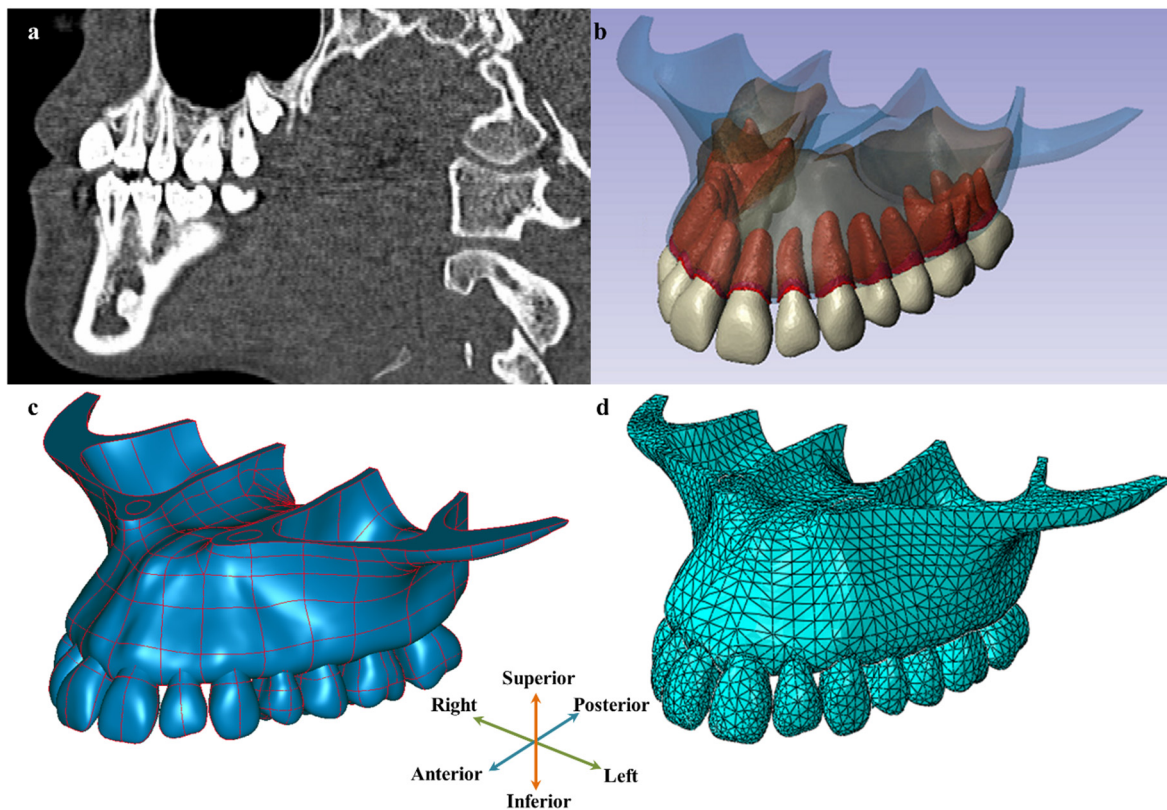


**Fig. 4.2** CT based maxillary modelling: (a) DICOM images processed and segmented in ScanIP; (b) Masks generated for each dental material in ScanIP; (c) NURBS surfaces created in Rhinoceros; (d) Full meshed FE model in Abaqus.

The surface models were imported into Rhinoceros (Robert McNeel & Associates, Seattle, US) for further processing. The patch boundary structures were generated from contour and boundary lines, based on which the ordered grids were created within every patch on the object, leading to the creation of non-uniform rational basis spline (NURBS) surfaces

(Fig. 4.2c). The processed surfaces were exported as IGES files for FE modelling. Abaqus 6.11 was employed for finite element analysis (FEA). The full model consists of 982,158 nodes and 541,729 10-node quadratic tetrahedral (C3D10) elements (Fig. 4.2d) in accordance with a mesh convergence test similarly to those reported in literature [124]. The meshes of the PDLs, which were the regions of interests, were locally refined for the purpose of better accuracy.

### ***4.2.2 Loading and boundary conditions***

In this study, translational and uncontrolled tipping tooth movements in mesio-distal direction were simulated. For the former, the tipping force was directly applied onto the bracket on the maxillary teeth. For the latter, a moment with a specific moment to force (M/F) ratio was applied in couple with the tipping force aiming to generate pure translation. In order to apply the theoretically correct translational orthodontic force, the location of CRe should be determined first. This was achieved, with an assumption that the maxillary teeth involved are morphologically symmetric in the mesio-distal context, by applying an uncontrolled tipping force and iterating moments to counteract the moment generated by the tipping force until the tooth recorded a zero angle of rotation. The increment of iteration of 0.5Nmm was found effective herein.

Orthodontic force ranging from 0.075 N to 3 N (7.5 g to 300 g) was first applied for tipping. The same set of tipping force and a coupled moment with M/F ratio specified was also applied to generate bodily movement of the canine (Fig. 4.3b). For simplicity, the influences of friction and slipping in the arch wire were not considered [113, 117].

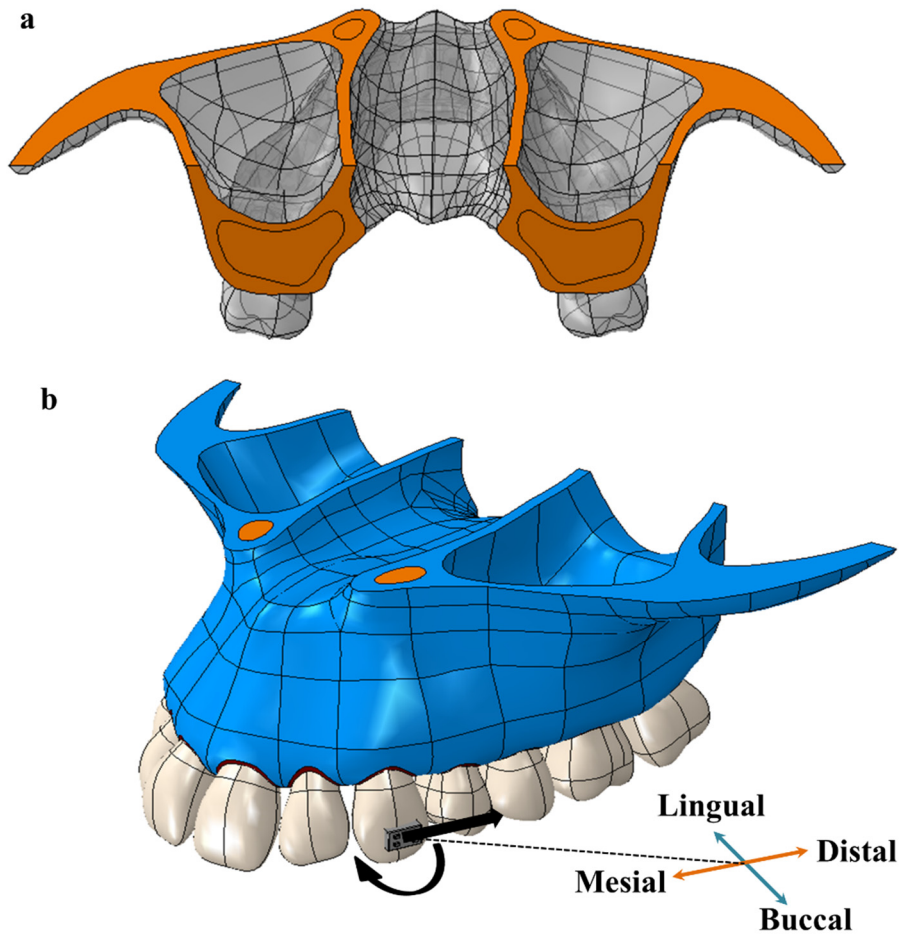


**Fig. 4.3** (a) Boundary condition (full constraints on bone sections); (b) loading condition (for translation) consisting a distally directed orthodontic force and a moment to counteract rotation.

It was assumed that the far-field surfaces of bone sections were fully fixed as the kinematic boundary condition (Fig. 4.3a). Local ( $\sigma_H$ ) and volume-averaged hydrostatic stresses (VAHS) within the PDL are evaluated in the FEA framework, as follows,

$$\sigma_H = \frac{\sigma_1 + \sigma_2 + \sigma_3}{3} = \frac{\sigma_{xx} + \sigma_{yy} + \sigma_{zz}}{3}$$

$$VAHS = \frac{\sum_i^n |\sigma_{H,ele}^i| V_{ele}^i}{\sum_i^n V_{ele}^i}$$

where  $\sigma_1$ ,  $\sigma_2$  and  $\sigma_3$  are the principal stresses;  $\sigma_{xx}$ ,  $\sigma_{yy}$  and  $\sigma_{zz}$  are the normal stresses in the Cartesian coordinate system,  $\sigma_{H,ele}$  and  $V_{ele}$  are elemental hydrostatic stress and elemental

volume respectively. The hydrostatic stress, the negative of pressure in mechanics context, was adopted as the mechanical indicator to OTM or PDL activity that is equivalent to and correlates with fluid or capillary blood pressure, as also employed by several previous studies [93-95, 113, 125].

#### **4.2.3 Material Properties**

All the materials except the PDL were assumed to be isotropic and linearly elastic in this study [37], as summarised in Table 4.1 [45-47, 92, 113]. The PDL has been acknowledged in a series of studies as a non-linear material and the incorporation of nonlinearity of the PDL can significantly alter the FEA results [42, 43]. In this study, a hyperelastic material model was adopted, which defined the strain energy stored in a unit volume as a function of the strain at a point of the material to correlate with the experiment based stress-strain curves [45, 92, 121]. While the rapid characterisation of soft tissue PDL properties has become clinically possible [126, 127], this strain energy driven behaviour was derived via a least-square fitting of the strain-stress curve in the study by Cattaneo et al. [92], which defined the non-linear behaviour under both tension and compression. The fitting was performed within Abaqus material evaluator, and a 3<sup>rd</sup> order Ogden equation was found to provide the closest match to the experimental data [113, 128].

**Table 4.1** Material properties

Material	Young's Modulus (MPa)	Poisson's Ratio
Cortical Bone	14,700	0.31
Alveolar Bone	490	0.3
Tooth (Dentin)	18,600	0.31

PDL	Hyperelastic	0.45
Bracket	210,000	0.3

---

### 4.3 Results

The FE study revealed that an M/F ratio of approximately 9.7, 10.2 and 8.8 can generate the translational movements of lateral incisor, canine and first premolar, respectively, with no tipping for the current subject, where the angle of rotation reached zero. The CRe was then calculated to be located approximately 13.0 mm, 14.9 mm and 11.0 mm apical to the crown for lateral incisor, canine and first premolar, respectively (Table 4.2).

**Table 4.2** M/F ratios and CRe location

	<b>M/F ratio</b>	<b>CRe location (measured apical from crown) (mm)</b>	<b>Distance between CRe and Crest /Length of root</b>
<b>Lateral incisor</b>	9.7	13.0	47.3%
<b>Canine</b>	10.2	14.9	43.6%
<b>First premolar</b>	8.8	11.0	5.4%

Stress distribution of maxillary canine was exemplified. The simulation of translational movement of the canine was successfully achieved with the proper hydrostatic stress distribution, i.e. compression on the distal surface and tension on the mesial surface without rotation (Figs. 4.4 and 4.5). It was found that a light bodily force of 0.1 N (10 g), equivalent to a 0.1 N (10 g) tipping force and a moment with M/F ratio 10.2, did not render the hydrostatic stress in the canine PDL higher than 4.7 kPa (Fig. 4.4a), the foregoing hypothesised lower threshold triggering OTM. Upon applying an increased bodily force of 0.3 N (30 g), an area



## CHAPTER 4: OPTIMISE ORTHODONTIC FORCE

of resultant hydrostatic stress over 4.7 kPa was observed on both the compression and tension sides of the cervical region of distal and mesial surfaces of the canine PDL (Fig. 4.4b). Such a hydrostatic stress induced OTM-activated area grew considerably upon further raising the orthodontic force to 0.75 N (75 g), virtually covering most of the compression and tension sites of the PDL (Fig. 4.4d). When a translational force increased to 1 N (100 g), a small region showing excessive stress (i.e. over the systolic pressure of 16 kPa) developed (Fig. 4.4e) and became significantly more visible as the force further increased to 1.5 N (150 g) (Fig. 4.4f). As expected, heavier forces ranging from 2 N to 3 N (200 g to 300 g) led to larger areas of excessive hydrostatic stress. As a result, the maximum hydrostatic stress within the PDL induced by a light tipping force of 0.3 N (30 g) and a moment with M/F ratio of 10.2 reached the lower OTM threshold 4.7 kPa (i.e. capillary pressure), while that produced by the force system of 1 N (100 g) reached the upper OTM threshold 16 kPa (i.e. systolic pressure) in some regions.

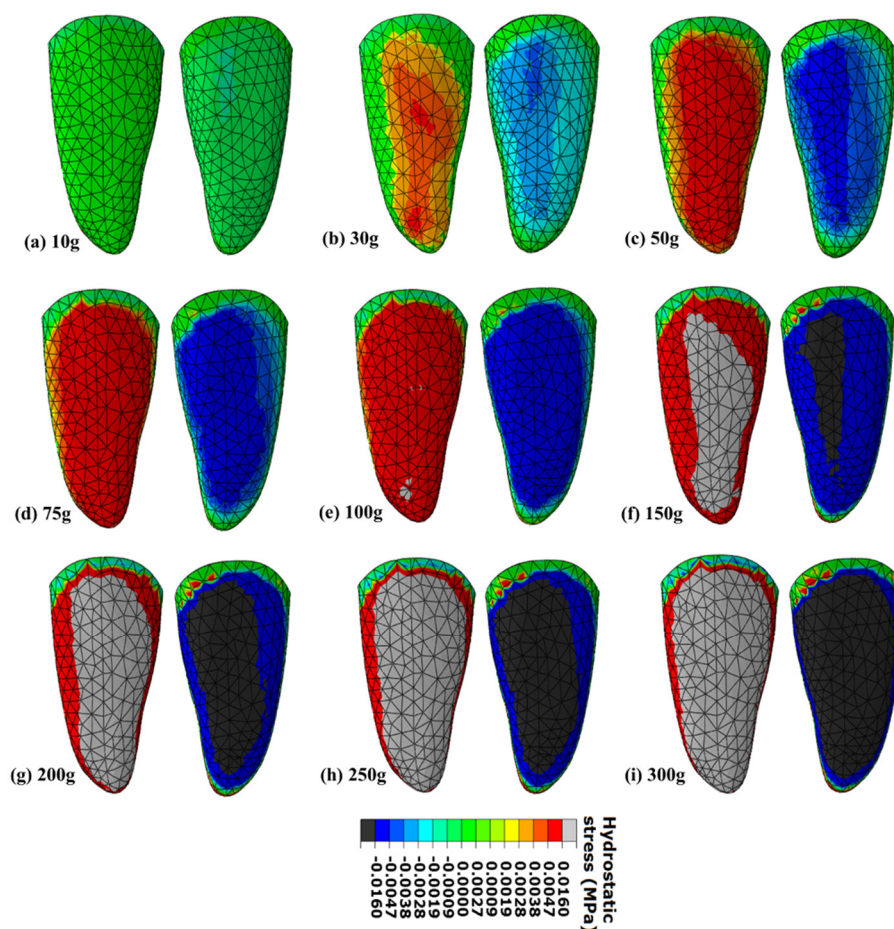


**Fig. 4.4** Selected hydrostatic stress distribution of canine PDL during translation under forces of (a) 0.1 N (10 g), (b) 0.3 N (30 g), (c) 0.5 N (50 g), (d) 0.75 N (75 g), (e) 1 N (100 g), (f) 1.5 N (150 g), (g) 2 N (200 g), (h) 2.5 N (250 g) and (i) 3 N (300 g); The left is the distal surface (compression site) and the right is the mesial surface (tension site). Deep red and blue areas indicate compressive and tensile hydrostatic stresses over capillary pressure of 4.7 kPa while grey and black areas indicate compressive and tensile hydrostatic stresses over systolic pressure of 16 kPa.

The uncontrolled tipping movement, on the other hand, generated both compression and tension on distal and mesial surfaces due to the tipping rotation of the canine (Fig. 4.5). When a light tipping force of 0.1 N (10 g) was applied, no region had the hydrostatic stress higher than 4.7 kPa until a tipping force of 0.14 N (14 g) was applied, which induced a stress higher than 4.7 kPa at both cervical and root apical areas (Figs. 4.5a and b). A further increase of force magnitude to 0.5 N (50 g) induced small areas of excessive pressure (higher than

systemic pressure of 16 kPa) at the cervical region of the PDL (Fig. 4.5c). These areas were further enlarged with tipping forces increased to 3 N (300 g) as seen in Figs. 4e-i.

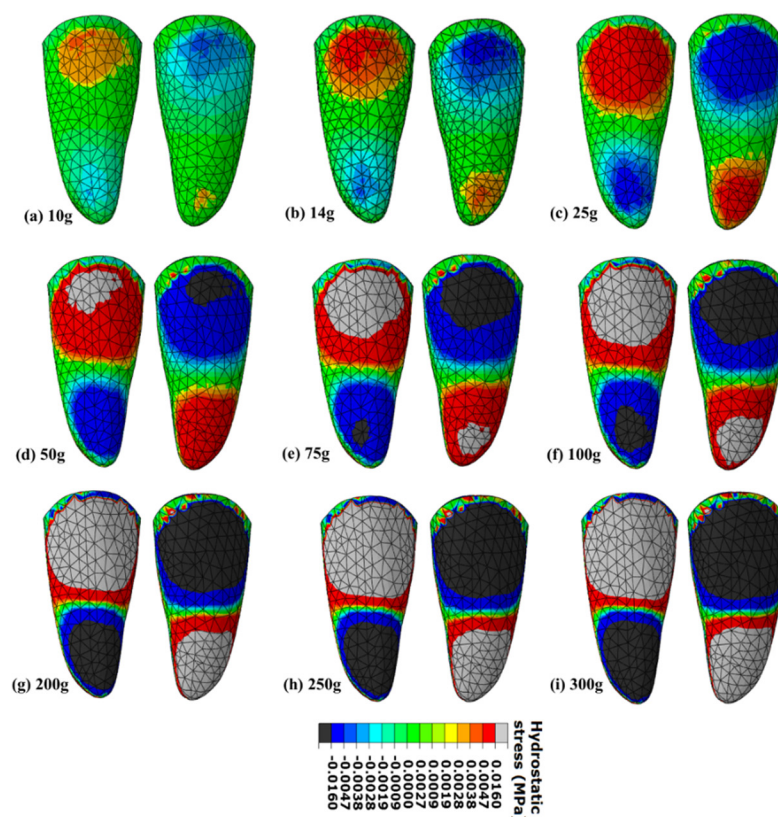


**Fig. 4.5** Selected hydrostatic stress distribution of canine PDL during tipping under forces of (a) 0.1 N (10 g), (b) 0.14 N (14 g), (c) 0.25 N (25 g), (d) 0.5 N (50 g), (e) 0.75 N (75g), (f) 1 N (100 g), (g) 2 N (200 g), (h) 2.5 N (250 g) and (i) 3 N (300 g); The left is the distal surface and the right is the mesial surface. Deep red and blue areas indicate compressive and tensile hydrostatic stresses over 4.7 kPa (capillary pressure) while grey and black areas indicate compressive and tensile hydrostatic stresses over 16 kPa (systolic pressure).

Similar trends can be observed with the lateral incisor and first premolar. For the translational movement of maxillary lateral incisor, the “OTM-effective” hydrostatic stress (i.e. over 4.7 kPa) on the PDL was initiated under a bodily force of 0.25 N (25 g) and it occupied the majority of the distal and mesial surfaces when a bodily force reached 0.5 N (50 g). The “OTM-lagging” hydrostatic stress (stress over 16 kPa) initially appeared under a bodily force of 0.8 N (80 g) and the excessively stressed area occupied the majority of both surfaces

when a bodily force was over 1.5 N (150 g). For the tipping movement, a fairly light uncontrolled tipping force of 0.075 N (7.5 g) could introduce a small area in the PDL where the hydrostatic stress was over 4.7 kPa, forming an “OTM-activated” region; whereas when the tipping force was increased to 0.25 N (25 g), the PDL commenced developing a small area with excessive stress over 16 kPa.

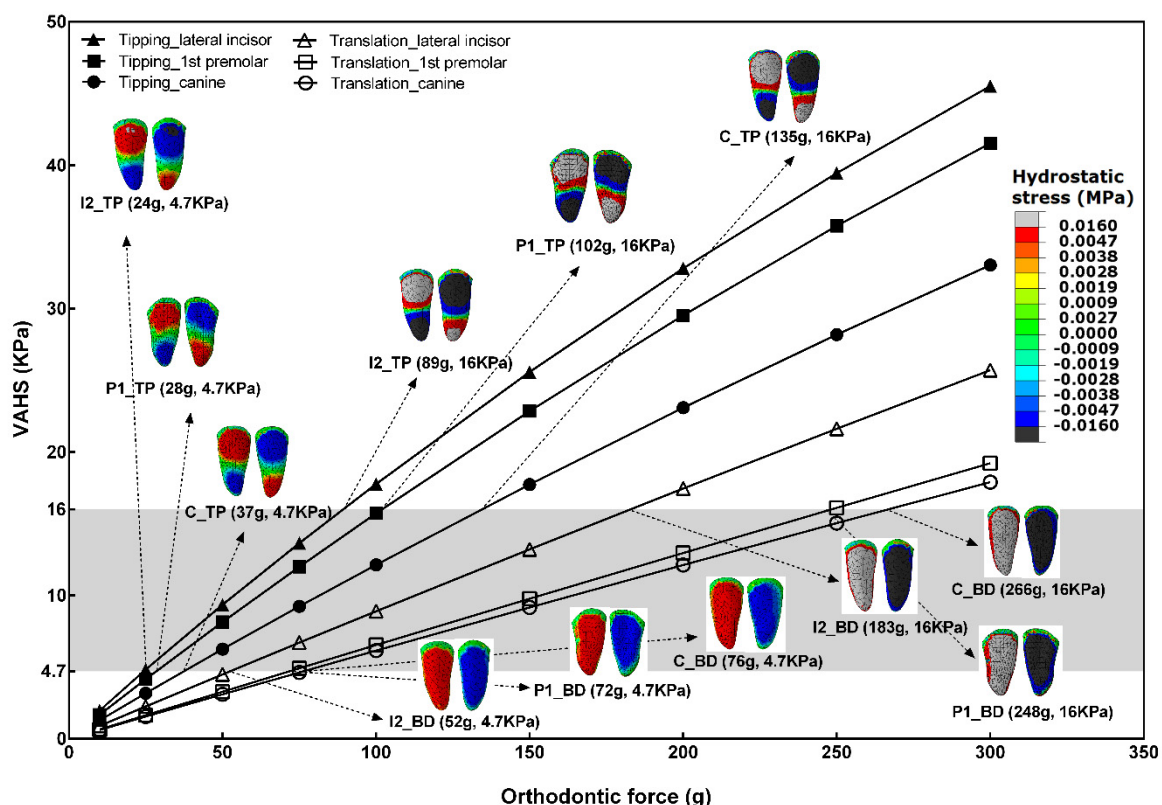


**Fig. 4.6** VAHS vs. orthodontic forces with stress distributions resulted from the threshold forces; P, I, C represent maxillary 1<sup>st</sup> premolar, lateral incisor and canine respectively; TP and BD represent tipping and bodily movements respectively; Grey region represents optimal zone.

The first premolar had 0.3 N (30 g) and 1 N (100 g) as the translational forces that initiated the OTM-activated region and OTM-decelerating region, respectively. For the tipping movement of the first premolar, 0.09 N (9 g) and 0.25 N (25 g) were found to be the threshold launching the abovementioned OTM-activated and -decelerating region respectively, as summarised in Table 4.3.

## CHAPTER 4: OPTIMISE ORTHODONTIC FORCE

The VAHS of the PDLs in the maxillary lateral incisor, canine and first premolar versus a range of orthodontic forces for tipping and translational movements is plotted in Fig. 4.6. As the orthodontic forces increased, VAHS increased in a nearly linear relationship for both tooth movement types (translation and tipping). A stronger overall PDL response was observed for the tipping movement compared with the bodily movement in all these three teeth. All correlation curves can be well fitted by quadratic equations with R-squared values ranging from 0.9996 to 1 for both the tipping movement and translation. The orthodontic forces actuating the lower (4.7 kPa) and upper (16 kPa) volume-averaged hydrostatic stress thresholds were accordingly summarised in Table 4.3. The corresponding stress distributions induced by these critical orthodontic forces were displayed in Fig. 4.6.

**Table 4.3** Optimal orthodontic forces for maxillary teeth estimated by local and volume-averaged stresses (4.7kPa and 16kPa as lower and upper thresholds)

	Optimal forces defined by local hydrostatic pressure		Optimal forces defined by VAHS	
	Translation	Tipping	Translation	Tipping
<b>Lateral incisor</b>	0.25 - 0.8N (25 - 80g)	0.075 - 0.25N (7.5- 25g)	0.52 - 1.83N (52 - 183g)	0.24 - 0.89N (24 - 89g)
<b>Canine</b>	0.35-1N (35 - 100g)	0.14 - 0.5N (14-50g)	0.76 - 2.66N (76 - 266g)	0.37 - 1.35N (37 - 135g)
<b>First premolar</b>	0.3 - 1N (30 - 100g)	0.09 - 0.25N (9 - 25g)	0.72 - 2.48N (72 - 248g)	0.28 - 1.02N (28 - 102g)

### 4.4 Discussion

The objective of an orthodontic treatment is to shift maloccluded teeth a predetermined distance in a prescribed direction. Clinically, the success of such therapy heavily hinges on the localisation of the CRe of each tooth and the accuracy of M/F ratios. It has been

## CHAPTER 4: OPTIMISE ORTHODONTIC FORCE

mathematically calculated and reported by a number of researchers that CRe is located at 24% to 52% of the distance from the alveolar crest to the root apex [129-132]. However, this indeed presents a large range and the determination of additional moments to minimise tipping movements from bodily translation remains inaccurate. It is noted that most of the existing methods considerably simplified the morphology of dental structure. A sophisticated mathematical deduction of CRe localisation however makes it difficult for orthodontists to follow clinically. As an alternative in practice, clinicians tend to employ M/F ratios for a specific type of tooth movement based on clinical experience, without completely comprehending the precise location of CRe of a tooth, based on which the M/F ratio should be calculated. As a result of underestimation of the variation from patient to patient contributing to the inaccurate determination of CRe location and M/F ratios, repeated visits to orthodontists for adjustment of orthodontic forcing system have to be necessitated. The consequences can be inefficient remedy for malocclusion and longer treatment duration, thereby compromising the effectiveness of orthodontic therapy.

This study demonstrated a patient-specific case where the accurate location of CRe and M/F ratios can be computationally determined without compromising the morphological sophistication of real dental structure. As summarised in Table 4.2, the locations of CRe and M/F ratios varied among maxillary teeth. However, as the force magnitude varied, the M/F ratio and hence location of CRe did not change for a specific tooth and movement type, despite the nonlinearity of the PDL. This was consistent with the results of the computational study conducted by Nyashin, Nyashin [133] in which no change of CRe location was found unless varying force directions. The consideration of patient's specification can significantly enhance the efficiency and effectiveness of an orthodontic treatment by accurately perceiving the M/F ratios based on the pre-determined CRe location. The location of CRe calculated in this study was consistent with the work presented by Cattaneo, Dalstra [134] who also found CRe lower

## CHAPTER 4: OPTIMISE ORTHODONTIC FORCE

than the recommended values. Although only one sample was analysed herein and the results cannot be applied to all the population, it can be advocated that accurate patient-specific estimation of CRe should be necessitated in orthodontics practice, with computation-based methodology being one option.

For the translation, as revealed by the FEA results, a force of 0.35 N (35 g) with M/F ratio of 9.7, a force of 0.25 N (25 g) with M/F ratio of 10.2 and a force of 0.3 N (30 g) with M/F ratio of 8.8 started to locally initiate OTM activities in the maxillary lateral incisor, canine and first premolar, respectively. This was a result of local hydrostatic pressure higher than 4.7 kPa, the level of capillary blood pressure in the PDL, and hence induced the partial occlusion of the PDL, launching a certain extent of OTM [93, 113]. On the other hand, force levels of 1 N (100 g), 0.8 N (80 g) and 1 N (100 g) with corresponding moments resulted in hydrostatic stress of a localised small region higher than the systolic pressure (16 kPa), which can render the PDL vasculatures of lateral incisor, canine and first premolar respectively to completely collapse locally [93, 114]. It may therefore initiate PDL necrosis and hyalinisation which has been regarded as a condition to decelerate OTM [135, 136].

In comparison, for the tipping movement, a lower level of orthodontic forces were recorded to commence (0.075 N (7.5 g), 0.14 N (14 g) and 0.09 N (9 g) for lateral incisor, canine and first premolar respectively) and impede (0.25 N (25 g), 0.5 N (50 g) and 0.25 N (25 g) for lateral incisor, canine and first premolar respectively) OTM. This can be explained by the fact that a tipping force exerts an additional unbalanced moment with respect to CRe compared with its translational counterpart. This significant difference therefore necessitates accurate patient-specific measurement of CRe in clinic. Based on anatomically accurate and structurally integral model, the present methodology enables a clinician to precisely locate the CRe.

## CHAPTER 4: OPTIMISE ORTHODONTIC FORCE

In this study, we presented two biomechanical indicators to quantify the effects of the magnitudes and orientations of the applied orthodontic forces on the PDL responses. The first adopted the localised hydrostatic stress (Figs. 4.3 and 4.4), and the second used the overall VAHS in the PDL (Fig. 4.6). It should be noted that the stress distribution is rather non-uniform in the region of interest, while the tooth movement follows almost a rigid body motion, thus imposing challenge in using the local hydrostatic stress to drive OTM. To address this issue and eliminate localised stress concentration induced from anatomical and mesh irregularities, the current study adopted the VAHS, which acts as a more sensible indicator to measuring the overall compression and tension on the PDLs. As per VAHS, a wider range of and overall higher orthodontic forces were evaluated to be associated with the lower and upper stress thresholds of triggering OTM. It is demonstrably more reasonable to use the VAHS, rather than local hydrostatic pressure  $\sigma_H$ , to describe and possibly predict the outcomes of orthodontic treatments. This agrees with the results obtained by Sarrafpour, Swain [123] who suggested that the extent of overall disturbance to blood supply can be manifested in the volume-averaged hydrostatic stress.

A number of studies have been conducted to determine the optimal orthodontic forces, which are in good agreement with the current study. An experiment conducted by Lee [137] concluded that the optimum force level for human maxillary canine distalisation is between 1.5 N and 2.6 N (150 g and 260 g). Similar results were obtained by Storey and Smith [110] who found that 1.5 N to 2 N (150 g to 200 g) is the optimal force range for bodily movement of human mandible canine. Likewise, Iwasaki, Haack [138], from their clinical study, found that when retracted at a higher stress of 13 kPa, distal human maxillary canine movement averaged at a higher rate than that was under 4 kPa. In addition, a non-linear regression analysis by Ren, Maltha [139] based on nine studies on human canines showed that a statistically established orthodontic force-OTM rate curve peaks at approximately 2.72 N (272



## CHAPTER 4: OPTIMISE ORTHODONTIC FORCE

g), following which OTM rate decreases. However, the study quantitatively investigating optimal force range for the lateral incisor is scarce. These findings are consistent with the results of the present study as most of optimum ranges fall within the optimal range obtained herein, e.g. 0.76 N to 2.66 N (76 g to 266 g) for canine bodily movement. The current FE procedure is therefore validated by comparing with the literature reporting optimal orthodontic translational force and can provide important references and approaches for future clinical applications.

On the other hand, some literature suggested conflicting results with the present study [140-142]. Lee [140] found that the maximum OTM rates were obtained for tipping movement with orthodontic force averaging between 3.37 N and 3.88 N (337 g and 388 g) while similar range (3.54 N to 3.75 N (354 g to 375 g)) was obtained for the maximum OTM rates under translational force. Andreasen and Zwanziger [142] reported a higher range of optimal orthodontic forces (up to 5 N (500 g)) for tipping movements of maxillary teeth. These studies used controlled tipping forces, whose experimental conditions differed from the current protocol where ideal translation and uncontrolled tipping can be accurately simulated. It should also be pointed out that the results of tipping movement highly depend on the location of force application with the correct M/F ratio being exactly the distance from the CRe to the bracket where the force is applied. The bracket positions, however, can greatly diverge from case to case, which contributes to the deviation of results of different studies investigating teeth tipping. On the other hand, different orthodontic bodily movements are comparable as M/F ratios can be adjusted. In other words, orthodontic tipping forces from different experiments and analyses can hardly be systematically compared due to different points of force application.

The argumentation supporting this OTM effective zone hypothesis, especially the establishment of the systolic pressure as the upper threshold, could be that the hydrostatic

## CHAPTER 4: OPTIMISE ORTHODONTIC FORCE

stress over capillary pressure may not occlude the microvasculature of the stressed PDL completely, whereas a further increase in the systolic pressure may be likely to obstruct blood circulation. Thus the level of activation of cells might be reduced due to the deprivation of nutrient and signalling delivered via the microvasculature and hence impedes OTM. The activity amplification of OTM-relevant cells and factors within or in the vicinity of the PDL due to a higher stress, induced by a larger orthodontic force, is overwhelmed by the activity decline due to the loss of blood supply.

Tooth movement is more like a rigid body motion and therefore a localised measure as elemental hydrostatic stress  $\sigma_H$  may not be suitable. From this study, it can be observed from Fig. 4.6 that when using the VAHS as an indicator, a small area of high hydrostatic stress (i.e. over 4.7 kPa, in deep blue/red area) is unlikely to be sufficient to trigger active OTM for both bodily and tipping movement of the entire tooth. Instead, when a large deep blue/red area covers the majority of PDL volumes, OTM would then be probably initiated. The same principle can be applied for the lagging stage of OTM, in which a large grey/black area covering the PDL corresponds to the endpoint of the optimal zone (grey zone in Fig. 4.6).

Visible deep red/blue regions indicating effective local hydrostatic stress and grey/black regions indicating excessive local hydrostatic stress in Fig. 4.6 were observed, when the volume average (namely global) VAHS reached 4.7 kPa and 16 kPa, respectively. This is dramatically opposed to the less convincing evaluative approach based on the localised hydrostatic stress, where regardless how small the area of excessive stress is, the existence of effective and excessive stress areas implies the initiation and deceleration of OTM locally respectively. It is therefore reasonable to hypothesise that only when the majority of the PDL volume on both compression and tension sides are stressed to the extent beyond relevant critical limits (either lower or upper threshold), OTM can start to occur or decelerate, whereas small area of the PDL being locally stressed beyond the limits may not trigger OTM. It can be

## CHAPTER 4: OPTIMISE ORTHODONTIC FORCE

further hypothesised that within the optimal force range, or OTM-effective zone, the area of local excessive stress (over 16 kPa) is allowed as long as the global stress, namely VAHS, does not exceed 16 kPa. This is supported by a previous experiment in which only a small proportion of human PDL fibroblasts responded to the elevation of hydrostatic pressure of 20 to 50 mmHg that just exceeds capillary perfusion pressure [95].

One limitation of the current study is that the thresholds on both tension and compression sides were assumed to be the same, i.e. apposition and resorption are equally sensitive to hydrostatic tensile and compressive stress. The other limitation is that the computationally calculated optimum ranges could still be too wide due to uncertainty about the clinical preference towards the thresholds, and variation in capillary pressure from subject to subject. It was reported that the capillary blood pressure can be ranged between 15 and 35 mmHg (equivalent to 2 kPa and 4.7 kPa) [112, 129]. An underestimation of this lower threshold will increase the range of optimal orthodontic force. In addition, the lower threshold (4.7 kPa) represents a fairly conservative therapeutic strategy where moderate PDL occlusion may take place, whereas the upper threshold (16 kPa) represents a more aggressive regime where a rapid OTM featuring complete PDL occlusion, which could however increase the risk of excessive PDL necrosis and hence orthodontic root resorption and OTM deceleration.

It is therefore suggested that further on-human experiments should be conducted to validate the modelling results and advance our understanding on the optimum ranges of orthodontic forces, particularly how to relate biomechanical and physiological thresholds to the biological and cellular events in OTM. Despite some uncertainties arisen, the optimal magnitude of orthodontic force should be close to and slightly smaller than the upper bound of the optimal range (i.e. 16 kPa). The factor of safety applied to ensure the selected optimal force being smaller than the upper bound should be based on the clinical judgment of individual patients.

### 4.5 Conclusions

The study revealed that there was a variety of locations of CRe among maxillary teeth, which led to different M/F ratios when mimicking the translation. It is therefore suggested that a universal M/F ratio and CRe localisation based on past experience can be problematic when applied to an arbitrary patient in clinic. One should take into account a patient's specification and determine where to apply the orthodontic forces for tooth translation. The present study conceptualised such a convenient and precise FE method for this purpose.

A biomechanical comparison with the past literature came down in favour of using volume average hydrostatic stress. The measure of global pressure, as a better descriptive indicator to prediction of OTM, validated the proposed hypothesis of OTM effective zone. It was thus implied that only when the majority of the PDL volumes are stressed to a critical level, either the OTM-effective level (VAHS of 4.7 kPa) or the OTM-lagging level (VAHS of 16 kPa), OTM, as a rigid body-resembling motion, would be carried forward from a previous stage to the next. The current study has the potential to provide orthodontic professionals with an elaborate insight into how the PDL responds to effective OTM, thereby facilitating the planning of orthodontic conducts based on optimising the regime of the orthodontic forcing system.

## CHAPTER 5

### CANTILEVER THE DENTURE

Implant-supported fixed partial denture with cantilever extension can transfer excessive load to the bone around implants and stress/strain concentration potentially leading to bone resorption. This study investigated the effects of implant configurations supporting three-unit fixed partial denture (FPD) on the stress and strain distribution in the peri-implant bone by combining clinically measured time-dependent loading data and finite element (FE) analysis. A 3-dimensional mandibular model was constructed based on computed tomography (CT) images. Four different configurations of implants supporting 3-unit FPDs, namely three implant-supported FPD, conventional three-unit bridge FPD, distal cantilever FPD, and mesial cantilever FPD were modelled. The FPDs were virtually inserted to the molar area in the mandibular FE models. The FPDs were loaded according to time-dependent *in vivo* measured 3-dimensional loading data during chewing. The von Mises stress (VMS) and equivalent strain (EQS) in peri-implant bone regions were evaluated as mechanical stimuli.

During the chewing cycles, the regions near implant necks and bottom apexes experienced high VMS and EQS than the middle regions in all implant-supported FPD configurations. Higher VMS and EQS values were also observed at the implant neck region adjacent to the cantilever extension in the cantilevered configurations. The patient-specific dynamic loading data and CT based reconstruction of full 3D mandibular allowed us to model the biomechanical responses more realistically. The results provided data for clinical assessment of implant configuration to improve longevity and reliability of the implant-supported FPD restoration.

### 5.1 Introduction

Implant-supported fixed partial dentures (FPDs) have become a predictable, reliable and biocompatible restoration procedure for partial edentulous patients. However, the surgical feasibility of implantation within the mandibular posterior region can be low for specific anatomic restrictions, such as insufficient bone volume and position of mental foramen. In such cases, FPDs with cantilever extensions can be an alternative to avoid additional surgical procedures prior to or concomitant to the insertion of implants [143, 144]. Despite positive clinical outcomes of FPDs with cantilever extensions, there have been concerns in long-term biomechanical consequence and relevant technical complications [144]. Furthermore, some clinical retrospective studies reported that the extent of marginal bone loss at the implant-supported FPD with cantilever extension was relatively higher than those without cantilever extension [145, 146].

The causes for loss of osseointegration can generally be related to two factors, i.e. peri-implant tissue infections (Fig. 5.1) and occlusal overloading. A recent clinical study revealed that there is clear clinical evidence that combined factors related to implant hardware, clinical handling, and patient characteristics may cause marginal bone loss [147]. They also speculated that the mechanism behind the action of combined factors is bone micro-fractures or other types of bone injury that leads to inflammation, in turn triggering bone resorption. Therefore, the optimal loading condition on an implant is one of the critical contributors to the long-term outcome. Biomechanically, peri-implant bone remodelling is driven by mechanical stimuli [28, 148, 149]. It is thus essential to quantify the mechanical stimuli generated by the transferred functional occlusal loading on the implant for optimisation.

Finite element analysis (FEA) has shown compelling advantages in quantifying the mechanical stimuli in peri-implant bony tissues. Several FEA studies investigated the effects

of the implant configuration for the partial FPDs on the stress/strain in peri-implant bone [150, 151], and suggested that occlusal forces on cantilevers were amplified by leverage effects which might result in severe strain in peri-implant bone. Nevertheless, most computational studies were conducted with various assumptions and simplifications, such as sectional bone model geometry, homogeneous properties and loading conditions. It is recognized that the results of FEA investigating the stress distribution around the implant are strongly dependent on load conditions as well as model geometry [148, 152, 153]. Therefore, more realistic model geometry and clinical patterns of masticatory loading should be incorporated into such simulation to gain more meaningful biomechanical insights into the effects of implant configuration involving cantilever design.



**Fig. 5.1** (a) Oedematous swelling of peri-implant mucosa; (b) Peri-implant fluctuant swelling [154].

In this study, we created the FE models of full mandible with three-unit implant-supported FPDs, which are commonly applied in the mandibular posterior area, to investigate the effect of implant configuration on the bone stress/strain distributions. The functional 3-dimensional (3D) time-dependent dynamic loads on implants supporting FPDs were measured in a specific subject with 3-unit implant-supported FPD under different implant configurations using a newly developed load measuring device [155]. The measured *in vivo* loading data was assigned onto the corresponding implants in FE models to better reflect the real clinical

scenario. The chapter will report new biomechanics insights into 3-unit implant-supported FPDs and the configurational effects on bone stress/strain distribution under *in vivo* measured loading condition.

### 5.2 Materials and Methods

#### 5.2.1 Clinical data acquisition

A 67-year-old healthy female subject, who had three implants (MKIII RP)<sup>ii</sup> in her left mandibular free-end partially edentulous region, i.e. second premolar (P2), first molar (M1) and second molar (M2) (Fig. 5.2a-c), was recruited. The 3D dynamic loads exerted on implants were measured using a piezo-electric force transducer (Z18400)<sup>iii</sup> (Fig. 5.2d where the horizontal axis represents time) [155-157]. The experimental condition was established based on the implant configurations depending on the number and position of working implants for a 3-unit FPD. In the first configuration, three implants were used to support three-unit FPD (namely, three implant-supported FPD: 3iFPD). The second was a conventional bridge (two implant-supported FPD: 2iFPD) with the central implant left idle. Also with two implants active, the third and fourth configurations were distal and mesial cantilever bridges (two implant-supported distal cantilevered FPD: 2idcFPD and mesial cantilevered FPD: 2imcFPD), respectively (Fig. 5.2e-h). Loads were measured during chewing a piece of gum (free zone; weight about 1.6 g)<sup>iv</sup>. The same superstructure was used for different configurations so that the occlusal contacts remained the same in all test configurations. The opposite dentition was natural teeth and the condition of occlusal contacts was adjusted in the usual manner to be in

---

<sup>ii</sup> Nobel Biocare Holding AG, Zurich, Switzerland.

<sup>iii</sup> Kistler instruments AG, Winterthur, Switzerland.

<sup>iv</sup> Lotte Co., Tokyo, Japan.



harmony with other teeth before load measurement. The characteristics of the load measuring device and the experimental procedure were described in detail elsewhere [157].

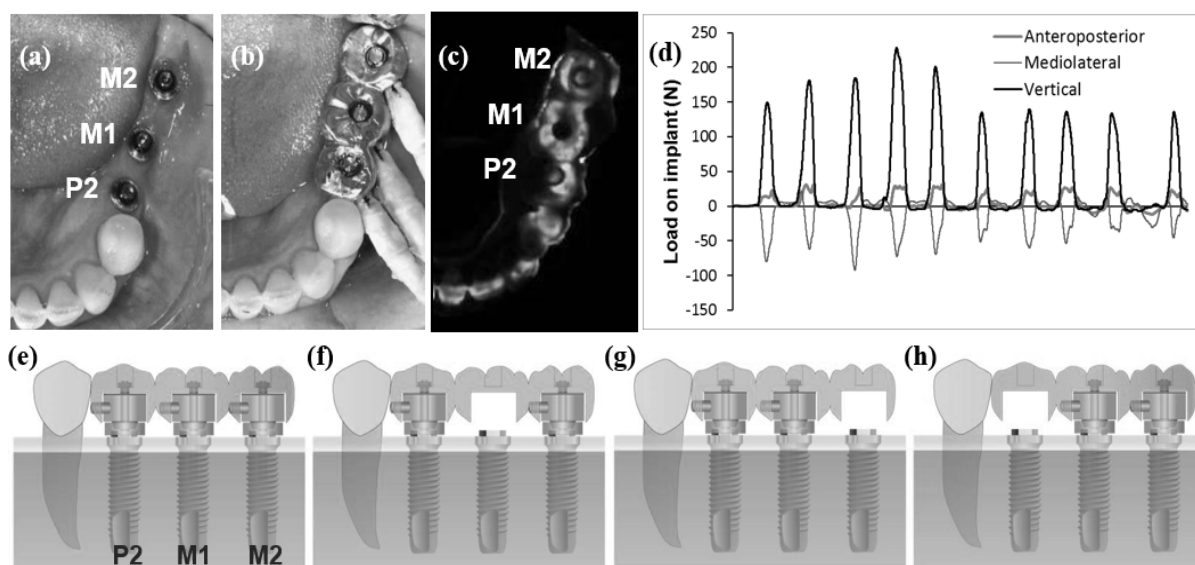


**Fig. 5.2** Intra oral views and occlusion of the subject (a-c), example of in vivo actual measured load on the implant, (d) and experimental conditions for in vivo load measurement (e-h); (a) Implants, with 3.75mm diameter and 13.0mm length, in the patient's left mandibular molar region, (b) After setting the load measuring device, (c) Occlusal contacts (Centric interocclusal record), (d) An example of in vivo actual measured load on the implant during chewing a piece of gum, (e) 3iFPD: Three implants (P2, M1, M2) were used, (f) 2iFPD: Two implants (P2, M2) were used, (g) 2idcFPD: Two implants (P2, M1) were used, (h) 2imcFPD: Two implants (M1, M2) were used.

The study protocol was approved by the research ethics committee of the Tohoku University Graduate School of Dentistry under the registration number of 22-33. A written informed consent was obtained from the patient after full explanation of the procedure.

### 5.2.2 *Finite element (FE) analysis*

The computed tomography (CT) images were segmented using ScanIP 4.3<sup>v</sup> based on greyscale thresholds and processed in Rhinoceros 3D<sup>vi</sup> to create 3D geometric models with non-uniform rational B-spline (NURBS). Three implants were modelled on the basis of identical specifications of the implants received by the subject. Tapered and cemented abutments were modelled complying with Esthetic Abutment RP<sup>vii</sup> design and these were connected to each implant with titanium abutment screws<sup>viii</sup>. The superstructure geometry was designed conforming to the real shape of the crowns of the subject. The implants, abutments, screws and superstructures were modelled using SolidWorks 2013<sup>ix</sup>.

The position and angulation of each implant was determined with reference to X-ray cephalometric images of the subject. The solid models were imported to FEA program Abaqus 6.9<sup>x</sup>. Four different FE models were constructed representing different clinical scenarios, i.e. 3iFPD, 2iFPD, 2idcFPD and 2imcFPD (Fig. 5.3a-d). The same superstructure was considered for all four different FE models.

The adaptive mesh was employed and a mesh convergence test was carried out [124]. For these different cases, the final meshes contain 392,691 (3iFPD), 250,317 (2iFPD), 353,825(2idcFPD), and 314,008 (2imcFPD) degrees of freedom using quadratic tetrahedral elements with hybrid formulation (C3D10H) to ensure smoothness of contact interfaces (Fig.

---

<sup>v</sup> Simpleware Ltd, Exeter, UK.

<sup>vi</sup> RobertMcNeel & Associates, Seattle, USA.

<sup>vii</sup> Nobel Biocare Holding AG, Zurich, Switzerland.

<sup>viii</sup> Nobel Biocare Holding AG, Zurich, Switzerland.

<sup>ix</sup> SolidWorks Corp, Waltham, MA, USA.

<sup>x</sup> Dassault Systèmes, Tokyo, Japan.

5.3e). All components as well as the interfaces between the implant and surrounding bone were completely fixed.

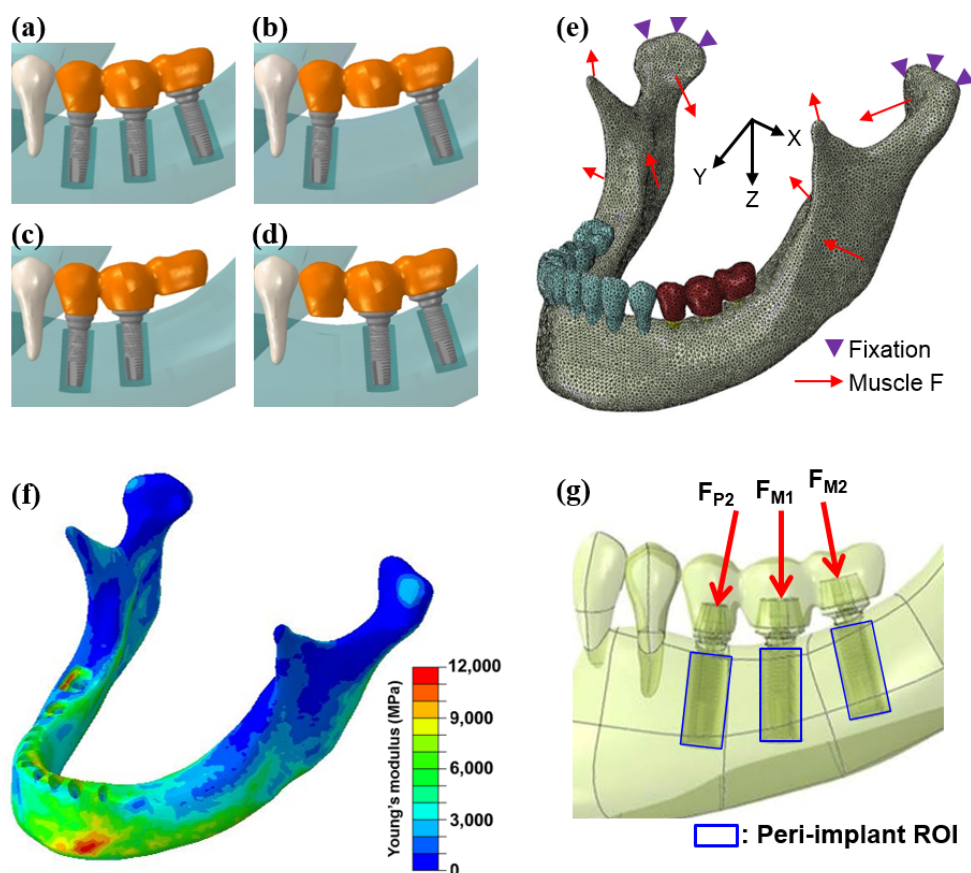


**Fig. 5.3** Process of FE model construction. (a) virtual insertion of all three implants (3iFPD) to the mandibular masks created in ScanIP, (b) 2iFPD, (c) 2idcFPD, (d) 2imcFPD, M1 was inclined 3 degrees to P2 and M2 was inclined 11 degrees to P2, to the posterior direction, respectively. Also, M1 was inclined 2 degrees to P2 and M2 was inclined 5 degrees to P2, to the lateral (buccal side) direction respectively. (e) Final meshed model meshed in ABAQUS (example of the 3iFPD case). Global 3D coordinate was defined as follows, X-axis: left (+) - right (-), Y-axis: anterior (+) - posterior (-), and Z-axis: upper (+) - lower (-), respectively, (f) Site-specific material properties of osseous tissues assigned based on the HU values from the CBCT data through a FORTRAN program in ABAQUS user subroutine, (g) Region of interests (ROIs): peri-implant and the loading position (red arrows show example of load vector in 3iFPD).

Material properties are summarized in Table 5.1. The bone is assigned heterogeneous properties based on the CT Hounsfield unit data (Fig. 5.3f). Site-specific material properties in the bony structure may to a certain extent affect the localized FE results [89], and hence further enhance the fidelity of the model and more accurately capture the biomechanical responses.

**Table 5.1** Materials properties adopted in FE modelling

Materials	Young's Modulus(MPa)	Poisson's ratio
Bone [89]	Heterogeneous	0.30
Teeth [158]	20,000	0.20
Ti (Implant, Abutment, Screw) [159]	110,000	0.35
Gold casting crown [160]	91,000	0.33

The 3D loads on implants measured *in vivo* during gum chewing were analysed using the global 3D coordinate (Fig. 5.3e) [156, 157, 161]. The maximum magnitude of the 3D load exerted on each implant in each chewing cycle was determined in all configurations. The average of maximum magnitudes in the first 10 chewing cycles was then calculated for applying to the FEA as a loading condition (Table 5.2). The loads were applied on the top surface of the abutment on each implant, consistent with the height of the load measuring point *in vivo* (Fig. 5.3g).

The mandibular models were supported by the masticatory muscles and temporomandibular joints. The magnitudes and directions of the masticatory muscles and their

positioning on the mandible were derived based on previous studies [162]. The boundary conditions were prescribed to the corresponding mandibular condyles. Consequently, the mandibular models were loaded and constrained in equilibrium.

**Table 5.2** The average of maximum magnitudes in the first 10 chewing cycles during gum chewing (N)

	P2			M1			M2		
	X-axis	Y-axis	Z-axis	X-axis	Y-axis	Z-axis	X-axis	Y-axis	Z-axis
<b>3iFPD</b>	-16.5	17.9	74.9	17.8	-1.9	84.9	19.5	-59.8	160.6
<b>2iFPD</b>	-4.8	31.1	136.5				20.3	-71	191.2
<b>2idcFPD</b>	6.4	-6.5	-24.2	8.6	-15.3	347.2			
<b>2imcFPD</b>				-2.2	-42.4	261.2	20.1	-30.4	92

Regions of interest (ROI) were placed at the peri-implant region, approximately 1.2 mm from the implant surface, for each implant (Fig. 5.3g). This region has often been considered as a key region for evaluating osseointegration and bone remodelling [153]. In order to obtain a thorough understanding of the biomechanical bone responses, von Mises equivalent stress (VMS) and equivalent strain (EQS) were analysed as mechanical stimuli for quantifying the bone responses in the peri-implant ROI [28, 39, 149].

### 5.3 Results

The distributions of VMS in peri-implant ROIs are displayed in two cross-sectional views (i.e. buccal and lingual sides) (Fig. 5.4a). A higher value of VMS is generally observed around neck and bottom apexes of the implants than around the middle regions. The VMS is relatively higher in the mesial side in P2 and distal side in M2 when the corresponding implants

are used. The higher VMS is also observed in a larger area around M1 in cantilevered configuration cases.

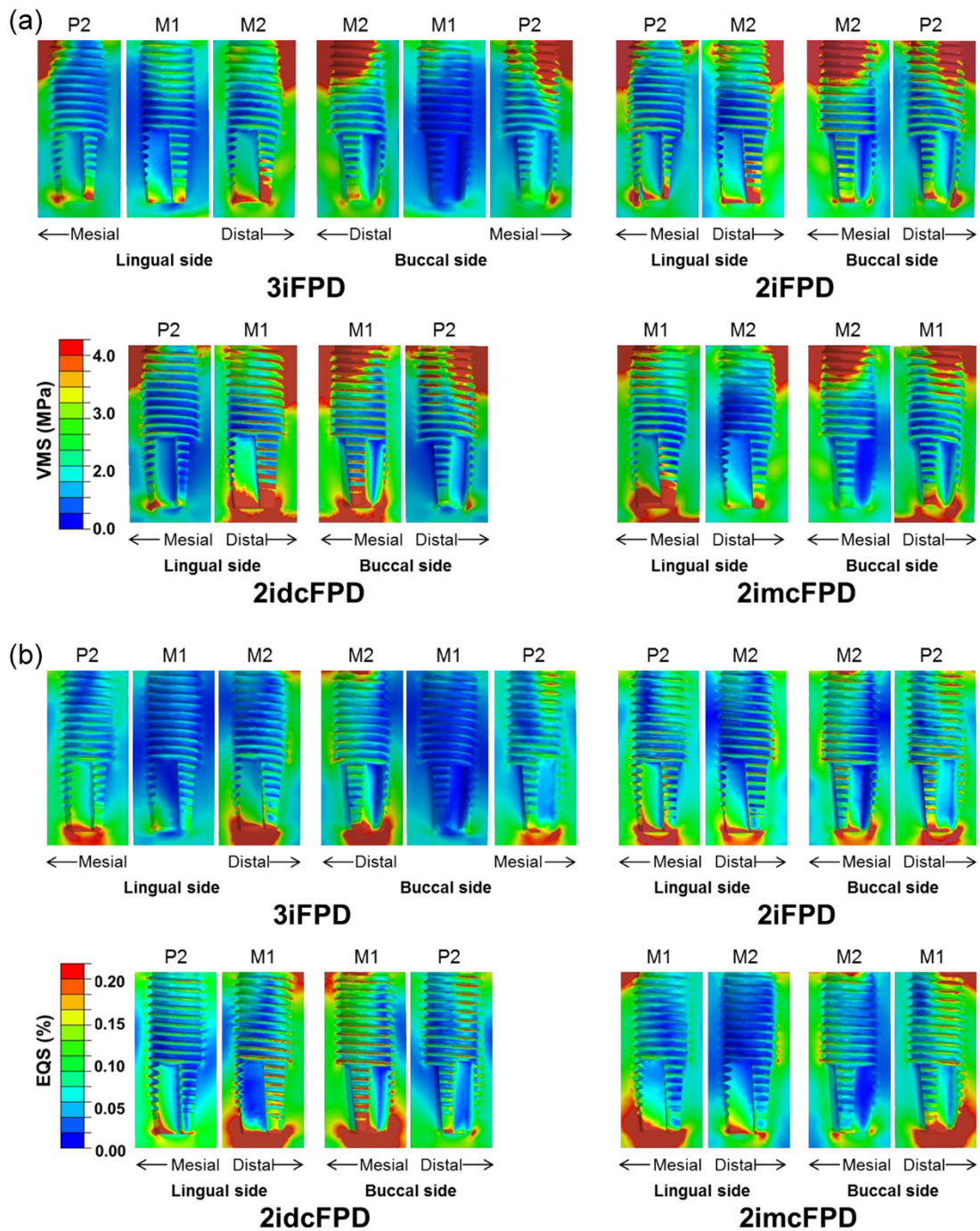


**Fig. 5.4** Comparison of the two sectional views (lingual and buccal) of mechanical stimuli distribution in peri-implant ROIs. (a) VMS, (b) EQS.

Distributions of EQS in the peri-implant ROIs are displayed in two cross-sectional views (Fig. 5.4b). A higher value of EQS is generally observed around the bottom apexes of the implants. In the neck areas, the higher magnitudes are noticeably present at the cantilever extension side of M1 in the cantilevered configurations.

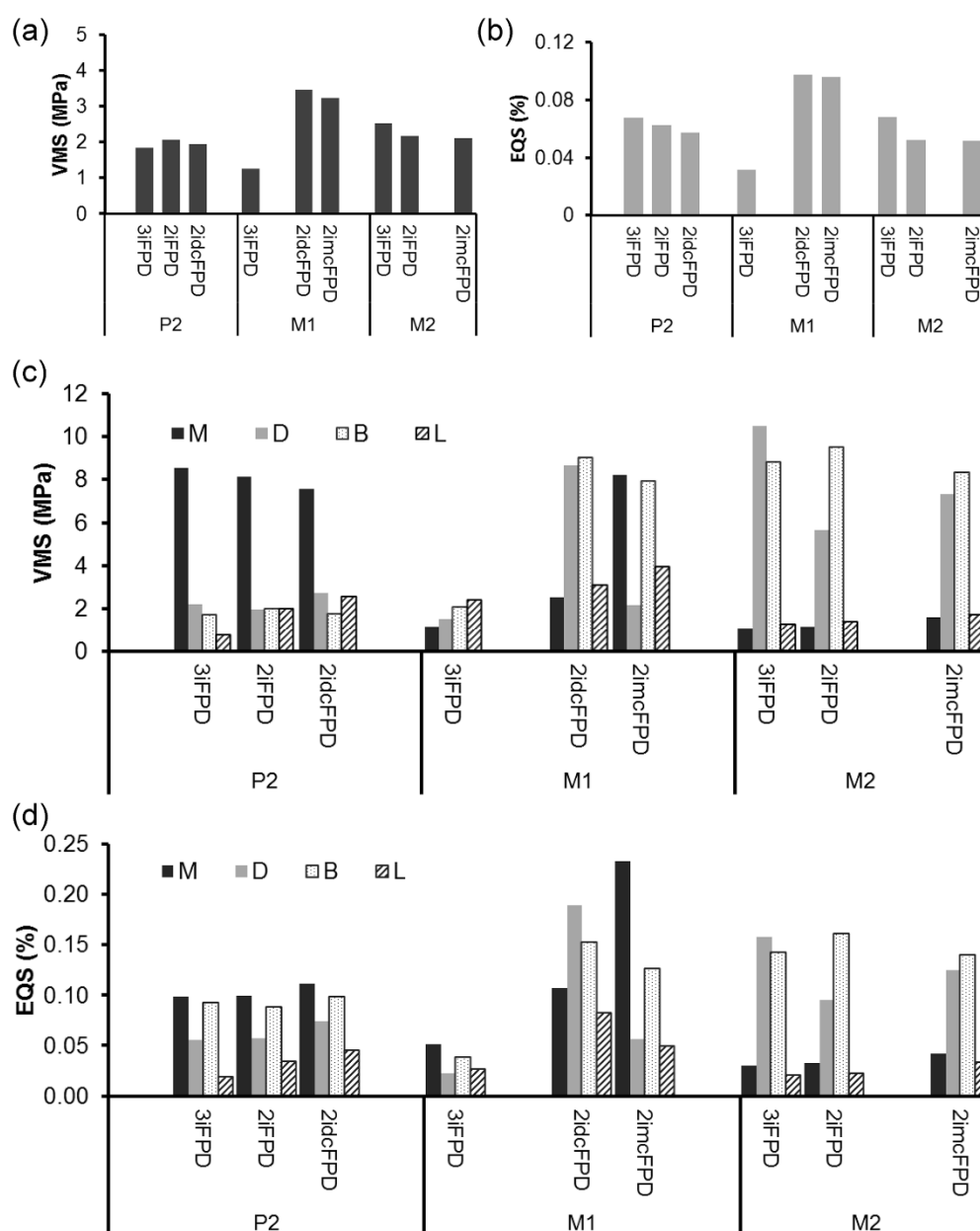


Fig. 5.5 Volume average of mechanical stimuli in peri-implant ROIs.

The volume average of VMS and EQS in the peri-implant ROIs are calculated (Fig. 5.5a, b). The values detected in M1 in the case of cantilevered configurations are much higher than those in the other cases. The regions around the implant neck are of primary interest in determining initiation of bone remodelling [28, 149, 153, 161]. To examine the bone responses in this region, the VMS and EQS are specifically calculated at the mesial, distal, lingual and buccal regions around the implant neck (Fig. 5.5c, d). The VMS on the mesial side is higher than the other three regions in P2. On the other hand, the VMS on distal and buccal sides are higher than the other two regions in M2. The EQS showed similar outcomes and the mesial side in M1 is the highest in the case of 2imcFPD. Both VMS and EQS are generally low on the lingual sides. It is noteworthy that in M1, the VMS and EQS distributions vary considerably depending on the implant configuration.

### **5.4 Discussion**

#### ***5.4.1 The FE modelling and analysis conditions***

The present models simulated different biomechanical conditions for this specific subject which revealed that the implant loading and subsequent bone stress/strain distribution were significantly affected by the implant configurations under approximately the same masticatory condition and the same superstructure.

Note that some loading conditions have been assumed in the previous FEA studies for biomechanical analysis of implant structure, which consistently exhibits a strong correlation between bone's response and loading [148, 152]. Here a recently developed in vivo load measuring device enabled us to obtain the genuine 3D time-dependent loads on implants in a patient-specific manner [155]. Although the loading scenario used in the present study represents only a fragment of real daily function of the specific subject, this study was the first



of its kind to incorporate 3D in vivo measured loads during mastication in the FE study, which is thought to more realistically reflect bone's responses.

A previous biomechanical study that investigated the strain distribution in the dentulous mandible under masticatory loading demonstrated that the buccal strains were constantly higher than the lingual strains in the molar area by using the whole mandible FE model with virtual muscle forces [163]. The present stress/strain results showed the good agreement with their results. Therefore, use of the 3D whole mandibular model for the computational simulation is of considerable benefits for realistically exploring the peri-implant bone responses even in the implant supported 3-unit FPD. In this study, the use of whole mandibular with both muscle and patient-specific occlusal forces as well as the heterogeneous FE model are thus thought to provide more credible insights into the biomechanics of the 3-unit implant-supported FPDs.

In addition, a higher VMS was generally observed in the mesial side in P2 and distal side in M2. Based on the loading conditions (Table 5.2), the load direction in Y-axis was positive (anterior) on P2 and negative (posterior) on M2 in all configurations except for the 2idcFPD. Those loads can cause the concentration of the compressive stress in the mesial side in P2 and the distal side in M2. In terms of the P2 in 2idcFPD, the applied load was upper-anterior direction, which can cause the concentration of the tensile stress in the mesial side in P2. Therefore, it is thought that the stress concentration in the peri-implant bone can be highly influenced by the loading direction on the implant. Also the stress/strain distribution might be affected by the non-parallel orientations of different implants.

### ***5.4.2 The influence of implant configuration on mechanical stimuli***

The VMS and EQS distributions within the bone surrounding the implants suggested sensible biomechanical responses. The VMS characterizes the distortion strain energies that

bony tissue withstand, which provides an indicator to measuring the degree of overall stress as a result of functional load [164]. The magnitude of peri-implant VMS can be a critical measure of damage to osseointegration [152]. The VMS distribution and volume averages suggested that M1 region is most prone to the loss of osseointegration in the cases of cantilevered configurations. In particular, the neck area of implants can be of the highest risk of failure, followed by the apex and middle regions. This finding is in good agreement with previous computational studies [150, 151]. In addition, recent retrospective study revealed that the bone loss level around implant in the FPDs with cantilever extension were significantly ( $p=0.047$ ) higher than those without cantilever extension in the mandibular posterior area, although the average observation period was less than 5 years [146].

On the other hand, EQS has been often correlated with bone remodelling activities [39, 149]. The EQS distributions and its volume average also suggested that M1 in the cantilevered configuration, where higher EQS was generated, has the potential to undergo most rapid bone apposition after implant placement and functioning [153]. However, it can also imply a higher risk of bone resorption upon overloading [28, 149]. Biomechanically, the concentration of EQS around implant necks may suggest that the risk of bone resorption around M1 in the case of cantilevered FPDs can be higher than that in the case of 3iFPD, especially in the distal aspect in the case of 2idcFPD and the mesial aspect in the case of 2imcFPD.

### ***5.4.3 Clinical implication and study limitation***

Within its limitations, the results suggested that the 3iFPD or 2iFPD appear to be more biomechanically favorable for the 3-unit implant supported FPDs based on the stimulus distribution and magnitudes. In the cantilevered design of 3-unit FPDs, the implant next to the cantilever extension may have a higher risk of failure, evidenced by visibly higher averaged VMS and EQS. Taking into account the influence of the loading condition on the stress/strain

in peri-implant bone, the cantilevered design of FDP should not be recommended in the subjects who have high occlusal bite forces or a history of bruxism [143]. The follow-up X-ray (S1) of this subject with 3iFPD showed a favourable condition of the osseointegration. Note that the bone remodelling outcomes depend on strain magnitude, frequency, and rate [165]. It implies that the EQS detected in the case of 3iFPD can be considered not to have damaging effect to the osseointegration. Further validation of the FE results with time-dependent clinical bone remodelling activities can provide useful information to predict the treatment outcome.

There are inherent limitations in the present study. First, all the interfaces between different materials were assumed to be fully bonded at the time of assessment. The interfacial stress/strain was not analysed for simplification so as to restrain our attention on the effect of implant configuration. Second, the *in vivo* measured implant loads might actually be different from the calculated occlusal load which was a reaction force generated by the derived muscle forces in the present model. Consequently, the resultant temporomandibular reaction forces could become asymmetric and also physiologically improper, although it was compensated by fully constraining the condyles in the present models. Further studies to identify the patient specific muscle forces are still needed. Third, the FEA results of this study were not validated with the clinical bone remodelling results. Further biologic and clinical follow-up studies on the bone remodelling would help establish a more comprehensive understanding of the role of occlusal loadings in preserving peri-implant tissues.

### **5.5 Conclusions**

This study provided a fundamental understanding of the local biomechanical responses of posterior mandibular bone to the construction of 3-unit implant-supported FPD restoration with different configurations, which may provide clinicians with meaningful insights into the

## CHAPTER 5: CANTILEVER THE DENTURE

pre-clinical assessment of implant-supported FPD treatment. The biomechanical effects of the configuration of implants-supported FPDs on the peri-implant bone were investigated *in silico*. The consideration of patient-specific loading data based on the different implant configurations and structurally detailed full mandible FE model allowed us to quantify the biomechanical responses more realistically. In the case of the cantilevered design of 3-unit FPDs, the implant adjacent to the cantilever extension may be of a high risk of loss of osseointegration.

## CHAPTER 6

# MULTI-STAGE BONE REMODELLING INDUCED BY DENTURES

This chapter aimed to develop a clinically validated bone remodelling algorithm by integrating bone's dynamic properties in a multi-stage fashion based on a four year clinical follow-up of implant treatment. The configurational effects of fixed partial dentures (FPDs) were explored using a multi-stage remodelling rule. Three dimensional (3D) real-time occlusal loads during maximum voluntary clenching (MVC) were measured with a piezo-electric force transducer and were incorporated into a computerized tomography (CT) based finite element (FE) mandibular model. Virtual X-ray images were generated based on simulation and statistically correlated with clinical data using linear regressions. The strain energy density (SED) driven remodelling parameters were regulated over the time considered. A linear single-stage bone remodelling algorithm, with constant remodelling parameters, was found to poorly fit with the linear regression line (low  $R^2$  and R), whereas a time-dependent multi-stage algorithm better simulated the remodelling process (higher  $R^2$  and R) against the clinical results.

The three-implant supported and distally cantilevered FPDs presented noticeable and continuous bone apposition, mainly adjacent to the cervical and apical regions. The bridged and mesially cantilevered FPDs showed bone resorption or no visible bone formation in some areas. Time-dependent variation of bone remodelling parameters is recommended to better correlate remodelling simulation with clinical follow-up. Caution should be taken when selecting the FPD with cantilever due to the risk of overloading bone resorption. The position of FPD pontics plays a critical role in mechanobiological functionality and bone remodelling.

### 6.1 Introduction

Implant-supported fixed partial dentures (FPDs) have been widely applied in partially or completely edentulous patients by virtue of their high 5-year (95.6%) and 10-year survival (93.1%) rates [166]. However, surgical limitations are often encountered in cases of anatomic restrictions such as insufficient bone volume and surgically-unfavourable position of the mental foramen, existing in the posteriorly-edentulous region [167]. Accordingly, with the overall low-profile regime and thus more bone conservation, financial advantage, as well as the controversies regarding potential complications, prostheses with cantilever extensions have been extensively used with divergent clinical outcomes [168, 169]. One major issue associated with the cantilever configuration is the prosthetic failure, including veneer and abutment screw fracture, screw loosening and peri-implantitis [170, 171]. Another critical issue is bone loss and resorption induced by cantilever FPDs (CFPDs), possibly stemming from mechanical overloading [167, 172].

To address the above issues numerous finite element analyses (FEA) have been conducted to comprehend the biomechanics of FPDs, with some emphasizing on the effects of prosthetic designs on the mechanobiology [153, 157, 173]. While the survival and success rates of an FPD heavily hinge on the osseointegration and bone remodelling [174], the bone remodelling outcomes, a critical contributor to the success of a restoration, have been noticeably lacking in existing literature involving FEA on fixed or removable dentures. Wolff's rule-based bone remodelling algorithms have been widely applied in dental implantology to understand, predict and optimize bone adaptation associated with various implant-supported prostheses [28, 153, 175].

Nonetheless, difficulties of validation and verification predominantly existed in many computational studies, a situation not limited to FPD- or bone remodelling-related FE studies.

First, it is challenging to know real-time loading *in vivo* for *in-silico* simulations, as the presumption of force magnitude and orientation can dramatically influence modelling results [161, 176]. Second, the validation of most FE models against clinical data is largely missing. Third, subject-specific heterogeneity and anisotropy of bony structure, contributing to the sophistication of dental and periodontal tissues, was largely neglected, thereby lowering the soundness of the computational modelling [89, 177]. Finally, linear bone remodelling algorithms adopted constant remodelling rate and reference stimulus, which often failed to reflect the dynamic sophistication in homeostatic conditions, i.e. a time-varying physiological responses in dental complexity [178].

The architecture, mass and homeostasis of a bone adapt to the external stimuli in a self-optimizing fashion. Bone forming osteoblasts, bone resorbing osteoclasts and other relevant factors are recruited and systematically coupled to implement the course of this adaptation, called bone remodelling. Pioneered and inspired by Wolff's law [179], researchers have proposed several computationally feasible models to describe and quantify the relationship between bone remodelling and external stimulus, the majority of which are analogous to a feedback control system, including the strain energy density (SED) based [180, 181], strain-based [182, 183], continuum damage [183, 184], cell coupling [185] and soft-tissue driven model [90, 186].

The foregoing long-established bone remodelling algorithm have the following limitations. Firstly, the bone remodelling rate, either of hypertrophy or atrophy, is deemed to be constant and not patient-specific. This fails to present and correlate with the genuine progression of bone remodelling where remodelling can occur non-linearly over time [181]. The bandwidth of a lazy zone, whose existence was questioned recently (Fig. 6.1) [187], and stimulus reference may also be inconstant [181]. Secondly, the patient-specificity was largely disregarded due to the scarcity of clinical data. An uncomprehensive literature review by us

shows that most of the studies adopted 0.004 J/g as the stimulus reference for the SED-based remodelling algorithm, which was originated in the studies by Huiskes *et al.* [188] and Weinans *et al.* [189] who estimated some bone remodelling coefficients based on the realism of the end configuration. The estimation could only be meaningful and correct using their specific 2D finite element (FE) model of proximal femur. Even larger error would arise if directly applying previously-defined parameters in models of other biological tissues such as dental structures and knee structures. Similarly, the widths of lazy zone were mostly defined as a fixed and sometimes arbitrary value without justification, with 10% being the most prevalent choice. Thirdly, the validations of simulations were considerably ignored. The remodelling parameters, adopted by the studies that did not directly employ the previously-estimated values, were usually determined from unquantified conclusion, e.g. a realistic bone density distribution, instead of statistical correlation with clinical data [190]. The inaccuracy also included the invalidated loading scenario and boundary conditions. Finally, there is still controversy over the role and weighing of mechano-stimulus on bone remodelling outcomes. Currently no bone remodelling rule can fully accommodate the sophistication of bone adaptation.

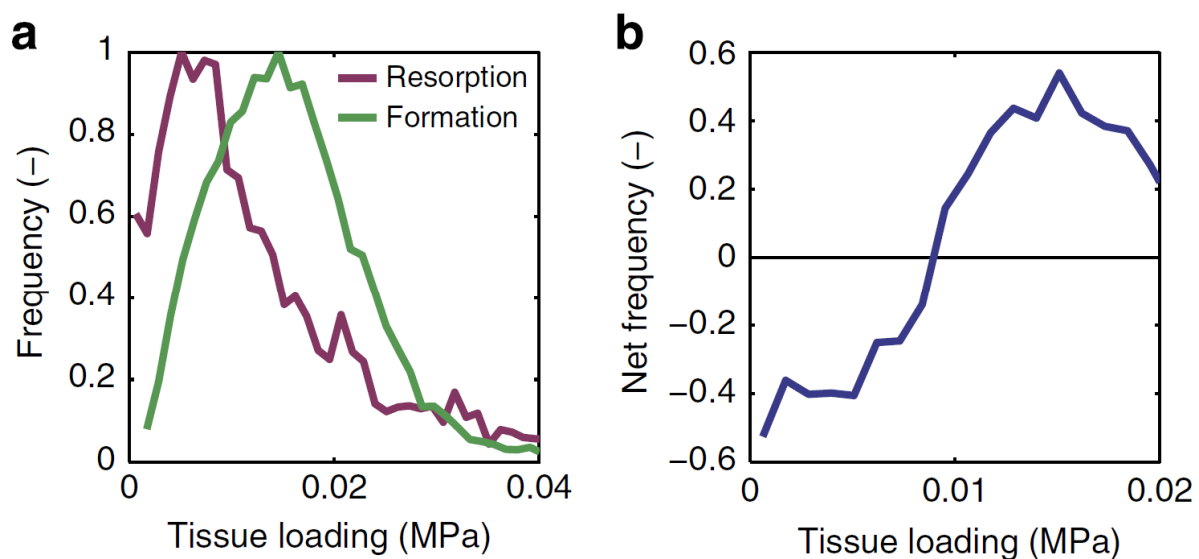




**Fig. 6.1** No lazy zone was found during human bone remodelling using high-resolution peripheral quantitative computed tomography (HR-pQCT) (a) Histograms of SED indicating bone resorption and apposition; (b) Bone remodelling, indexed as net frequency, versus loading [187].

This chapter aimed to establish an FEA-based bone remodelling algorithm by integrating the *in-vivo* occlusal loads and X-ray data at different time points during a four-year clinical follow-up. A multi-stage bone remodelling algorithm was compared with the traditional tri-linear counterpart. The effects of FPD designs on bone remodelling outcomes were studied systematically by using the new remodelling algorithm to provide clinical recommendations. Further, the randomness of parameter identification by Latin hypercube sampling (LHS) and surrogate modelling were incorporated to achieve a more accurate dynamic bone remodelling strategy and explore the contribution of mechanobiological stimulus to bone remodelling.

## 6.2 Materials and Methods

### 6.2.1 Clinical data acquisition

A 67-year-old female was recruited for the real-time dynamic loading measurements *in vivo*. A three-implant-supported FPD, with implant diameter of 3.75 mm and length of 13 mm, was installed in the subject's left mandibular free-end, a partially edentulous region spanning second premolar (P<sub>2</sub>), first molar (M<sub>1</sub>) and second molar (M<sub>2</sub>) areas (Fig. 6.2a & b). Dynamic loads during maximum voluntary clenching (MVC) with different FPD designs were recorded using a piezo-electric force transducer (Z18400, Kistler instruments AG, Winterthur, Switzerland) and their local maxima were tabulated (Table 6.1). The appropriate preload was generated to each transducer by tightening the screws, ensuring the output accuracy and stability. Approval of this study protocol was granted by the research ethics committee of

Graduate School of Dentistry, Tohoku University (registration number: 22-33). Full details of the experimental protocol can be found in Kobari *et al.* [157].

**Table 6.1** Real-time loading measurements during MVC.

	P <sub>2</sub> (N)			M <sub>1</sub> (N)			M <sub>2</sub> (N)		
	X	Y	Z	X	Y	Z	X	Y	Z
3I	9.3	10.8	57	12.8	-11.3	68.3	-4.4	-33.4	51.1
Br	36.3	21.9	106.2		N/A		-1.4	-38.3	59.4
DCBr	37.3	12	62.2	-8.8	-15.6	109.9		N/A	
MCBr		N/A		43.9	-29.3	209.9	-23.1	-25.2	10.9

3I: three-implant-supported FPD; Br: conventional bridge;

DCBr: distal cantilever bridge; MCBr: mesial cantilever bridge



**Fig. 6.2** (a) 67 year-old subject installed with FPD and piezo-electric force transducer; (b) top view of intra-oral experimental set-up.

### 6.2.2 Finite element modelling

The 3D FE model of patient's mandible was constructed based on the anatomical data obtained from an i-CAT CBCT scanner (Imaging Sciences International, Hatfield, Pa). The scans, with a resolution of 0.3 mm per slice, were taken one year after teeth extraction. The

image segmentation was performed with ScanIP 4.3 (Simpleware Ltd., Exeter, UK), followed by creation of non-uniform rational basis spline (NURBS) models using Rhinoceros (Robert McNeel & Associates, Seattle, US) [35].

Four FPDs with different configurations were modelled, namely three-implant-supported FPD (Model 3I), conventional bridge (Model Br), distal cantilever bridge (Model DCBr) and mesial cantilever bridge (Model MCBr) (Fig. 6.3a-d). The full mandible consisted of 932,848 quadratic tetrahedral elements, in which peri-implant ROIs (PROIs) were assigned extra fine meshes in accordance with a convergence test. PROIs are considered critically important to examining the osseointegration and bone remodelling [153].

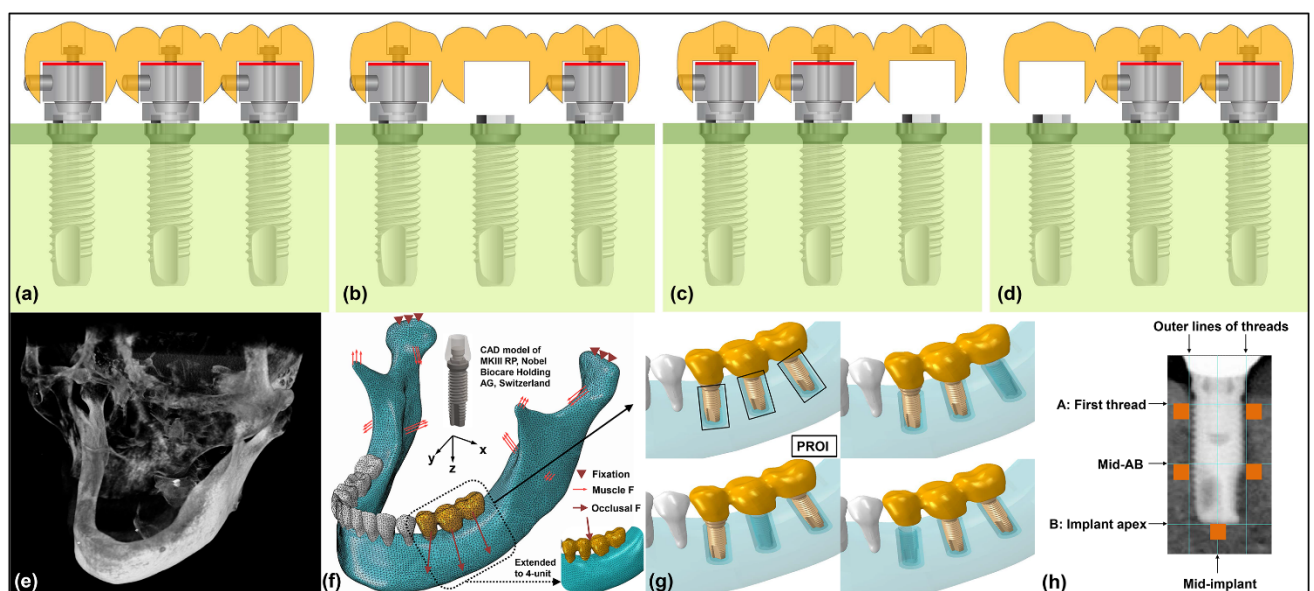


**Fig. 6.3** (a) Model 3I; (b) Model Br; (c) Model DCBr; (d) Model MCBr. From left to right: P2, M1, M2; (e) CBCT scans of edentulous mandible; (f) Meshed FE model with loading and boundary conditions; Note that force vectors are only for illustration and only the loads on Model 3I were visualized. For more detailed loading conditions, refer to Table 6.1; (g) FE models of various configurations; The boundaries of Peri-implant regions of interest (PROIs) are 1.2 mm from the implant surface; (h) ROIs localisation for each implant unit. Please refer to Reference 181 for better readability if needed.

The initial heterogeneous density of mandibular bone was interpolated from a linear relationship between measured Hounsfield unit ( $HU$ ) and apparent density  $\rho$  of bone as

$$\rho = \rho_{\min} + \frac{(\rho_{\max} - \rho_{\min})(HU - HU_{\min})}{(HU_{\max} - HU_{\min})} \quad (\text{Eq. 6.1})$$

where  $\rho_{\min}$  and  $\rho_{\max}$  stand for the minimum and maximum bone densities which were assigned as  $0.69 \text{ g/cm}^3$  and  $1.90 \text{ g/cm}^3$  respectively [39, 191].  $HU_{\max}$  and  $HU_{\min}$  are the maximum and minimum HUs of the scans.

The importance of incorporation of cortical bone orthotropy has been well acknowledged [192, 193]. Orthotropic cortical elastic moduli ( $E_{\text{cort1}}$ ,  $E_{\text{cort2}}$  and  $E_{\text{cort3}}$ ), shear moduli ( $G_{\text{cort12}}$ ,  $G_{\text{cort23}}$  and  $G_{\text{cort31}}$ ) and Poisson's ratios ( $\nu_{\text{cort12}}$ ,  $\nu_{\text{cort23}}$  and  $\nu_{\text{cort31}}$ ) and cancellous elastic modulus ( $E_{\text{can}}$ ) were determined and mapped to the Gaussian points in each element according to Carter and Hayes [183], Schwartz - Dabney and Dechow [177] and Hellmich, Kober [194]. These provide site-dependent and anisotropic properties of the cortical layer, as formulated in Eqs. 6.2-6.12.

The anisotropic properties of the cortical bone can be identified in terms of nine orthotropic parameters in the elasticity tensor, i.e.  $E_1$ ,  $E_2$ ,  $E_3$ ,  $G_{12}$ ,  $G_{23}$ ,  $G_{31}$ ,  $\nu_{12}$ ,  $\nu_{23}$ ,  $\nu_{31}$  (Eq. 6.2), where radial, circumferential and axial directions are denoted as subscripts 1, 2 and 3 respectively, while radial-circumferential, circumferential-axial and axial-radial planes are denoted as subscripts 12, 23 and 31 respectively. Nonlinear correlations between the elasticity parameters and elemental densities were established using curve fitting (Eqs. 6.3-6.8), based on the data reported by Schwartz - Dabney and Dechow [177] (Fig. 6.4a-c). However,  $R^2$  values for the fitted equations of orthotropic Poisson's ratios against density are significantly low (ranging from 0.023 to 0.15), using several different curve fitting strategies. The

correlations between orthotropic Poisson's ratios and HUs reported by Hellmich *et al.* [194] were therefore adopted (Eqs. 6.8-6.10 & Fig. 6.4d).

$$\begin{Bmatrix} \epsilon_{11} \\ \epsilon_{22} \\ \epsilon_{33} \\ \gamma_{12} \\ \gamma_{23} \\ \gamma_{31} \end{Bmatrix} = \begin{bmatrix} 1/E_1 & -\nu_{21}/E_2 & -\nu_{31}/E_3 & 0 & 0 & 0 \\ -\nu_{12}/E_1 & 1/E_2 & -\nu_{32}/E_3 & 0 & 0 & 0 \\ -\nu_{13}/E_1 & -\nu_{23}/E_2 & 1/E_3 & 0 & 0 & 0 \\ 0 & 0 & 0 & 1/G_{12} & 0 & 0 \\ 0 & 0 & 0 & 0 & 1/G_{23} & 0 \\ 0 & 0 & 0 & 0 & 0 & 1/G_{31} \end{bmatrix} \begin{Bmatrix} \sigma_{11} \\ \sigma_{22} \\ \sigma_{33} \\ \sigma_{12} \\ \sigma_{23} \\ \sigma_{31} \end{Bmatrix} \quad (6.2)$$

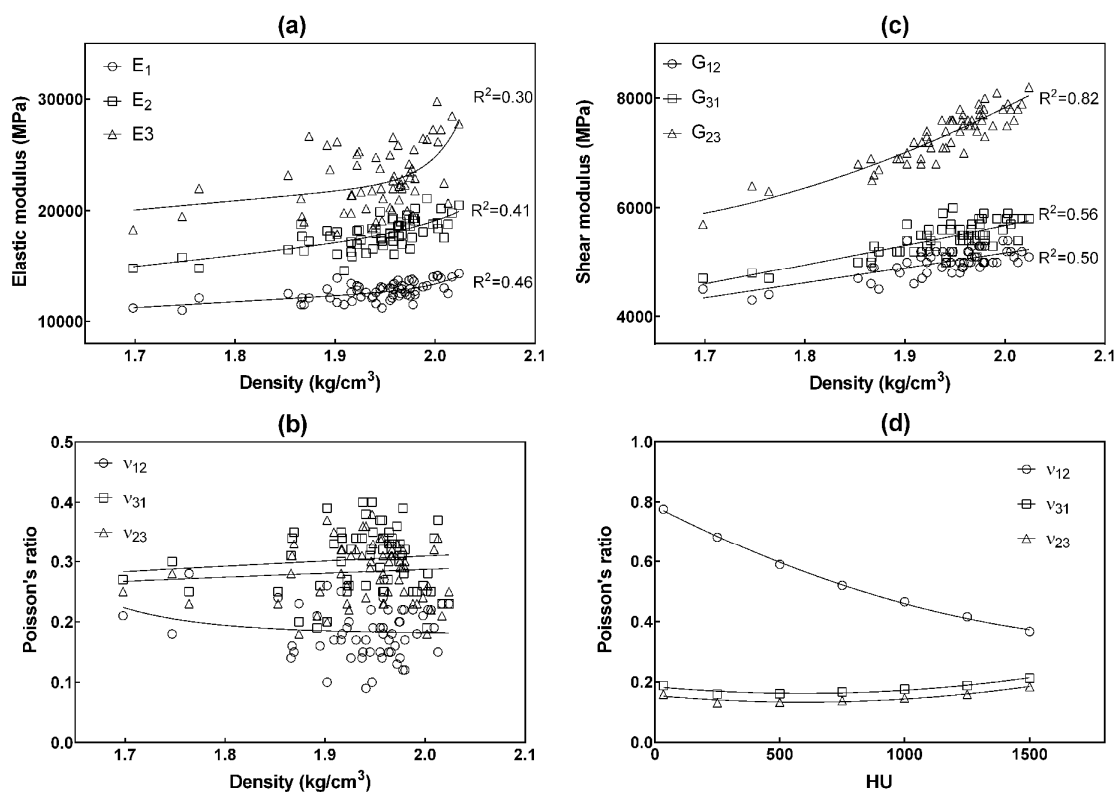


**Fig. 6.4** (a-c) Correlations of orthotropic constants (elastic moduli, shear moduli and Poisson's ratios) against density based on Schwartz - Dabney and Dechow [177]; (d) orthotropic Poisson's ratios correlated with HU, replotted from Hellmich *et al.* [194].

The local material orientations were identified by generating multiple sections accommodating the morphology of mandible so that each divided section resembles a cylinder

and hence features an orthogonal coordinate system [177]. Two field variables were set up in Abaqus subroutine, i.e. density and HU for the calculation of all nine engineering constants defining orthotropy, which are nine solution-dependent variables. The upper threshold for cancellous density is  $1.53 \text{ g/cm}^3$  [195] and the lower threshold for cortical density is  $1.70 \text{ g/cm}^3$  [177] for differentiating them.

$$E_{\text{cort1}} = 2.13 \times 10^{-17} \rho^{64.49} + 7329 \rho^{0.81} \quad (6.3)$$

$$E_{\text{cort2}} = 1.61 \times 10^{-8} \rho^{36.01} + 8243 \rho^{1.13} \quad (6.4)$$

$$E_{\text{cort3}} = 6.04 \times 10^{-18} \rho^{68.39} + 13821 \rho^{0.70} \quad (6.5)$$

$$G_{\text{cort12}} = 2448 \rho^{1.08} \quad (6.6)$$

$$G_{\text{cort31}} = 1155 \rho^{1.27} + 1159 \rho^{1.32} \quad (6.7)$$

$$G_{\text{cort23}} = 13792 \rho^{-3.827} + 758.7 \rho^{3.18} \quad (6.8)$$

$$v_{\text{cort12}} = 10^{-7} (HU)^2 - 4 \times 10^{-4} (HU) + 0.7856 \quad (6.9)$$

$$v_{\text{cort31}} = 6 \times 10^{-8} (HU)^2 - 8 \times 10^{-5} (HU) + 0.1843 \quad (6.10)$$

$$v_{\text{cort23}} = 6 \times 10^{-8} (HU)^2 - 8 \times 10^{-5} (HU) + 0.1553 \quad (6.11)$$

$$E_{\text{can}} = 3790 \rho^3 \quad (6.12)$$

The material properties were summarized in Table 6.2 [153]. Occlusal forces were applied on the superior surfaces of abutments as per Table 6.1. Muscular forces were derived and exerted as suggested in the literature [196]. Fixation was applied on the

temporomandibular joints and the teeth were constrained from moving upwards, allowing the reaction forces induced by occlusion (Fig. 6.3f) [153, 197, 198].

**Table 6.2** Material properties

<b>Materials</b>	<b>Elastic modulus (GPa)</b>	<b>Poisson's ratio</b>
Cortical bone	Heterogeneous and orthotropic	Heterogeneous and orthotropic
Cancellous bone	Heterogeneous and isotropic	0.3
Teeth	20	0.2
Titanium (implant, abutment, screw)	110	0.35
Gold (casting crown)	91	0.33

### 6.2.3 Multi-stage bone remodelling algorithm

Strain energy density (SED) based bone remodelling algorithm was adopted, in which the normalized SED per unit apparent density is the mechanical stimulus driving bone remodelling [153, 158]. It is defined by

$$\Xi = \frac{U}{\rho} \quad (6.13)$$

where  $\Xi$ ,  $U$  and  $\rho$  are mechanical stimulus (J/g), SED (J/cm<sup>3</sup>) and apparent density of bone (g/cm<sup>3</sup>), respectively. The local bone density changes if the external impetus exceeds the lower or upper threshold, defined by the reference stimulus ( $K$ ) and lazy zone with the bandwidth of  $2\delta$ . Thus, the density increment  $\Delta\rho$  during the time interval  $\Delta t$  can be formulated as

$$\Delta\rho = \begin{cases} C_a [\mathcal{E} - K(1+\delta)]\Delta t - C_{or} [\mathcal{E} - K(1+\delta)]^2 \Delta t, & \text{if } \mathcal{E} > K(1+\delta) \\ 0, & \text{if } K(1-\delta) < \mathcal{E} < K(1+\delta) \\ C_{ur} [\mathcal{E} - K(1-\delta)]\Delta t, & \text{if } \mathcal{E} < K(1-\delta) \end{cases} \quad (6.14)$$

s.t.  $0.69 \text{ g/cm}^3 < \rho_{can} < 1.53 \text{ g/cm}^3$ ,  $1.70 \text{ g/cm}^3 < \rho_{cort} < 1.90 \text{ g/cm}^3$

where  $C_a$ ,  $C_{or}$  and  $C_{ur}$  are bone apposition, over-loading resorption and under-loading resorption rate constants, respectively [199]. In this study, each time increment  $\Delta t$  represents a month, hence 48 iterations for 4 years. The remodelling iterations, together with heterogeneous mapping of Young's modulus, were executed through a Fortran-compiled user subroutine in Abaqus as outlined in a flowchart (Fig. 6.5).

The initial reference values of remodelling parameters are listed in Table 6.3 [28, 153, 189]. X-rays were taken at the end of Year 1, 2, 3 and 4 after the installation of FPD, denoted as the time points of  $T_1$ ,  $T_2$ ,  $T_3$  and  $T_4$ , respectively. Four groups of algorithmic parameters were introduced to represent multiple stages of bone remodelling progression from  $T_0$  to  $T_1$  ( $T_{01}$ ),  $T_1$  to  $T_2$  ( $T_{12}$ ),  $T_2$  to  $T_3$  ( $T_{23}$ ) and  $T_3$  to  $T_4$  ( $T_{34}$ ), respectively (Table 6.3). It is noted that all the parameters for  $T_{01}$  are the same as those for  $T_{12}$  as the X-rays taking started at  $T_1$ . At the end of each year, the remodelling parameters are regulated to accommodate the change of virtual X-ray results for a better match to the clinical data. In particular, the volume average of apparent density and stimulus, as formulated in Eq. 6.15, were calculated for assessment of the bone remodelling outcomes.

$$\rho_{avg} = \frac{1}{V} \int_V \rho dV \approx \frac{\sum_i^n \rho_{ele}^i V_{ele}^i}{\sum_i^n V_{ele}^i}, \quad \mathcal{E}_{avg} = \frac{1}{V} \int_V \mathcal{E} dV \approx \frac{\sum_i^n \mathcal{E}_{ele}^i V_{ele}^i}{\sum_i^n V_{ele}^i} \quad (6.15)$$



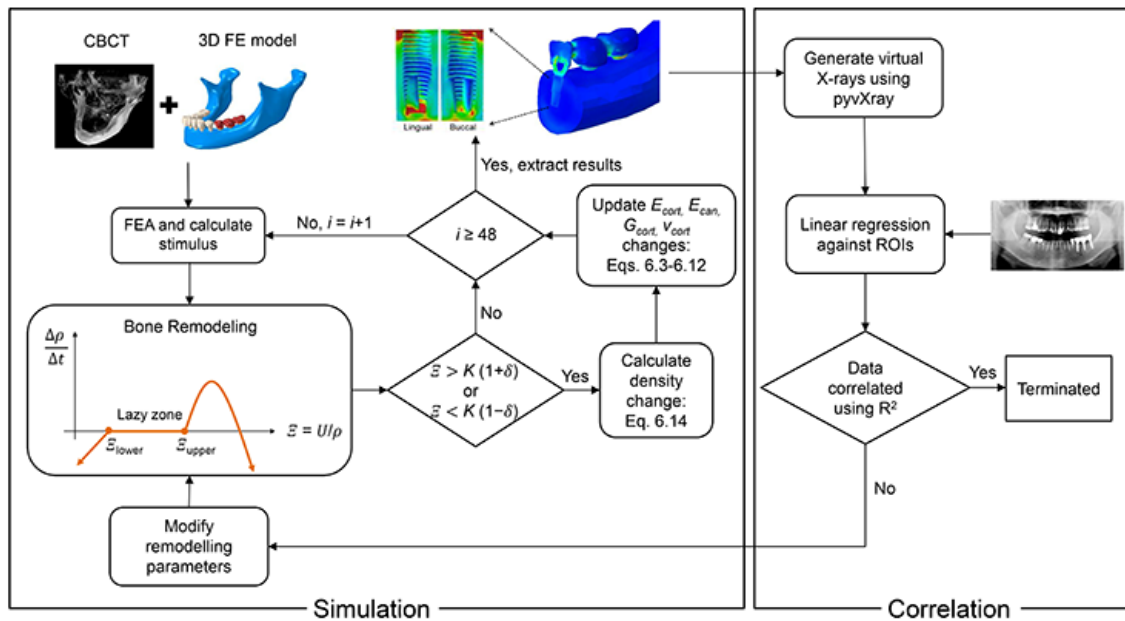


**Fig. 6.5** Flowchart of the SED-based bone remodelling algorithm and the correlation with clinical follow up. Please refer to Reference 181 for better readability if needed.

**Table 6.3** Multi-stage bone remodelling parameters

Symbol	Parameter	Reference	Value				Unit
			$T_{01}^*$	$T_{12}$	$T_{23}$	$T_{34}$	
$C_a$	Bone apposition rate	18	$C_{a01}$ (3.37)	$C_{a12}$ (3.37)	$C_{a23}$ (4.24)	$C_{a34}$ (5.64)	$\text{month} \cdot \text{g}/\text{cm}^5$
$C_{or}$	Over-loading resorption rate	600	$C_{or01}$ (5074)	$C_{or12}$ (5074)	$C_{or23}$ (793)	$C_{or34}$ (4484)	$\text{month}^3 \cdot \text{g}/\text{cm}^7$
$C_{ur}^{**}$	Under-loading resorption rate	18	$C_{ur01}$ (3.37)	$C_{ur12}$ (3.37)	$C_{ur23}$ (4.24)	$C_{ur34}$ (5.64)	$\text{month} \cdot \text{g}/\text{cm}^5$

$K$	Reference stimulus	0.004	$K_{01}$ ( $2.90 \times 10^{-5}$ )	$K_{12}$ ( $2.90 \times 10^{-5}$ )	$K_{23}$ ( $3.82 \times 10^{-5}$ )	$K_{34}$ ( $1.28 \times 10^{-4}$ )	J/g
$\delta$	Half bandwidth	0.1	$\delta_{01}$ (0.013)	$\delta_{12}$ (0.013)	$\delta_{23}$ (0.052)	$\delta_{34}$ (0.0075)	

\*All parameters for  $T_{01}$  are equal to those for  $T_{12}$

\*\* $C_a = C_{ur}$

#### 6.2.4 Model validation

In this study, the remodelling parameters were regulated in a time-dependent manner to match clinical X-ray follow-up data. The FE model and bone remodelling algorithm were validated by correlating with the clinical X-rays data obtained at  $T_1$ ,  $T_2$ ,  $T_3$  and  $T_4$ , respectively. Correspondingly, the FE-based virtual X-ray images were generated from the simulated density mappings at  $T_1$ ,  $T_2$ ,  $T_3$  and  $T_4$ , using pyvXray, a python program converting user-defined fields into virtual X-rays, which was also employed in other relevant studies [39, 200].

Fifteen ROIs, five for each implant area, were used to correlate simulated remodelling results with the four year clinical follow-up data. Specifically, the cervical, middle and apex regions at both mesial and distal ends were selected as ROIs, as shown in Fig. 6.3h. The changes of mean greyscale values of these 15 ROIs were calculated based on both clinical X-rays and FEA-driven virtual X-rays using MATLAB (MathWorks, Inc., Massachusetts, US).

A linear regression analysis was conducted, using GraphPad Prism 7 (GraphPad Software, Inc., CA, US), to evaluate the coefficients of determination ( $R^2$ ), coefficients of correlation ( $R$ ) and p-values.  $R^2$  and  $R$  were calculated for the correlation between the clinical and computational data, in terms of the annual changes in greyscale value which indicates density changes at 15 ROIs. The p-values were calculated to test against the null hypothesis

that the overall slope of fitted line is zero. It should be noted that, the linear regression was implemented for three time periods, i.e. T<sub>12</sub>, T<sub>13</sub> and T<sub>14</sub> for a better clinical relevance.

### 6.3 Results

#### 6.3.1 Model validation

Shown in Fig. 6.7 and Table 6.4 were the results of bone remodelling validation based on the linear regressions between the annual density change (%) of clinical X-rays and FEA virtual X-rays images. It was observed that the use of constant remodelling parameters resulted in statistically unsatisfactory R<sup>2</sup>, R and p-values over three time periods, i.e. T<sub>12</sub>, T<sub>13</sub> and T<sub>14</sub>. Thus, a strong linear correlation between the FE remodelling results and clinical data, which requires R not less than 0.7 [201], cannot be derived. Conversely, the multi-stage model, incorporating time-varying stage-based remodelling parameters, presented considerably higher R<sup>2</sup> and R and hence better association between FE remodelling results and clinical data, with the p-values less than 0.001. Specifically, the R<sup>2</sup> values from the multi-stage remodelling procedure were evaluated to be 0.61, 0.53 and 0.65 for T<sub>12</sub>, T<sub>13</sub> and T<sub>14</sub>, respectively and the corresponding R values were 0.78, 0.73 and 0.81 (Fig. 6.7). A strong correlation can therefore be obtained between the multi-stage bone remodelling results and the clinical follow-up data.

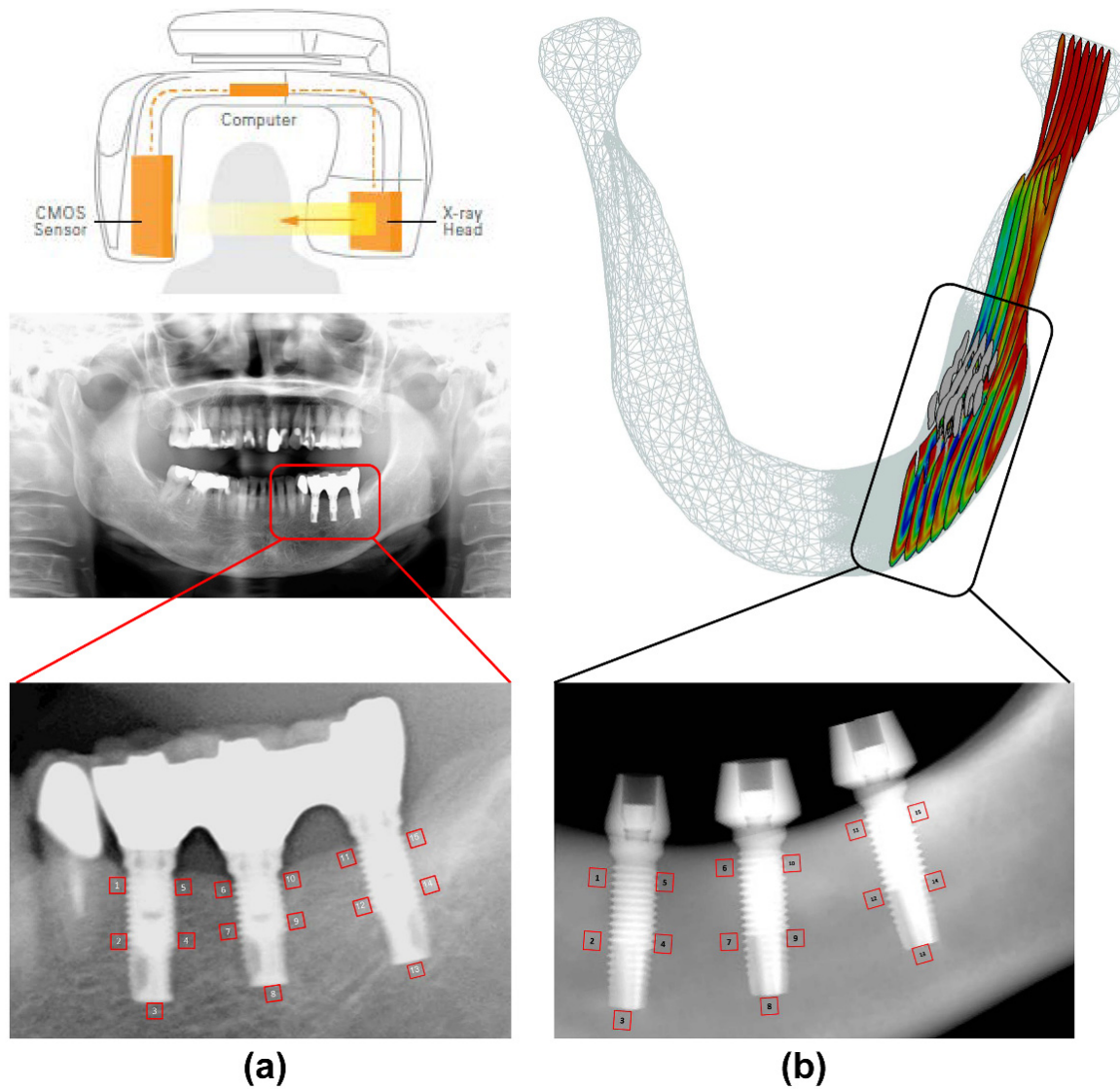


**Fig. 6.6** Estimation of mean greyscales of 15 ROIs, sized 30×30 pixels; **(a)** X-ray 4 years since the installation of FPD; **(b)** FEA-driven virtual X-ray obtained at Iteration 48 (Year 4).

**Table 6.4** Goodness of fit between simulation and experiment

Remodelling model	T <sub>12</sub>			T <sub>13</sub>			T <sub>14</sub>		
	R <sup>2</sup>	R	p value	R <sup>2</sup>	R	p value	R <sup>2</sup>	R	p value
Linear	0.26	0.49	0.0514	0.07	0.26	0.34	0.06	0.24	0.39
Multi-stage	0.61	0.78	0.0006	0.53	0.73	0.0022	0.65	0.81	0.0003

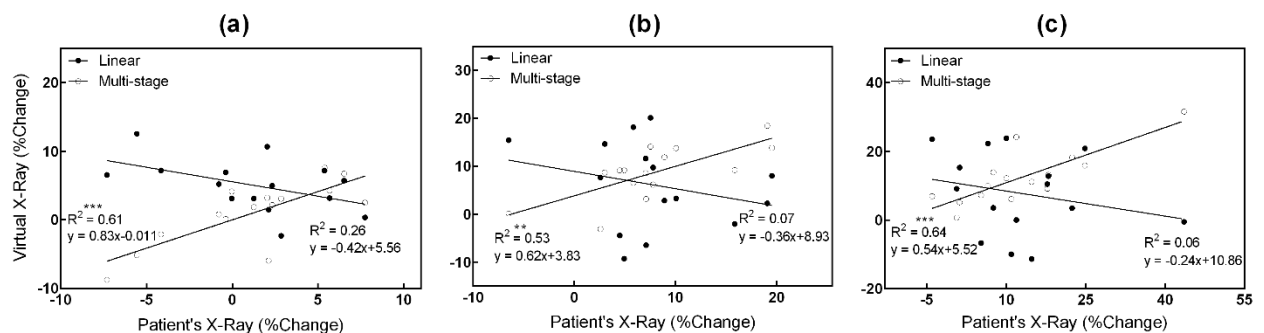


**Fig. 6.7** Statistical comparison between linear and multi-stage bone remodelling algorithms: linear regression analysis between the ROI greyscale changes of subject's four-year X-rays and FEA-based reversed X-rays, for (a) T<sub>12</sub>, (b) T<sub>13</sub>, (c) T<sub>14</sub>.

### 6.3.2 Effects of FPD configurations

The density contours from FEA-driven remodelling simulation indicated that both bone apposition and resorption, occurring in different patterns, could be observed in PROIs for the four different denture configurations (Fig. 6.8). Models 3I and DCBr generated positive bone gains around all of their supporting implants, whereas bone resorption was found in Models Br and MCBr. In the P<sub>2</sub> region, all three designs (Models 3I, Br and DCBr) induced noticeable bone apposition immediately around the mesial and distal aspects of the peri-implant neck and implant apex-cancellous bone interface areas (Fig. 6.8a). Both Models 3I and DCBr presented progressive appositional growth of bone throughout the four year period for the majority of PROIs, whereas Model Br exhibited an observable bone density decrease at the regions other than neck and apex. Similarly for the M<sub>1</sub> PROI, bone gains were appreciable in the areas close to the neck and apex at Month 24 but plateaued thereafter with Models 3I and DCBr (Fig. 6.8b). Model DCBr also showed apposition of apparent bone at the regions adjoining superior threads, while Model 3I resulted in a higher bone density in mid-

implant area. No detectable density change was visualized in Model MCBr, which was also true in area M<sub>2</sub> (Fig. 6.8c). The other two prosthetic configurations, Models 3I and Br, resulted in bone apposition largely around the distal necks, and moderately around the first few threads in Model Br.

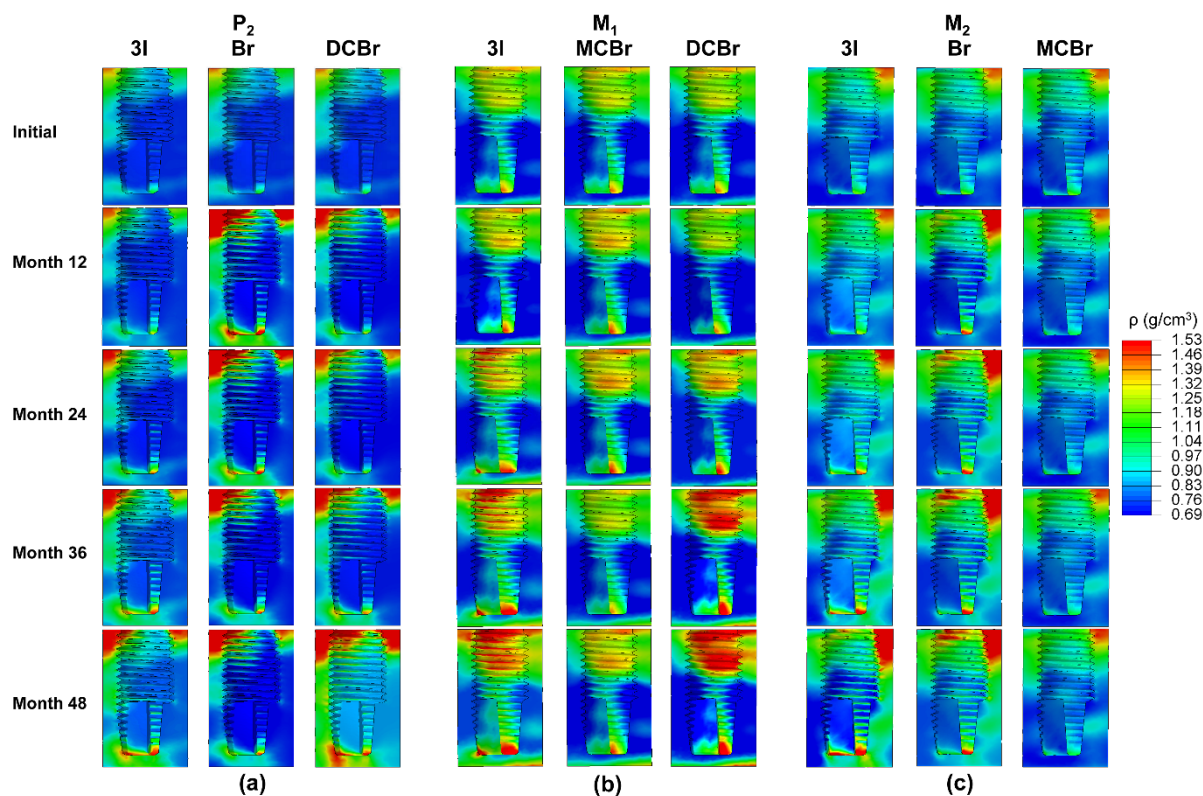


**Fig. 6.8** Contours of PROI density evolutions in mesial-distal cutting plane over 4 years at (a) P<sub>2</sub> area; (b) M<sub>1</sub> area; (c) M<sub>2</sub> area.

The aggregate quantifications of bone remodelling in terms of density and stimulus development in different prosthetic configurations were compared schematically in Fig. 6.9, where the responses differed dramatically. For the P<sub>2</sub> PROI, both Models 3I and DCBr exhibited similar trends with visible bone apposition towards T<sub>4</sub> but Model Br presented the opposite trend (Fig. 6.9a). The period T<sub>34</sub> saw accelerated bone growth in Models 3I and DCBr, with 29.7% and 39.5% being the total density increases over the four year period respectively. By comparison, the bridged prosthesis (Model Br) registered merely 2.7% bone density

apposition at Year 4, down from 9.3% increase at Year 1. Likewise, Models 3I and DCBr demonstrated comparatively noticeable bone apposition around the supporting implants in the M<sub>1</sub> regions (14.1% and 15.4% respectively in Fig. 6.9b & e). The growth rate plateaued at Month 42 for the 3-implant-support design and stayed relatively steady with Model DCBr since Month 8 following an unsubstantial trough. The bone remodelling activity around the M<sub>1</sub> region with Model MCBr was, by comparison, barely discernible with the bone density change less than 1% throughout the observation period. Similarly, this mesially cantilevered prosthetic design prompted virtually no bone gain in the vicinity of the M<sub>2</sub> region, with only 0.1% density increase (Fig. 6.9c & f). Its non-cantilevered counterparts, on the other hand, presented stable density increase spanning four years, up 8.1% and 10.5% respectively compared with the initial densities. In summary, Model 3I witnessed overall steady bone density increase around peri-implant regions, although marginal resorption occurred during the first year at the M<sub>1</sub> region. A similar pattern was recorded for Model DCBr with better bone formation outcomes than Model 3I, but perceptible bone resorption was found in Models Br and MCBr.

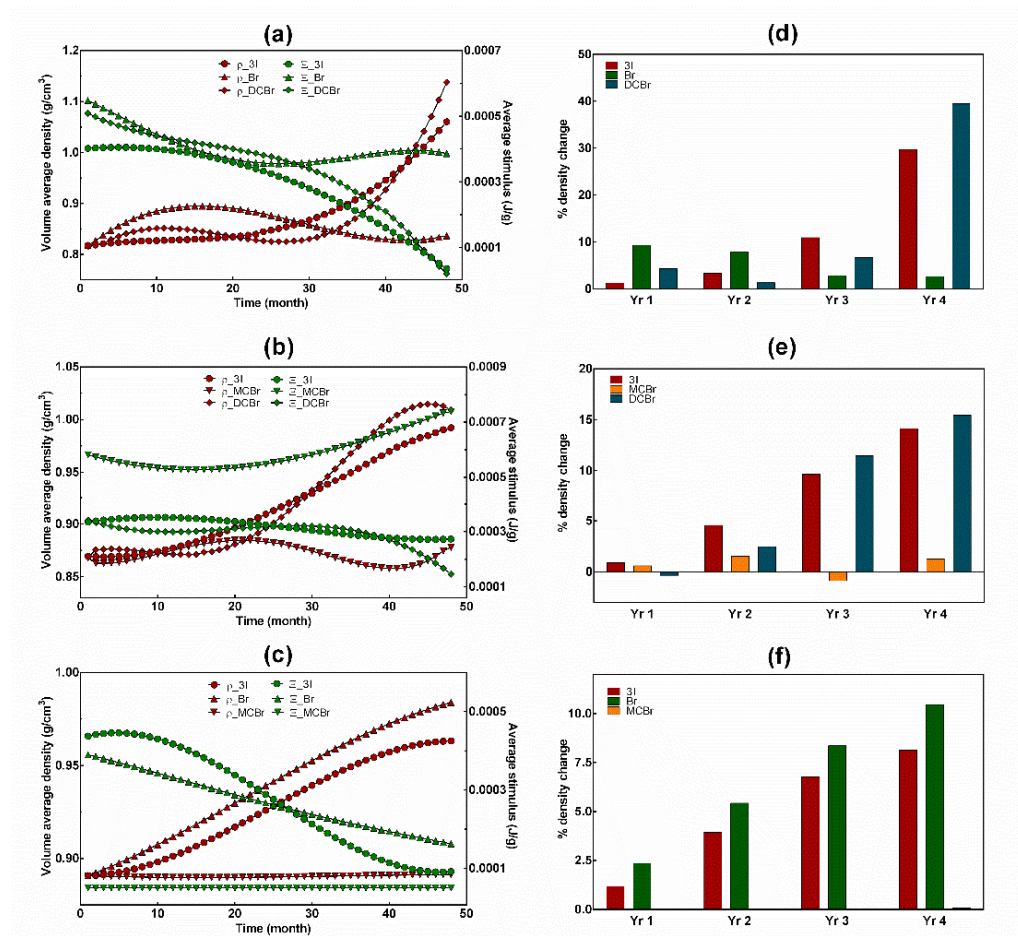


**Fig. 6.9** Volume average density and SED progression of PROIs over 4 years on (a) P<sub>2</sub> regions; (b) M<sub>1</sub> regions; (c) M<sub>2</sub> regions; quantification of density percentage changes at (d) P<sub>2</sub> regions; (e) M<sub>1</sub> regions; (f) M<sub>2</sub> regions. Please refer to Reference 181 for better readability if needed.

### 6.4 Discussion

One critical selection criterion for dental prosthetics is a satisfactory long-term bone remodelling outcome, which signifies a dynamic process. The bone remodelling rate, either of apposition or resorption, is not considered to be constant [178, 202]. The reference stimulus and bandwidth of the quiescent period of bone remodelling can also vary over time from a physiological perspective. The present study, through the correlation with the clinical follow-up, explored this phenomenon from a biomechanical standpoint. Despite the recognition of the unsteady nature of bone remodelling, most computational studies reported in existing literature



assumed constant remodelling parameters [28, 153, 175]. In this study, utilizing constant bone remodelling parameters, the FEA-based remodelling density change within ROIs were statistically inconsistent with the clinical X-ray data, as indicated by extremely low  $R^2$  and  $R$  as well as unacceptably high p-values (Table 6.4).

The refinement of computational remodelling by integrating with multi-stage remodelling parameters, i.e. adjusting the remodelling parameters yearly to better match clinical data over a 4-year period, was able to simulate the dynamic nature of bone adaptation properly with a significantly better correlation with the clinical follow-up data. This affirms that bone remodelling progression is non-steady with variant rates and stimulus references during the rehabilitation period (Table 6.3). Furthermore, the absence of clinical data could render the time interval of the bone remodelling simulation inconsistent without physical meaning. In other words, any arbitrary time unit proposed for remodelling simulation, e.g. hour, week, year, without the corresponding time-dependent *in-vivo* data for validation, has limited predictive capability and clinical relevance. On the other hand, the time step (iteration) used in the present simulation was validated to be equivalent to one month and thereby shown to be illustrative of the bone adaptation, both *in silico* and *in vivo*.

In the current study, it was suggested that the implant neck and apex regions underwent positive bone turnover as bone apposition occurred, regardless of the density variation over time in other regions. This is in agreement with other simulation studies [39, 153, 203], though the magnitude of appositional increases in the present patient-specific study was lower in general. This can be attributed to different bone morphologies, genders, ages and pathological factors associated with the subjects. However the results in this study were validated against follow-up clinical data, thus providing insights into the bone remodelling and associated biomechanics regarding implant supported FPD.

It is also noteworthy that at the P<sub>2</sub> PROI, both Models 3I and DCBr caused steep increases in bone density towards Month 48, while for other bone apposition cases the gain levelled off (Fig. 6.9a-c). This may be attributed to the resorption term (Eq. 6.14) starting to dominate the remodelling rate. Thus continuously increasing SED may, if the follow-up and corresponding FE-based remodelling simulation proceed further, decrease the overall PROI density. This differs from the results reported by Rungsiyakull *et al.* [153] who found all average densities of ROIs plateauing towards Month 48. The time-dependent regulation of remodelling constants enabled the current dynamic algorithm to better conform to the development of patient-specific bone remodelling at different timeframes.

The remodelling study indicates that the conventional prosthetic design, namely Model 3I may still be amongst the most reliable surgical options for stable bone growth surrounding all supporting implant units without visible net resorption over all the time intervals concerned. The more evenly distributed mechanobiological stimuli with Model 3I, in comparison with other configurations where the pontic structure exists, render three PROIs bearing relatively more balanced loads and hence potentially avoiding inordinate or insufficient stimuli to bony tissues as well as relevant osteocytes and physiological factors regulating bone turnover. Model Br, another typical FPD, may not be suitable for this particular patient due to the considerable bone resorption at the peri-mid-implant areas. Arguably the worst possible scenario occurred with the use of Model MCBr, in which no obvious total bone density variation emerged. Model DCBr, usually installed due to inadequate bone volume in posterior regions, generated similar bone density progression patterns to Model 3I and even higher bone appositional turnover than Model 3I.

The underperformance of Model MCBr can be ascribed to the higher and lower resultant occlusal loads on M<sub>1</sub> and M<sub>2</sub> units respectively (Fig. 6.10). The former caused overloading resorption and the latter underloading resorption. However it is challenging to

accurately define the terms “overloading” and “underloading” due to the difficulty in quantification of bone remodelling *in vivo*. According to Eq. 6.14, if  $\mathcal{E}$  falls within the lazy zone whose bandwidth  $2\delta$  can also vary over time, or if the difference between  $\mathcal{E}$  and upper threshold  $K(1 + \delta)$ , defining the effective increment of remodelling energy ( $\Delta_{\text{eff}}$ ), is approximately equal to the ratio of apposition rate  $C_a$  to overloading resorption rate  $C_{\text{or}}$ , (defined as  $R_{\text{ar}}$ ), the net bone density change is estimated to be zero. These can be elucidated through the following formulae.

$$(6.16) \quad \left\{ \begin{array}{l} \text{No density change: } \left\{ \begin{array}{l} \text{formation-resorption equilibrium: } \mathcal{E} - K(1 + \delta) = \frac{C_a}{C_{\text{or}}} > 0, \text{ or } \Delta_{\text{eff}} = R_{\text{ar}} \\ \text{lazy zone: } K(1 - \delta) < \mathcal{E} < K(1 + \delta) \end{array} \right. \\ \text{Net bone apposition: } \mathcal{E} - K(1 + \delta) < \frac{C_a}{C_{\text{or}}}, \text{ or } \Delta_{\text{eff}} < R_{\text{ar}} \\ \text{Net overloading bone resorption: } \mathcal{E} - K(1 + \delta) > \frac{C_a}{C_{\text{or}}}, \text{ or } \Delta_{\text{eff}} > R_{\text{ar}} \end{array} \right.$$

During the lazy zone driven quiescent transition, there is no or very little change in bone remodelling activity, as a consequence of inactivation of responsible cells [202, 204]. On the other hand, when bone remodelling-related cells are activated, both apposition and resorption can occur simultaneously [187]. The net change of bone density is then dependent on Eq. 6.16. It can be subsequently suggested that only when  $\Delta_{\text{eff}}$  exceeds  $R_{\text{ar}}$ , overloading resorption occurs, following a period of bone apposition with a decreasing rate. This explains the unfavourable outcomes with Model MCB<sub>r</sub>. The excessively high occlusal load on M<sub>1</sub> led to vigorous stimulation, high  $\Delta_{\text{eff}}$  and predominance of overloading resorption against apposition. The lazy zone was retained for the M<sub>2</sub> region with the low occlusal force. Conversely, Model DCB<sub>r</sub> induced more evenly distributed occlusal loads and generated beneficial remodelling outcomes.

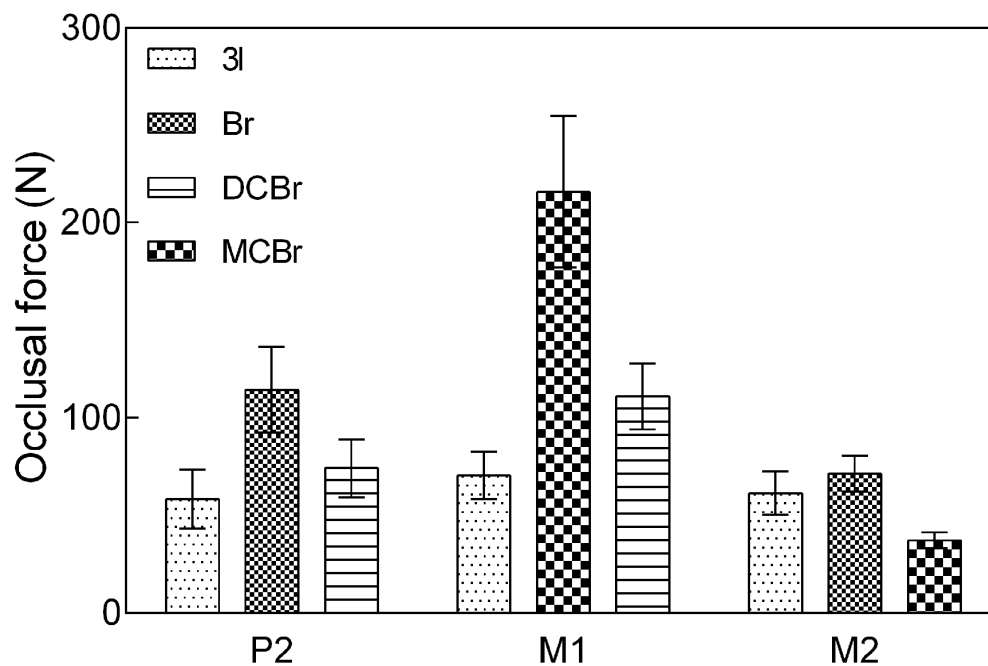


**Fig. 6.10** Average resultant occlusal forces induced by four models during MVC.

The multi-stage bone remodelling algorithm might be applied to other clinical scenarios in the future studies, e.g. different FPD configurations, implant-supported overdenture and orthopaedic treatments. In this paper, two four-unit FPD configurations, i.e. bridge Type 1 without supporting implant at M<sub>1</sub> region and bridge Type 2 without implant at P<sub>2</sub> and M<sub>1</sub> regions, are analysed further, where a 100 N occlusal load is applied in the middle of the crown [205]. From Fig. 6.11, it can be observed that the Type 2 FPD shows a faster appositional bone remodelling throughout the four year period compared with the Type 1 FPD which sees bone resorption at the P<sub>1</sub> region. However, it is advised that the accuracy of bone remodelling simulation heavily hinges on the availability of loading and medical imaging data of a specific patient.

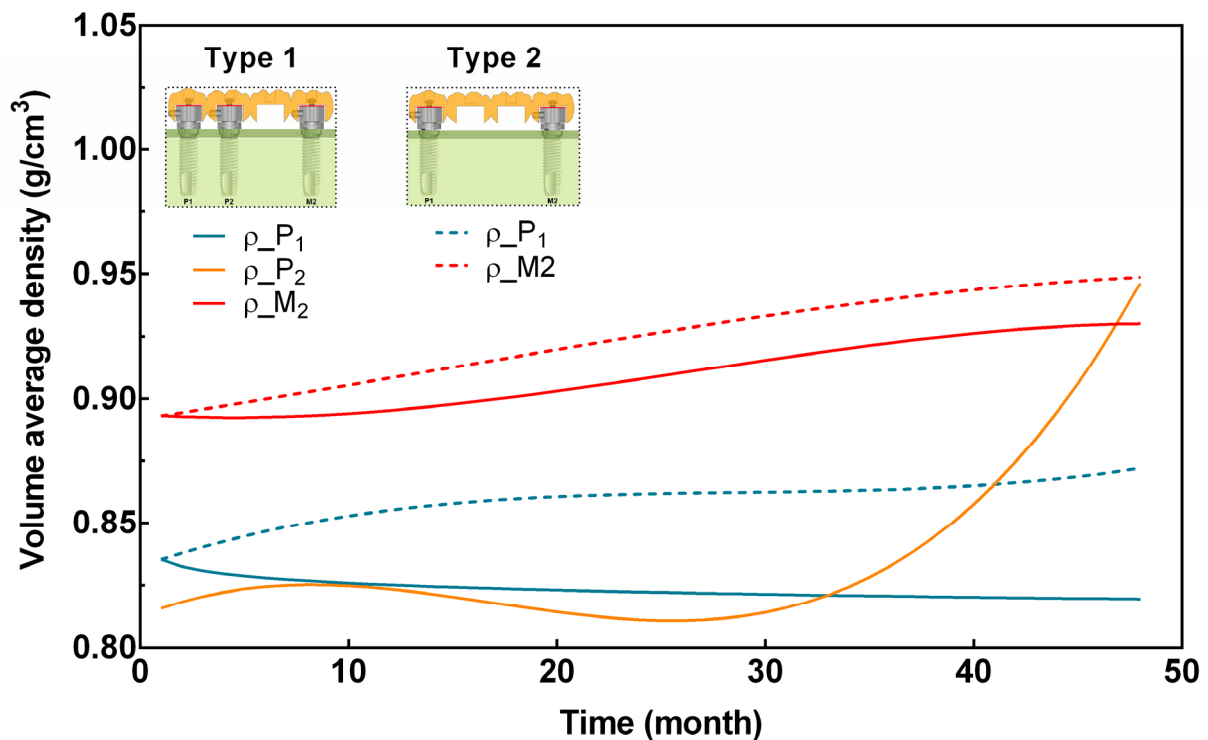


**Fig. 6.11** Preliminary analysis of bone remodelling of four-unit FPDs.

The results of the current study shed light on the clinical implications pertaining to FPD related oral restoration. The application of extended FPD should be critically assessed before implantation. In the case of bone volume insufficiency where a cantilevered FPD becomes necessary and thus the concerns of long-term bone remodelling outcomes arise, it was suggested to shorten the supporting implant [206], reduce dental arch [207], or introduce a pontics-supporting abutment [208]. In addition, peri-implantitis, one of the most common factors contributing to the bone resorption, was not diagnosed during the follow-ups in this study. This eliminated the influence of infection and provided sensible validation to the impact of occlusal loads on bone remodelling progress in different FPD configurations.

One limitation of the current study is the single sample which can hardly reflect the variety of patients and hence the common mechanobiological environment, though it can help comprehend the dynamics of bone remodelling induced by FPD in a patient-specific fashion.

The results and conclusions should be applied with caution before more samples can be recruited and studied. Although the bone remodelling parameters have physiological meanings, they were regulated in a statistical manner. Another improvement to further improve the bone remodelling algorithm is introducing surrogate model and systematically optimizing the remodelling parameters. Even higher  $R^2$  may be achieved by incorporating instantaneous time-dependent parameters with higher orders, which can be a focus of future study.

### **6.5 Conclusions**

This study has proved that a multi-stage nonlinear algorithm can effectively simulate bone remodelling and enable to better correlate with the clinical follow-up data. The results indicate that bone remodelling is a dynamic process whose time-dependency needs to be accommodated in the numerical simulation. The long-established computational protocol addressing bone remodelling, especially concerning with dental structures, requires the amendment to comply with such dynamic nature. For this particular patient, the distally cantilevered FPD outperformed all other designs, including the mesially cantilevered counterpart, which witnessed the worst bone resorption as a result of unbalanced mechanotransduction. The three-implant supported configuration was also considered to be clinically reliable in terms of favourable bone remodelling outcomes. The cantilevered FPD has uncertainty about its long-term bone remodelling outcome. It is therefore difficult to assure the clinical preference towards the FPD featuring cantilever extension without the association with occlusal loading data and patient specific conditions.

## CHAPTER 7

### MASTICATION IS NOT OPTIMALLY CONTROLLED

It has long been wondered how human mastication responds to major facial reconstruction. Measurements involving different principles have been applied to acquire or assess the muscular co-activation during normal or unhealthy stomatognathic functioning. Their accuracy and capability of direct quantification, especially when using alone, are however questioned. In this study we establish a clinically validated Sequential Kriging Optimisation (SKO) model, coupled with the finite element method (FEM) and *in vivo* occlusal records, to further the understanding of muscular functionality following a fibula free flap (FFF) surgery. The results, within the limitations of the current study, indicates the statistical advantage of agreeing occlusal measurements and hence the reliability of using the SKO model over the traditionally adopted optimality criteria. It is therefore speculated that mastication is not optimally controlled to a definite degree. It is also found that the maximum muscular capacity slightly decreases whereas the actual muscle forces fluctuate over the 28-month period.

### 7.1 Introduction

The human masticatory functionality and capability is fulfilled by the sophisticated co-activation of a group of masticatory muscles which contribute to the execution of chewing, biting, clenching, proper speech, jaw movement, etc. The patterns of mastication and hence stomatognathic performance may fundamentally change, if not in all likelihood deteriorate, following major oral interventions, such as the instalment of dental prosthesis and facial reconstruction [209-211]. Some studies however reported the opposite that the masticatory efficiency is not significantly compromised after oral surgeries [212, 213]. While the conflicting observations may be ascribable to various factors, such as the demographic variance of the subjects and different natures of cranio-maxillo-facial surgeries, a measurement system or technique for the mastication, normally functioning or potentially damaged, is particularly in demand.

For decades, electromyography (EMG) has been widely employed as a qualitative tool to describe muscular activities [214, 215] with however incapability or limitation in accurate quantification of , or wide-accepted correlation with, the joint reactions and the characteristics of motor skills, including the exact force magnitude, orientation and muscle force ratio [216]. Computer tomography (CT) is also frequently recruited to approximate the maximum capacity (MaxCap) of muscular magnitude and its direction. Optimisation methods accommodating static equilibrium, physiological constraints and objective criteria were also widely adopted to estimate the magnitude, orientation and activation ratio (AR) of muscle functioning groups during various movements [217, 218].

With often too many unknowns and insufficient equations, several objective functions have been proposed to address the indetermination of the static equilibrium due to the redundancy. Some most commonly applied optimality criteria include minimisation of



## CHAPTER 7: MASTICATION IS NOT OPTIMALLY CONTROLLED

summed muscle forces (Eq. 7.1) [219], minimisation of summed joint forces (Eq. 7.2) [220], minimisation of summed reaction forces (Eq. 7.3) and minimisation of summed elastic energies (Eq. 7.4) [217].

$$\text{Min } f_1 = \sum_{i=1}^i F_{M,i} \quad (7.1)$$

$$\text{Min } f_2 = \sum_{i=1}^i F_{J,i} \quad (7.2)$$

$$\text{Min } f_3 = \sum_{i=1}^i F_{R,i} \quad (7.3)$$

$$\text{Min } f_4 = \sum_{i=1}^i \left( \frac{l_{F,i}}{\cos^2 \alpha_i \cdot A_i} F_i^2 \right) \quad (7.4)$$

Not only were these optimality criteria chosen for the mathematical necessity but also the neurological hypothesis that the central nervous system (CNS) can systematically optimize to reduce the work or load bearing on joints and render the musculo-skeletal actions cost-efficient [221].

However, it is arguable whether these minimal principle are biologically and mathematically accurate. Firstly, it is still uncertain that which or any of these optimality criteria are the most universally correct, with conflicting results recorded. Minimal energy [217, 222], minimal AR [219] and combination of minimal muscle force and moment [223] criteria were respectively found to better agree with the EMG data for various groups of subjects compared with other criteria. There is no solid evidence and consensus about which or any of these optimality criteria can be applied to obtain the characteristics of muscle force. Meanwhile, some argue that this optimal feedback system does not exist in biological organisms [224]. Secondly, the simplification of both morphological and mathematical modelling, based on which the optimality strategies are applied, considerably lowers the

## CHAPTER 7: MASTICATION IS NOT OPTIMALLY CONTROLLED

validity. For ease of programming, the formulation has to assume single point constraints for attachments of masticatory muscles, occlusal and TMJ contacts (Table 7.1). In reality they however exhibit multiple contact points which can be different from single point scenario. Thirdly, the resultant joint and muscle force directions are pre-supposed and hence ineluctably disregards the physiological variance among the population and limits the degree of freedom. Finally, although it is acknowledged that the muscular activity control system tends to consume the minimal amount of energy [225], whose form is yet uncertain, it is reasonable to doubt the chance that this seemingly precise regime can generate a global optimal set of solutions at any arbitrary time during any random movement, with any single-objective optimisation methodology. To sum up, a systematic and quantitative methodology to accurately obtain the muscular characteristics, especially in conjunction with computing techniques, is yet to be established.

Table 7.1: Nomenclature

$F_{Ma}$	Left masseter muscle force
$F_{MP}$	Left medial pterygoid muscle force
$F_T$	Left temporalis muscle force
$F_{LLP}$	Lateral pterygoid (left) muscle force
$F_{RLP}$	Lateral pterygoid (Right) muscle force
$F_O$	Occlusal force measurement
$F_R$	Reaction force due to clenching
$\overline{F_O}$	Average occlusal measurement
f	Function of coefficient of determination

C	Mandibular canine
P <sub>1</sub>	Mandibular first premolar
P <sub>2</sub>	Mandibular second premolar
M <sub>2</sub>	Mandibular second molar
R <sup>2</sup>	Coefficient of determination
F	Muscle force matrix
F <sub>M</sub>	Muscle force
TMJ	Temporomandibular joint
F <sub>J</sub>	Joint force, i.e. TMJ reaction force
M0, M4, M16, M28	Before surgery, 4, 16 and 28 months after the surgery

The present study aims to (1) propose a more easily validated and hence physiologically and mathematically convincing approach to estimate muscular activity, with a mandibulectomy follow-up case; (2) compare the computational method, coupled with the Sequential Kriging Optimisation (SKO) technique, with previous optimality principles using statistical models; (3) analyse the muscular behaviour following the mandibular resection at different rehabilitation stages.

## 7.2 Methods

### 7.2.1 Clinical treatment and medical imaging analysis

The research protocol was approved by the research ethics committee of the Tohoku University Graduate School of Dentistry, with the reference number 26-34. Full written informed consent was obtained for the use of CT images.

## CHAPTER 7: MASTICATION IS NOT OPTIMALLY CONTROLLED

A male patient aged 66, diagnosed with the squamous-cell carcinoma at the right molar gingiva in August 2013, was recruited to undergo mandibular reconstruction with osteotomised fibular free flap (FFF). The fibular bone was harvested, segmented and modelled to accommodate the defect morphology, followed by the installation of a titanium reconstruction plate (Synthes, Solothurn, Switzerland) which was configured to be fixed monocortically (Fig. 7.1). The CT scans were performed before the surgery and at 4, 16 and 28 months after the surgery, denoted as M0, M4, M16 and M28 respectively. A removable partial denture was inserted to this patient 6 months after the surgery. However, the patient did not use it for mastication due to the hesitation in biting on the reconstructed side. The periodontal conditions of the remaining teeth and the removable partial denture was maintained at the Maxillofacial Prosthetics Clinic in Tohoku University Hospital every three months.

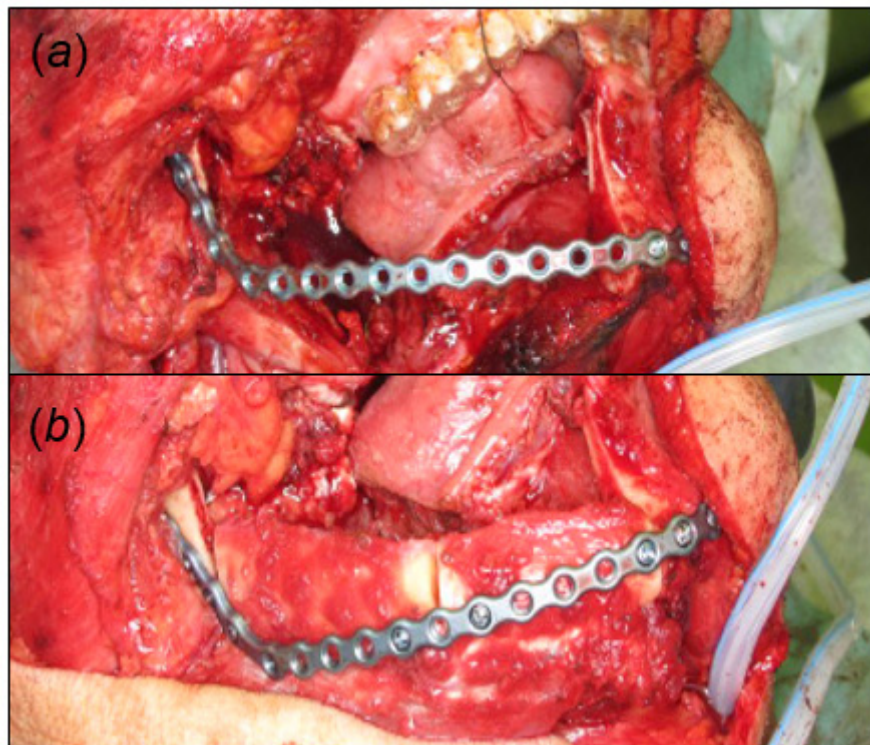


**Fig. 7.1.** (a) Intraoperative schematic of FFF affixed to the titanium fixation plate. (b) The flap pedicles were anastomosed with the thyroid artery and the external jugular vein.

The occlusal forces on the remaining teeth were measured at M4, M16 and M28 with a film to identify pressure (Dental Prescale 50H, type R, Fuji Photo Film Co., Tokyo, Japan) [216, 226] (Fig. 7.2a). The force magnitudes were calculated by film scanning using a device that is pre-calibrated (Occluzer FPD 707, Fuji Photo Film Co.). Bite records were acquired using impression of silicone (Flexicon, injection type, GC Co., Tokyo, Japan) to localise coloured points on the film and hence the occlusal contact regions on the lower arches (Fig. 7.2b & c).

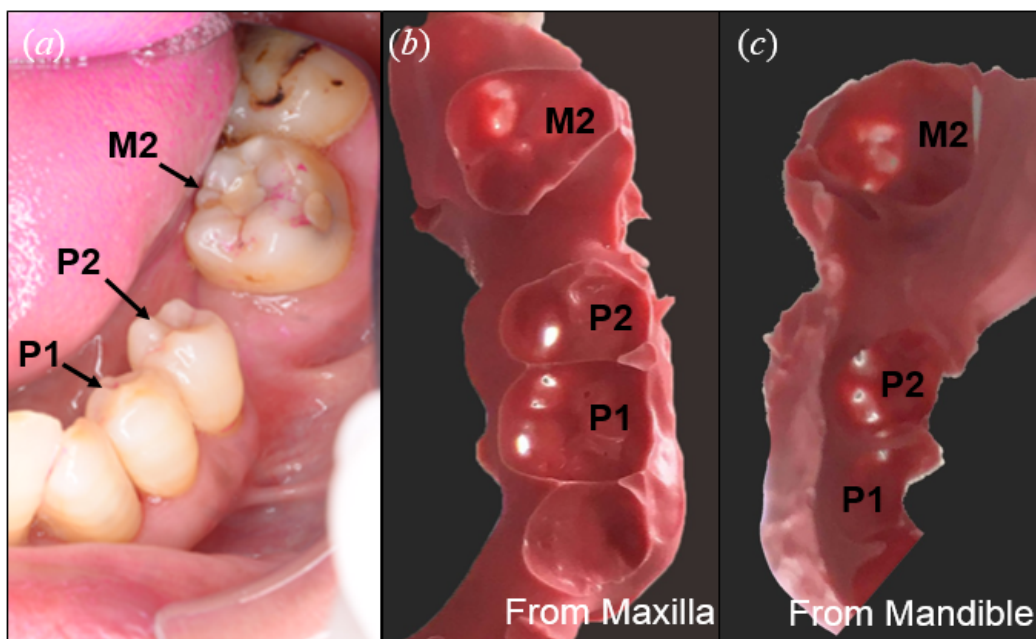


**Fig. 7.2.** (a) Occlusal force measurement using pressure-indicating film. (b) Silicone impression as bite records from maxilla view, (c) from mandible view.

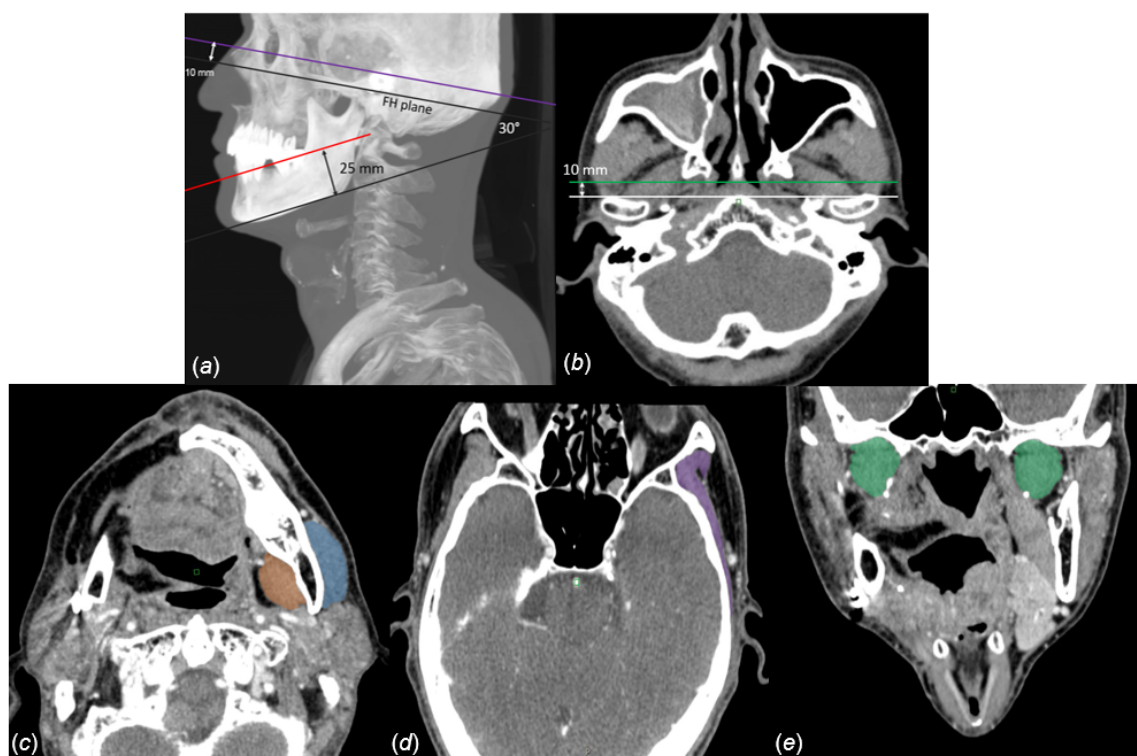


**Fig. 7.3.** Estimation of muscle physiological cross-sectional areas (PCSA). (a) Reference planes for measuring PCSA of  $F_{Ma}$  (red line),  $F_{MP}$  (red line) and  $F_T$  (purple line) and (b)  $F_{LP}$  (green line). (c) Examples of muscle PCSA of Ma and MP, (d) T and (e) LP.

Maximum muscle construction instantaneous force ( $F_{max}$ ), or the maximum muscular capacity (MMC) is calculated by multiplying the physiological cross-sectional area (PCSA) with a scaler of  $40 \text{ N/cm}^2$  [216, 227-229]. Thus, each muscle force was determined according to the following formula:

$$F_{max} = \text{PCSA} \times 40 \quad (7.5)$$

The PCSA were determined from the muscle cross-sections measured using the CT sectional images of this patient. The measurement was conducted according to the previous methods [229, 230]. The reference plane of temporalis was defined as a plane parallel to the FH plane, 10 mm upper from FH plane. The reference plane of lateral pterygoid was defined as a plane perpendicular to the FH, 10 mm medio-anterior from the lateral pole of the

mandibular condyles along the muscle direction. In total eleven measurements of the Ma, MP and T were taken on each side, 5 mm above and below at 1 mm interval. For LP muscles, the measurements were taken on the on each side, 5 mm anterior and posterior at 1 mm interval.

### 7.2.2 Finite element modelling

CT images at M0, M4, M16 and M28 were registered and segmented with ScanIP 7.0 (Simpleware Ltd, Exeter, UK) and Amira 4.1.2 (Mercury Computer Systems, Inc., Chelmsford, MA, USA), based on which NURBs were generated using Rhinoceros (Robert McNeel & Associates, Seattle, US) and imported into Abaqus 6.11. The bony tissues featured CT-based heterogeneous distribution, calculated from the interpolation among the minimum and maximum densities and Hounsfield units ( $HU$ ) (Eq. 7.6) [89]. The orthotropic cortical layer was also incorporated, employing the curve fitting results in a previous study [181]. It is assumed that the periodontal ligament (PDL) is hyperelastic, complying to a 3rd order Ogden strain energy ( $U$ ) formulation (Eq. 7.7) [90, 231], where  $\bar{\lambda}_i$ ,  $n$ ,  $J^{el}$  are the deviatoric principal stretch, order number, determinant of the elastic deformation gradient, respectively, and  $\mu_i$ ,  $\alpha_i$ , and  $D_i$  are material constants [128]. The full details of FE modelling, including the material properties, can be found in a previous literature [Yoda, 2016, under review].

$$\rho = \rho_{\min} + \frac{(\rho_{\max} - \rho_{\min})(HU - HU_{\min})}{(HU_{\max} - HU_{\min})} \quad (7.6)$$

$$U = \sum_{i=1}^n \frac{2\mu_i}{\alpha_i^2} (\bar{\lambda}_1^{\alpha_i} + \bar{\lambda}_2^{\alpha_i} \bar{\lambda}_3^{\alpha_i} - 3) + \sum_{i=1}^n \frac{1}{D_i} (J^{el} - 1)^{2i} \quad (7.7)$$

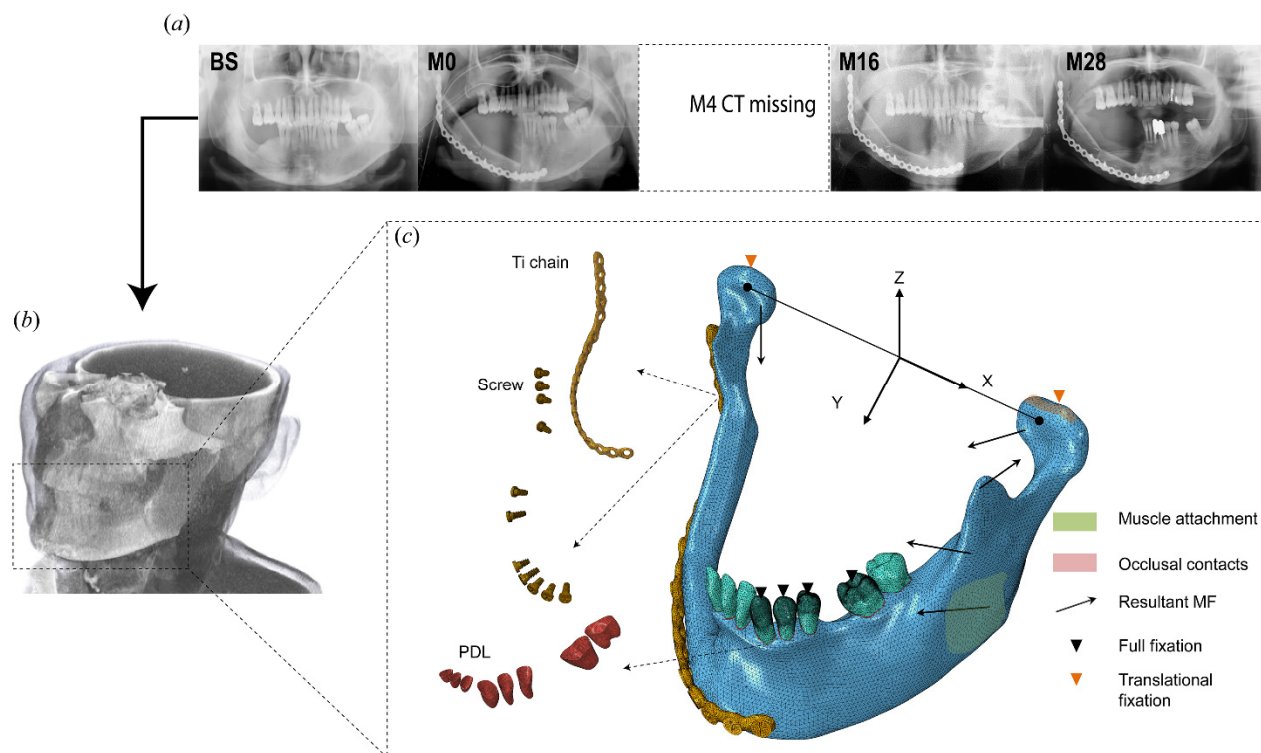


**Fig. 7.4.** (a) CTs of patient at different stages. (b) Segmentation of CT images at M16. (c) FE model with illustration of loading and boundary conditions; Model of M16 is shown.

### 7.2.3 Inverse identification of muscle force

The optimisation problem can be defined to extract a series of design variables by minimising the differences between the measurement statistics and computational results. In this study, these variables are defined in Eq. 7.8 and contained in a muscle force matrix  $\mathbf{x} = [F_{Ma_x}, F_{Ma_y}, F_{Ma_z}, F_{MP_x}, F_{MP_y}, F_{MP_z}, F_{T_x}, F_{T_y}, F_{T_z}, F_{LP_x}, F_{LP_y}, F_{LP_z}]^T$  with the subscripts denoting Cartesian components. The optimisation constraints, based on a series of previous literature and CT measurement of this study, are established for the minimum and maximum magnitudes and muscle groups ratios that restrict the relative magnitudes among different groups of muscles [196, 217, 220, 232-235]. The identification problem is then defined mathematically as the following.



$$\left\{ \begin{array}{l} \min -f(\mathbf{F}) = -f(\mathbf{F}_{Ma}, \mathbf{F}_{MP}, \mathbf{F}_T, \mathbf{F}_{LLP}, \mathbf{F}_{RLP}) \\ \text{s.t. } 1.56 \leq M_a/P_m \leq 2.15, 0.83 \leq M_a/T \leq 2.15, \\ 1.72 \leq M_a/P_1 \leq 4.07, 0.53 \leq P_m/T \leq 1.16, \\ 1.15 \leq P_m/P_1 \leq 2.61, 0.99 \leq T/P_1 \leq 4.92, \\ 59 \text{ N} \leq M_a \leq 372 \text{ N}, \\ 39 \text{ N} \leq P_m \leq 264 \text{ N}, \\ 34 \text{ N} \leq T \leq 279 \text{ N}, \\ 34 \text{ N} \leq P_1 \leq 382 \text{ N} \end{array} \right. \quad (7.8)$$

$$R_i = \left| \sum_{m=1}^k \mathbf{R}_{i(m)} \right| \quad (7.9)$$

$$\text{Coefficient of determination function: } f(\mathbf{B}) = 1 - \frac{\sum_{i=1}^n (F_{oi} - R_i(\mathbf{B}))^2}{\sum_{i=1}^n (F_{oi} - \overline{F_o})^2} \quad (7.10)$$

where  $F_{oi}$ ,  $R_i$  and  $\mathbf{R}_i$  are occlusal load measurements, resultant reaction forces and vector of nodal reactions on C, P<sub>1</sub>, P<sub>2</sub> and M<sub>2</sub> respectively and  $\overline{F_o}$  is the average measurements of occlusal loads. m and i denote the total number of nodes within the maxilla-mandibular contact area domain and the number of groups of reaction forces or occlusal measurements, respectively.

### 7.2.4 Linear programming

The linear optimisation problem is defined such that muscle forces, occlusal and TMJ loads satisfy the static equilibrium of force and moments as follows:

$$\sum \vec{F} = \sum_{i=1}^{n_m} \vec{F}_m + \sum_{i=1}^{n_j} \vec{F}_j + \sum_{i=1}^{n_o} \vec{F}_o = 0$$

$$\sum \vec{M} = \sum_{i=1}^{n_m} \vec{r}_m \times \vec{F}_m + \sum_{i=1}^{n_j} \vec{r}_j \times \vec{F}_j + \sum_{i=1}^{n_o} \vec{r}_o \times \vec{F}_o = 0$$

where  $F_m$ ,  $F_j$  and  $F_o$  are muscular, joint and occlusal forces and  $n_m$ ,  $n_j$  and  $n_o$  are numbers of muscular, joint and occlusal forces involved.  $r_m$ ,  $r_j$  and  $r_o$  are moment arms for each muscular group and evaluated from the CT images assuming single force vector, muscle attachment and contact.

### 7.3 Results

#### 7.3.1 Optimisation

The optimal Latin Hypercube sampling technique was carried out to obtain initial training points uniformly in the design space. Then, the above-mentioned SKO was utilised to identify the muscle forces with 50 sequential training points per iteration. The convergence history of expected improvement  $E(I)$  was plotted in Fig 7.5. It can be seen that at the beginning M4, M16 and M28 had large values of  $E(I)$ , indicating the optimisation (identification) processes need more training points to obtain final global optimums. When the optimisation progressed, the newly-added sequential training points had fewer contributions to acquiring better optimums. After 8, 3 and 5 iterations of sequential sampling of M4, M16 and M28, the parallelised SKO converged (i.e., the EI became small enough to obtain a global optimum). In order for SKO to converge to the final optimum, the sequential training points were yielded in the vicinity of the optimums and the boundaries of the design space. Taking M4 for an example, it was observed that SKO yielded 217 (out of 400) training points that are considered design boundary points, in which the Kriging models have a large uncertainty. It was also found that 221 points located in the neighbourhood of the final optimum, which had only 5% difference from the optimum in at least one dimension of the design space.

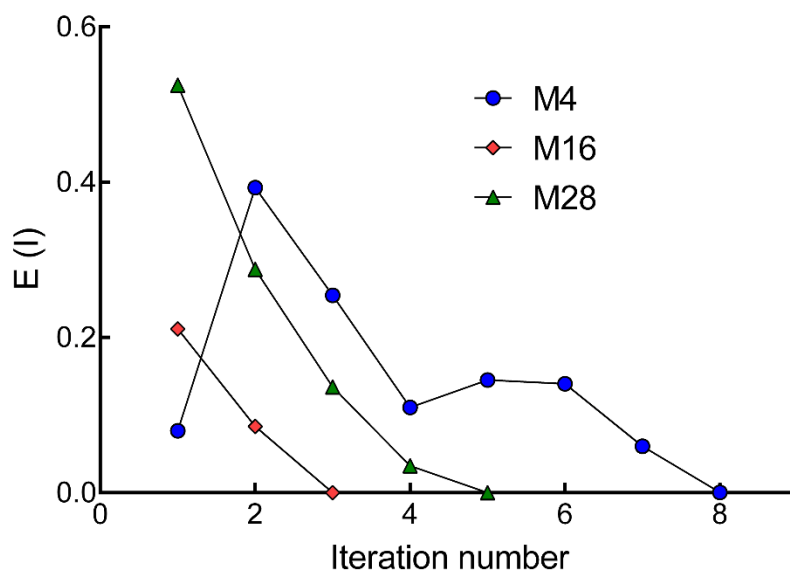


**Fig. 7.5.** History of  $E(I)$  during the identification process.

### 7.3.2 Occlusal and medical imaging analysis

The occlusal loads at M6, M16 and M28 were calculated and presented in Fig. 7.6. It can be observed that the right mandibular C, one of the remaining teeth after surgery, bore significantly less occlusal loads, 10.1 N at M6 and 11.9 N at M16, compared with P1, P2 and M2 at Month 4 and 16. It is therefore implied that P1, P2 and M2 were the primary teeth implementing the occlusal duty. M28, before which a crown was introduced, saw no sign of biting or clenching with C. In addition, occlusal loading increases were recorded from M6 to M28 for all remaining teeth. However it is noted that the standard deviation (SD) was significantly high for M28 measurements, indicating a substantial discrepancies among multiple measuring results.

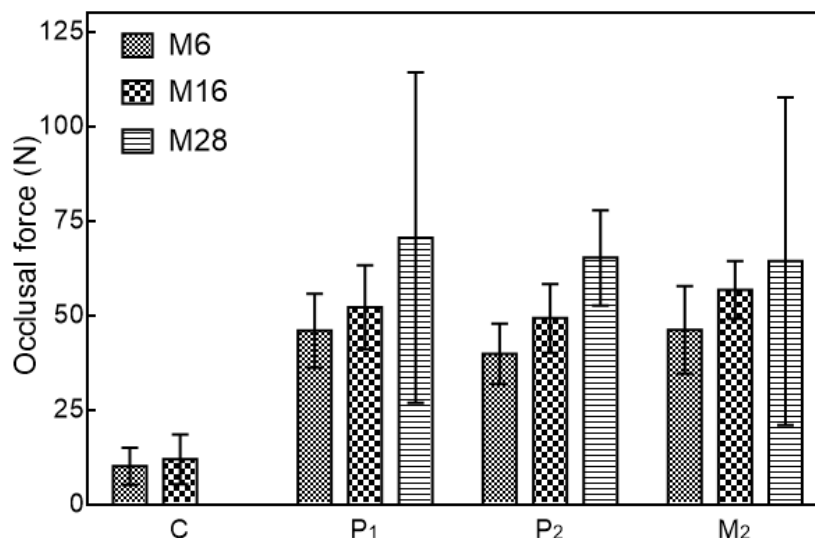


**Fig. 7.6.** Occlusal loading changes with standard deviations, 6, 16 and 28 months after mandibular reconstruction

### 7.3.3 Muscular force identification

The PCSA were measured and presented in Fig. 7.7a. Generally the decline trends can be observed for most of the time and muscle groups from M0 to M16, except for LLP and RLP which saw a slight capacity growth from M0 to M4 and from M16 to M28. In addition, no significant change can be recorded from M16 to M28 for all groups. The similar trend, due to the linearity, occurred to the maximum capacity of masticatory muscles which were estimated accordingly and presented in Fig. 7.7b. All five groups of muscles experienced visible declines in magnitude from M4 to M16 and kept relatively unchanged thereafter (Fig. 7.7b). The maximum capacities of Ma, MP, T, LLP and RLP were calculated to be 196.0 N – 206.5 N, 145.4 N – 151.3 N, 147.1 N – 151.7 N, 181.7 N – 191.2 N and 186.2 N – 203.6 N, respectively (Eq. 7.5). LLP and RLP, the only muscle pair of this resected mandible, presented comparably similar magnitudes throughout the entire observation period.

On the other hand, the actual muscle forces, based on the optimisation results, presented different time-dependent patterns. The magnitude of Ma slightly decreased during

the treatment period while a slight increase of T magnitude was registered from M4 to M16, followed by almost no change approaching M28. By comparison, MP saw virtually no variation in magnitude, fluctuating at around 116 N. LLP and RLP, on the contrary, varied greatly with a decrease at M16 and a subsequent increase at M28. It was also indicated that MP and T exercised up to 80.3% of their corresponding maximum capacity during clenching whereas Ma, LLP and RLP used up to 58.2%, 57.3% and 49.8% of maximum muscle capacity, respectively.

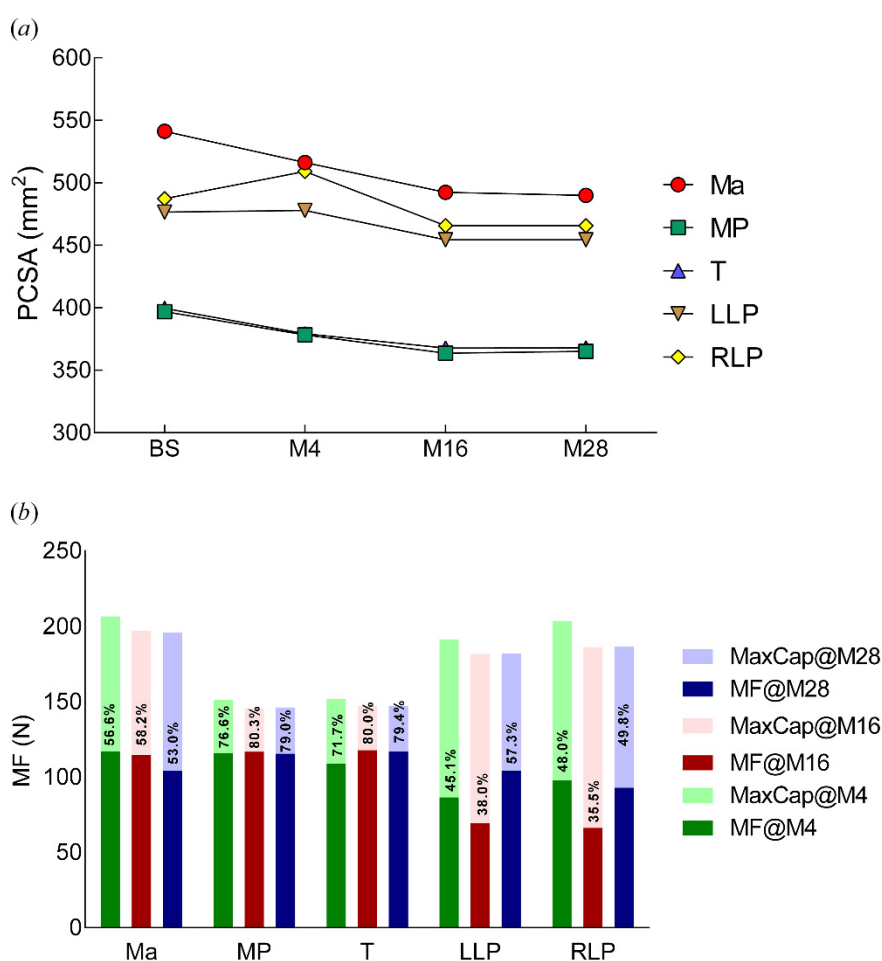


**Fig. 7.7.** (a) PCSA changes before and after surgery. (b) CT-derived maximum muscle capacities and calculated muscle force magnitudes at M4, M16 and M28; AR are also shown on top of each bar

The linear regression analysis showed that SKO technique yielded very high  $R^2$  values, i.e. 0.92, 0.97 and 0.84 for M4, M16 and M28 respectively. The scatters generated by SKO were well fitted by the regression line  $y = x$ . Conversely,  $R^2$  values determined from the linear optimality methods were extremely low and corresponding scatters were poorly fitted by the regression line, indicating that using traditionally applied optimality criteria, it is unlikely to obtain realistic occlusal loads (Fig. 7.8a). As a result, the displacement contours generated by the linear optimality methods are visibly deviated from those by SKO method (Fig. 7.8b).

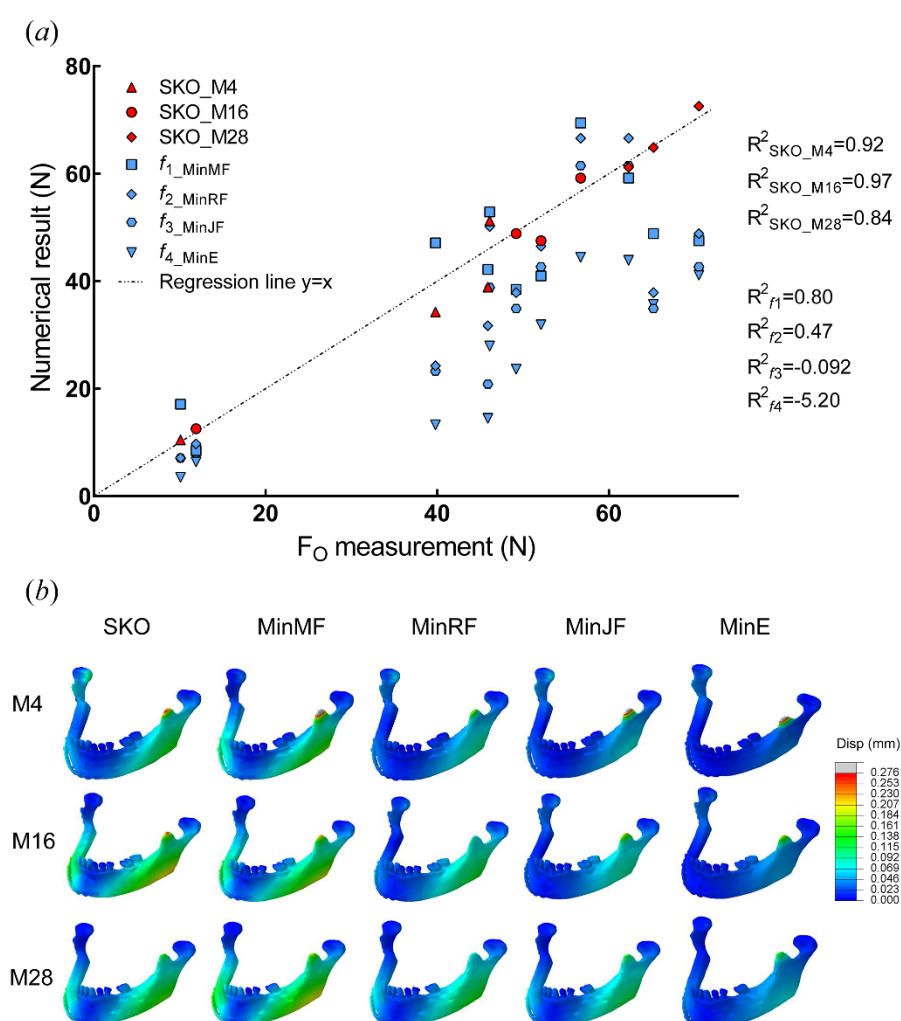


**Fig. 7.8.** (a) Regression analysis between occlusal force obtained from optimisation techniques and experimental measurements; MF, RF and JF represent muscle force, reaction force and

joint force respectively. (b) displacement contours at M4, M16 and M28, using different optimisation techniques.

### 7.4 Discussion

#### 7.4.1 SKO vs. optimality criteria

In this study the problem was approached in an inverse manner by investigating the occlusal measurements with SKO technique, by minimising the discrepancies between the empirical and FEA-based results. From the optimisation perspective, SKO can allow to exploit local regions and explore sparse regions (i.e., the boundary of the design space) of the design space to iteratively drive the identification. The local exploitation could improve the local accuracy of the Kriging models around the final optimums while the global exploration was beneficial to enhance the overall accuracy of the Kriging models. SKO provided a flexible optimisation way to identify the muscular forces in an adaptive manner by combining these two sequential sampling strategies. Besides, parallelised sequential sampling enabled to run multiple simulation models at each iteration, which could take advantage of the ever-growing computational capacity to accelerate the identification process. Furthermore, SKO is generally recognised as a global optimisation algorithm. Thus, SKO is more likely to avoid converging to local optimums, compared to traditional gradient-based algorithms such linear programming.

The SKO method in this study accurately evaluated the muscle force magnitudes and directions during maximum intercuspation at different rehabilitation time points, by virtue of the *in vivo* measurements of occlusal loads. In contrast, the fundamental of some formerly proposed principles assumes that the input or output, MF, RF and JF in this case, or the combination of both tends to be systematically minimised during muscle co-activation, a presumption not limited to the muscular activities involved in mastication or clenching [217-

221]. Our comparative results have shown that SKO can detail the resultant muscular force magnitudes and directions with very high  $R^2$  values against occlusal measurements, ranging from 0.84 to 0.97, attesting to its accuracy. Conversely, the optimal control theory based criteria resulted in occlusal loads significantly diverging from the experimental measurements (Fig. 7.8).

### ***7.4.2 The irrationality of optimality for mastication***

The deduction herein is that while our neuro-musculo-skeletal system still tends to reduce, if not to minimize the consumption of energy, MF in this study being an example, or the potential detriment to tissues, e.g. RF or JF during mastication, it is unlikely to provide an absolute optimal behaviour which may define the limit our body can hardly achieve. It is sufficiently good rather than optimally best [224]. The CNS may be as complex as a computing power but would address the masticatory coordination in a way different from the single-objective optimisation method which seeks ideal solutions based on a large number of statistically randomised samples and corresponding outputs. On the other hand, the CNS has no capability of foreseeing results but to accumulatively reference constant feedbacks from the biochemical environments. This inherent distinction between human and computer can contribute to the unfavourability of using traditional optimality criteria to understand muscular activation and functionality. Despite the ongoing popularity of minimisation strategy applied in human locomotion and neuroscience researches, the forgoing conclusion is agreed by some literature which suggest that the preferable muscular patterns, e.g. during gaiting, arm or wrist movements and running may not be consistent with or dominated by a single-objective scheme minimising metabolic consumption [236-240]. However, it is not until this study that there is evidence for the irrationality of using a single optimality criterion to obtain masticatory muscle activity during mastication. Further, it is speculated that as the mastication has a relatively



narrower range of motion, compared with other types of locomotion such as gaiting and running, the CNS may have smaller domain of control to beneficially adjust the muscular activity, i.e. reduce the cost or harm.

### ***7.4.3 Clinical implications and limitations of this study***

Masticatory functionality, the most important part of stomatognathic performance, has been directly or indirectly measured using a variety of methods, including EMG [214], CT-based imaging analysis [241], gnathodynamometer [211], colour-changing gum [242], gummy jelly [243], questionnaires [244] and above-mentioned optimality criteria [217]. None of these methods alone can produce the quantification of muscle force magnitude and direction. This study provides such a novel approach to address the problem with its advantages of matching the clinical data. It was also indicated that a heavier maximum occlusal force was associated with a superior performance of mastication [245]. Therefore, the measurement of muscle force is a clinical significant to assess the recovery of stomatognathic performance.

The results show that the maximum capacity of muscular contraction can slightly decrease at the early stage of rehabilitation (Fig. 7.7b), possibly caused by the reduction of PSCA (Fig.7.7a). This was consistent with the study by Dicker *et al.* [246] where the shrinkage of PSCA was found for Ma and MP 18 months after the advancement bilateral sagittal split osteotomies. Similarly, Katsumata *et al.* [241] also reported the reduction of Ma PSCA following mandibular setback osteotomy. This could be attributable to the muscular atrophy as a consequence of the dissection of bony and muscular tissues and hence the regional interference with the blood supply [247-249]. Nonetheless, it is found that the decline of PSCA ceased after M16, indicating a stabling functioning condition for muscles of the resected regions undergoing some rehabilitation. The activation ratio and actual muscle force generated, however, witnessed dissimilar patterns with quite irregular fluctuations (Fig. 7.7b). The

## CHAPTER 7: MASTICATION IS NOT OPTIMALLY CONTROLLED

activation ratios of Ma and T with complete dentitions were reported to be between 70.3% and 77.7% [216], which is higher than AR of Ma, i.e. 53.0% - 58.2% and on par with that of T, i.e. 71.7% - 80.0% calculated in this study. This implies that the hesitation of the patient to bite, especially using the resected side, has a major effect on Ma, reducing its activation ratio by supposedly 20% from the normal. Furthermore, inconsiderable consecutive decreases in Ma force magnitude were recorded throughout the follow-up, echoing with, in spite of the different type of surgery, the study by Nakata *et al.* [250] in which the Ma activity was measured to slightly decrease 31 months after mandibular prognathism. By comparison, MP presented no significant change from M4 to M28 in both the maximum muscular capacity, activation ratio and hence the actual resultant muscle force. Similar patterns were observed with LLP and RLP for which the activation ratios and actual muscle force decreased from M4 to M16 and subsequently increased and surpassed the M4 values at M28. The loss of some major masticatory muscles in the resection side (right side) causes the non-physiological oral biomechanical situation, which can change the muscle activities for stabilizing the reconstructed mandible. The higher AR of MP and T might thus be related with the stabilisation of mandibular position.

One of the limitations of this study is the sample size. Only one patient, who underwent a major mandibular resection, is followed up. While it is not advocated, given the uniqueness of the case, to implicitly apply the proposed phenomenon to a large population, especially to those with normal masticatory functionality, the findings of this study shed lights on the insight into a more realistic masticatory pattern. The future study will therefore recruit more samples with demographic and clinical variances. Additionally, the present study focused on the static equilibrium when the occlusion occurs, whereby its dynamic characteristics were not investigated. Furthermore, the high standard deviation of occlusal measurements at M28 can render the evaluation of muscular activity less accurate, although it indicates the instability of

## CHAPTER 7: MASTICATION IS NOT OPTIMALLY CONTROLLED

masticatory patterns not long after the introduction of the dental crown. Since there is no occlusal loading data available pre-surgically, comparison between pre- and post-surgical muscular activity is impossible. Over the last decade, the many digital CAD/CAM technology have been used in the dental treatment [251]. Recently, the novel application of computational optimisation methods for manufacturing the dental prosthesis using clinical *in vivo* data, *in silico* method and 3D printing system was reported [252]. The method for calculating the muscle forces introduced in this study can improve the accuracy and reliability of such computational methods, which can greatly contribute to the future development of the digital solutions in dentistry.

## **CHAPTER 8**

### **CONCLUSIONS**

This thesis has explored a wide range of theories, algorithms and applications related to dental biomechanics, with the emphasis on the dynamics presented. The conclusions, contributions, recommendations and future study possibilities will be summarised in this chapter.

### 8.1 Orthodontics

The dynamic natures of dental structure, both in narrow and broad senses, is largely under-studied. The natural frequency and corresponding mode shapes, playing an important role in the assessment of periodontal health, have been evaluated extensively however with limitations and inaccuracy, mainly due to the assumptions used. A better accuracy means a more realistic and complete simulation model with more realistic property modelling which are adopted in our investigation, accommodating the sophistication of the morphology and property. It is shown that the integrity of the model and preciseness of the PDL property modelling are important in extracting the dynamic properties and hence the behaviours of tooth-PDL-bone complex. The mode shape, of the same integrity of modelling, is however not affected by the property change. The first several mode shapes of a complete human maxilla indicate that the external energy tends to be transferred in a linguo-buccal manner.

The dynamic property of the tooth-PDL-bone complex enables the possibility of introducing an external stimulus, cyclic force being an example, to interact with the structure and induce an amplified response as a result of resonance effect. Attempts have been made to clinically investigate the effect of mechanically induced vibration on OTM, which contributed to the invention of several commercially available devices specialised in orthodontics. The results were however conflicts and the safety issues have not been systematically addressed. Our comparative study, consisting of a clinical trial with the size of 13 patients and a computational simulation, provides with the evidence that vibration of frequency less than the first local natural frequency can dramatically amplify the PDL hydrostatic stress. This may trigger the relevant regulating chemicals and factors in the microvasculature more activated, thereby enhancing OTM. The increase of pressure level is however lower than the upper threshold of the excessive compression and tension and hence ensures the safety whereby the PDL will not undergo harmful necrosis. It is also advocated, based on the results of the current

## CHAPTER 8: CONCLUSIONS

thesis, that single-tooth vibration targeting the tooth to be moved and frequency higher than 30 Hz should be applied for better efficacy.

The other important part of orthodontic force is the static part, i.e. the magnitude. The optimal orthodontic force is always necessitated however with difficulties, one of which being the accurate localisation of the CRe. It is revealed in the thesis that a universal M/F ratio and CRe based on past experience can be inaccurate when applied to an arbitrary patient in clinic. A patient's specification should be taken into consideration. A convenient and precise method is conceptualised so that M/F ratio and CRe location of a tooth can be determined. The results show that the volume average could be an effective indicator for description and prediction of OTM, which validates the proposed hypothesis of OTM effective zone. This further implies that the tipping point of OTM is the time when the majority of the PDL volume is compressed or stretched to a critical level, i.e. the OTM-effective level (VAHS of 4.7 kPa) or the OTM-lagging level (VAHS of 16 kPa). This is also the moment when OTM, a rigid body-resembling motion, is carried forward from a previous stage to the next.

This thesis has the potential to provide the orthodontic professionals with an elaborate insight into how the dynamic properties of hard and soft tissue complex of dental structure respond to the external stimulation, thereby facilitating the orthodontic planning more effectively.

### **8.2 Oral Rehabilitation and Bone Remodelling**

This thesis investigates the configurational effects of the implanted fixed partial denture on biomechanical response and bone remodelling outcomes. A fundamental comprehension is supplemented from a computational perspective based on a heterogeneous and orthotropic model. It is advised to incorporate patient-specific loading data if possible.

## CHAPTER 8: CONCLUSIONS

The results show that the cantilevered design of a 3-unit FPD may have the risk of loss of osseointegration in the implant adjacent to the cantilever extension.

Our subsequent study approves that the mesially cantilevered FPD may see the highest potential of overloading resorption while its distally cantilevered counterpart outperform other configurations. The results are validated by the 4-year follow-up of a subject undergoing the installation of an implanted-FPD, and our newly developed multi-stage nonlinear bone remodelling algorithm. It is indicated that bone remodelling is a dynamic course whose time-dependency needs to be accommodated in the numerical simulation. The traditional tri-linear bone remodelling algorithm, based on constant remodelling parameters, should be amended to comply with such dynamic nature within the computational limitation. The optimisation methods, e.g. response surface method, sequential Kriging optimisation technique, based on the dimension of the problem, can be effectively employed to fulfil the calculation of the multi-stage parameters.

### **8.3 Muscle**

A 28-month follow-up of a jaw reconstruction case helps us understand that the co-activation of mastication may not be optimally controlled. The linear regression analysis suggests that our SKO optimisation derived muscle forces align with the occlusal measurements while conventional optimality criteria generate very small  $R^2$ , indicating a significant disagreement with clinical data. It is also indicated that the muscular functionality changes during oral rehabilitation time, echoing with the changes of occlusal loading measurements. The mechanism of muscular control involving mastication is however yet to be explored and advanced.

### **8.4 Closing Remarks**

Some take-home messages from this thesis, if any, are prepared herein. Firstly, one should always consider the dynamic properties, for the better accuracy and potential illumination on the relevant applications. Secondly, sample size of a clinical experiment is a critical problem limiting the validation of a computational simulation. Thirdly, a limited validation is significantly sounder than no validation. A researcher in this field should always reach out to seek potential interdisciplinary collaborations. Fourthly, if a computational modelling, including but not limited to image segmentation and finite element modelling, consumes a large amount of manual efforts, it may not be an effective tool applied for daily practices and commercialisation. It can still serve as a valuable research methodology. Finally, be both bold and conscientious towards assumptions for a simulation.



## REFERENCES

1. Kai D. Funke, D., *The Anatomy of a Tooth*. Available from <http://funkesmiles.com/patient-info/patient-education/tooth-anatomy/>. 2018.
2. McCoy, C. *The periodontium*. 2013; Available from: <https://www.studyblue.com/notes/note/n/the-periodontium-1-the-gingiva-and-periodontal-ligament/deck/7535863>.
3. Sherwood, I.A., *Essentials of operative dentistry*. 2010: Boydell & Brewer Ltd.
4. Smith, S. *What is Dentin?* 2013; Available from: <http://www.wisegeek.com/what-is-dentin.htm>.
5. Ireland, R., *Advanced dental nursing*. 2010: John Wiley & Sons.
6. Dibart, S., *Practical Advanced Periodontal Surgery*. 2011: John Wiley & Sons.
7. Gray, H., *Anatomy of the human body*. 1918: Lea & Febiger.
8. Kinney, J., S. Marshall, and G. Marshall, *The mechanical properties of human dentin: a critical review and re-evaluation of the dental literature*. *Critical Reviews in Oral Biology & Medicine*, 2003. **14**(1): p. 13-29.
9. Kinney, J., et al., *Resonant ultrasound spectroscopy measurements of the elastic constants of human dentin*. *Journal of biomechanics*, 2004. **37**(4): p. 437-441.
10. Tanne, K., et al., *An evaluation of the biomechanical response of the tooth and periodontium to orthodontic forces in adolescent and adult subjects*. *Journal of Orthodontics*, 1998. **25**(2): p. 109-115.
11. Natali, A.N., *Dental biomechanics*. 2003: CRC Press.
12. Fung, Y.-C., *Biomechanics: mechanical properties of living tissues*. 2013: Springer Science & Business Media.
13. Fill, T., et al., *Experimentally Determined Mechanical Properties of, and Models for, the Periodontal Ligament: Critical Review of Current Literature*. *Journal of Dental Biomechanics*, 2011. **vol. 2011**.
14. Pietrzak, G., et al., *A nonlinear elastic model of the periodontal ligament and its numerical calibration for the study of tooth mobility*. *Computer Methods in Biomechanics & Biomedical Engineering*, 2002. **5**(2): p. 91-100.
15. Jónsdóttir, S., E. Giesen, and J. Maltha, *Biomechanical behaviour of the periodontal ligament of the beagle dog during the first 5 hours of orthodontic force application*. *The European Journal of Orthodontics*, 2006. **28**(6): p. 547-552.
16. Seong, W.-J., et al., *Elastic properties and apparent density of human edentulous maxilla and mandible*. *International journal of oral and maxillofacial surgery*, 2009. **38**(10): p. 1088-1093.

## CHAPTER 8: CONCLUSIONS

17. Huang, H.M., et al., *Natural frequency analysis of periodontal conditions in human anterior teeth*. Ann Biomed Eng, 2001. **29**(10): p. 915-20.
18. Huang, H.M., et al., *Dynamic finite element analysis of the human maxillary incisor under impact loading in various directions*. Journal of Endodontics, 2005. **31**(10): p. 723-727.
19. Huang, H.M., et al., *Damping effects on the response of maxillary incisor subjected to a traumatic impact force: a nonlinear finite element analysis*. J Dent, 2006. **34**(4): p. 261-8.
20. Lee, S.Y., et al., *In vivo and in vitro natural frequency analysis of periodontal conditions: an innovative method*. J Periodontol, 2000. **71**(4): p. 632-40.
21. Wang, C.H., et al., *Natural frequency analysis of tooth stability under various simulated types and degrees of alveolar vertical bone loss*. Proceedings of the Institution of Mechanical Engineers Part H-Journal of Engineering in Medicine, 2008. **222**(H6): p. 983-989.
22. Xin, H.T., et al., *Nonlinear finite element analysis of the vibration characteristics of the maxillary central incisor related to periodontal attachment*. Medical & Biological Engineering & Computing, 2009. **47**(11): p. 1189-1195.
23. Shen, L.-K., et al., *Effects of periodontal bone loss on the natural frequency of the human canine: a three-dimensional finite element analysis*. J Dent Sci, 2009. **4**(2): p. 81-86.
24. Li, M.Y., et al., *Modal analysis of maxillary central incisor tooth*. African Journal of Biotechnology, 2009. **8**(19): p. 5088-5096.
25. Li, W., et al. *Monitoring natural frequency for osseointegration and bone remodeling induced by dental implants*. in *Computational Intelligence for Measurement Systems and Applications, 2009. CIMS'A'09. IEEE International Conference on*. 2009. IEEE.
26. Rasmusson, L., et al., *Implant Stability Measurements Using Resonance Frequency Analysis in the Grafted Maxilla: A Cross-Sectional Pilot Study*. Clinical Implant Dentistry and Related Research, 1999. **1**(2): p. 70-74.
27. Li, W., et al., *Finite element based bone remodeling and resonance frequency analysis for osseointegration assessment of dental implants*. Finite Elements in Analysis and Design, 2011. **47**(8): p. 898-905.
28. Lin, D., et al., *Mandibular bone remodeling induced by dental implant*. Journal of biomechanics, 2010. **43**(2): p. 287-293.
29. Rungsiyakull, C., et al., *Bone's responses to different designs of implant-supported fixed partial dentures*. Biomechanics and Modeling in Mechanobiology, 2014: p. 1-9.
30. Kau, C.H., J.T. Nguyen, and J. English, *The clinical evaluation of a novel cyclical force generating device in orthodontics*. Orthodontic Practice US, 2010. **1**(1): p. 10-15.
31. Leethanakul, C., et al., *Vibratory stimulation increases interleukin-1 beta secretion during orthodontic tooth movement*. Angle Orthodontist In-Press, 2015.

## CHAPTER 8: CONCLUSIONS

32. Bouziane, A., et al., *Outcomes of nonsurgical periodontal therapy in severe generalized aggressive periodontitis*. Journal of periodontal & implant science, 2014. **44**(4): p. 201-206.
33. Nishimura, M., et al., *Periodontal tissue activation by vibration: intermittent stimulation by resonance vibration accelerates experimental tooth movement in rats*. Am J Orthod Dentofacial Orthop, 2008. **133**(4): p. 572-83.
34. Li, Z., et al. *Modal analysis of a tooth-PDL-bone complex*. in *Information Science and Technology (ICIST), 2014 4th IEEE International Conference on*. 2014. IEEE.
35. Chen, J., et al., *A comparative study on complete and implant retained denture treatments – A biomechanics perspective*. Journal of Biomechanics, 2015. **48**(3): p. 512-519.
36. Chandra, S., et al., *Textbook of Dental and Oral Histology with Embryology 2007*: Jaypee Brothers Medical Publishers (P) Ltd. 366.
37. Field, C., et al., *Mechanical responses to orthodontic loading: a 3-dimensional finite element multi-tooth model*. Am J Orthod Dentofacial Orthop, 2009. **135**(2): p. 174-81.
38. Li, W., et al., *Fibre reinforced composite dental bridge. Part II: numerical investigation*. Biomaterials, 2004. **25**(20): p. 4995-5001.
39. Field, C., et al., *Prediction of mandibular bone remodelling induced by fixed partial dentures*. Journal of biomechanics, 2010. **43**(9): p. 1771-1779.
40. O'Brien, W.J., *Dental materials and their selection*. 1997: Quintessence Publ. Chicago.
41. Chen, J., et al., *A periodontal ligament driven remodeling algorithm for orthodontic tooth movement*. J Biomech, 2014. **47**(7): p. 1689-95.
42. Toms, S.R. and A.W. Eberhardt, *A nonlinear finite element analysis of the periodontal ligament under orthodontic tooth loading*. Am J Orthod Dentofacial Orthop, 2003. **123**(6): p. 657-65.
43. Cattaneo, P.M., M. Dalstra, and B. Melsen, *Strains in periodontal ligament and alveolar bone associated with orthodontic tooth movement analyzed by finite element*. Orthod Craniofac Res, 2009. **12**(2): p. 120-8.
44. Limbert, G., et al., *A transversely isotropic hyperelastic constitutive model of the PDL. Analytical and computational aspects*. Computer methods in biomechanics and biomedical engineering, 2003. **6**(5-6): p. 337-345.
45. Poppe, M., C. Bourauel, and A. Jager, *Determination of the elasticity parameters of the human periodontal ligament and the location of the center of resistance of single-rooted teeth a study of autopsy specimens and their conversion into finite element models*. J Orofac Orthop, 2002. **63**(5): p. 358-70.
46. Smith, H., *Basic Anatomical and Physiological Data for Use in Radiological Protection*. 1995, Oxford: Elsevier Science Ltd.
47. Manly, R., *Density and Refractive Index Studies of Dental Hard Tissues : II. Density Distribution Curves 1,2*. Journal of Dental Research, 1939. **18**: p. 203.

## CHAPTER 8: CONCLUSIONS

48. Caughey, T. and M. O'Kelly, *Effect of damping on the natural frequencies of linear dynamic systems*. The Journal of the Acoustical Society of America, 1961. **33**(11): p. 1458-1461.
49. Craig, R. and A.J. Kurdila, *Fundamentals of Structural Dynamics*. 2nd ed. 2006: John Wiley & Sons Inc.
50. Chowdhury, I. and S.P. Dasgupta, *Computation of Rayleigh damping coefficients for large systems*. The Electronic Journal of Geotechnical Engineering, 2003. **8**(0).
51. Clement, R., et al., *Quasi-automatic 3D finite element model generation for individual single-rooted teeth and periodontal ligament*. Comput Methods Programs Biomed, 2004. **73**(2): p. 135-44.
52. Sandstedt, C., *Einige beitrage zur Theorie der Zahnregulierung*. Nord Tand Tidsskr, 1904. **5**: p. 236-48.
53. Oppenheim, A., *Tissue changes, particularly of the bone, incident to tooth movement*. The European Journal of Orthodontics, 2007. **29**(suppl 1): p. i2-i15.
54. Kitaura, H., et al., *Effect of cytokines on osteoclast formation and bone resorption during mechanical force loading of the periodontal membrane*. The Scientific World Journal, 2014. **2014**.
55. Meikle, M.C., *The tissue, cellular, and molecular regulation of orthodontic tooth movement: 100 years after Carl Sandstedt*. The European Journal of Orthodontics, 2006. **28**(3): p. 221-240.
56. Roberts-Harry, D. and J. Sandy, *Orthodontics. Part 11: orthodontic tooth movement*. British dental journal, 2004. **196**(7): p. 391-394.
57. Masella, R.S. and M. Meister, *Current concepts in the biology of orthodontic tooth movement*. Am J Orthod Dentofacial Orthop, 2006. **129**(4): p. 458-68.
58. Meikle, M.C., *The tissue, cellular, and molecular regulation of orthodontic tooth movement: 100 years after Carl Sandstedt*. Eur J Orthod, 2006. **28**(3): p. 221-40.
59. Schwarz, A., *Tissue changes incidental to orthodontic tooth movement*. Int J Orthod, 1932. **18**: p. 331-52.
60. Bassett, C.A.L. and R.O. Becker, *Generation of electric potentials by bone in response to mechanical stress*. Science, 1962. **137**(3535): p. 1063-1064.
61. Bien, S.M., *Fluid dynamic mechanisms which regulate tooth movement*. Advances in oral biology, 1966. **2**: p. 173.
62. Singh, G., *Textbook of orthodontics*. 2015: JP Medical Ltd.
63. Rubin, C., et al., *Prevention of postmenopausal bone loss by a low-magnitude, high-frequency mechanical stimuli: a clinical trial assessing compliance, efficacy, and safety*. J Bone Miner Res, 2004. **19**(3): p. 343-51.
64. Rubin, C., et al., *Anabolism. Low mechanical signals strengthen long bones*. Nature, 2001. **412**(6847): p. 603-4.

## CHAPTER 8: CONCLUSIONS

65. Darendeliler, M.A., P.M. Sinclair, and R.P. Kusy, *The effects of samarium-cobalt magnets and pulsed electromagnetic fields on tooth movement*. Am J Orthod Dentofacial Orthop, 1995. **107**(6): p. 578-88.
66. Darendeliler, M.A., et al., *Effects of pulsed electromagnetic field vibration on tooth movement induced by magnetic and mechanical forces: a preliminary study*. Aust Dent J, 2007. **52**(4): p. 282-7.
67. Ward, K., et al., *Low Magnitude Mechanical Loading Is Osteogenic in Children With Disabling Conditions*. Journal of Bone and Mineral Research, 2004. **19**(3): p. 360-369.
68. Kopher, R.A. and J.J. Mao, *Suture growth modulated by the oscillatory component of micromechanical strain*. J Bone Miner Res, 2003. **18**(3): p. 521-8.
69. Sriram, D., et al., *Effects of mechanical stimuli on adaptive remodeling of condylar cartilage*. J Dent Res, 2009. **88**(5): p. 466-70.
70. Tanaka, E., et al., *Low-intensity pulsed ultrasound in dentofacial tissue engineering*. Annals of biomedical engineering, 2015. **43**(4): p. 871-886.
71. Bowman, S., *The effect of vibration on the rate of leveling and alignment*. Journal of clinical orthodontics, 2014. **48**(11): p. 678-688.
72. Woodhouse, N., et al., *Supplemental Vibrational Force During Orthodontic Alignment A Randomized Trial*. Journal of dental research, 2015. **94**(5): p. 682-689.
73. Leethanakul, C., et al., *Vibratory stimulation increases interleukin-1 beta secretion during orthodontic tooth movement*. The Angle Orthodontist, 2015. **86**(1): p. 74-80.
74. Pavlin, D., et al., *Cyclic loading (vibration) accelerates tooth movement in orthodontic patients: A double-blind, randomized controlled trial*. Seminars in Orthodontics, 2015. **21**(3): p. 187-194.
75. Klepac, R.K., et al., *Reports of pain after dental treatment, electrical tooth pulp stimulation, and cutaneous shock*. The Journal of the American Dental Association, 1980. **100**(5): p. 692-695.
76. Jones, M. and C. Chan, *Pain in the early stages of orthodontic treatment*. Journal of clinical orthodontics: JCO, 1992. **26**(5): p. 311-313.
77. Ngan, P., et al., *The effect of ibuprofen on the level of discomfort inpatients undergoing orthodontic treatment*. American Journal of Orthodontics and Dentofacial Orthopedics, 1994. **106**(1): p. 88-95.
78. Horowitz, L., L. Kehoe, and E. Jacobe, *Multidisciplinary patient care in preventive dentistry: idiopathic dental pain reconsidered*. Clinical preventive dentistry, 1990. **13**(6): p. 23-29.
79. Kehoe, M.J., et al., *The effect of acetaminophen, ibuprofen, and misoprostol on prostaglandin E2 synthesis and the degree and rate of orthodontic tooth movement*. The Angle orthodontist, 1996. **66**(5): p. 339-350.
80. Proffit, W.R., H.W. Fields Jr, and D.M. Sarver, *Contemporary orthodontics*. 2014: Elsevier Health Sciences.

## CHAPTER 8: CONCLUSIONS

81. Lim, H.-M., K.K. Lew, and D.K. Tay, *A clinical investigation of the efficacy of low level laser therapy in reducing orthodontic postadjustment pain*. American Journal of Orthodontics and Dentofacial Orthopedics, 1995. **108**(6): p. 614-622.
82. Marie, S., M. Powers, and J. Sheridan, *Vibratory stimulation as a method of reducing pain after orthodontic appliance adjustment*. Journal of Clinical Orthodontics, 2003. **37**(4): p. 205-208.
83. Ottoson, D., A. Ekblom, and P. Hansson, *Vibratory stimulation for the relief of pain of dental origin*. Pain, 1981. **10**(1): p. 37-45.
84. Louis, C. *Many Cutbacks but Not for Straight Teeth*. 2009; Available from: <http://www.nytimes.com/2009/04/16/fashion/16SKIN.html>.
85. Malek, S., M.A. Darendeliler, and M.V. Swain, *Physical properties of root cementum: part I. A new method for 3-dimensional evaluation*. American Journal of Orthodontics and Dentofacial Orthopedics, 2001. **120**(2): p. 198-208.
86. Yee, J.A., et al., *Rate of tooth movement under heavy and light continuous orthodontic forces*. American Journal of Orthodontics and Dentofacial Orthopedics, 2009. **136**(2): p. 150. e1-150. e9.
87. Almeida, M.A., et al., *Stability of the palatal rugae as landmarks for analysis of dental casts*. The Angle Orthodontist, 1995. **65**(1): p. 43-48.
88. Brezniak, N. and A. Wasserstein, *Root resorption after orthodontic treatment: Part 2. Literature review*. American Journal of Orthodontics and Dentofacial Orthopedics, 1993. **103**(2): p. 138-146.
89. Liao, Z., et al., *Computational modeling of dynamic behaviors of human teeth*. Journal of Biomechanics, 2015. **48**(16): p. 4214-4220.
90. Liao, Z., et al., *Biomechanical investigation into the role of the periodontal ligament in optimising orthodontic force: a finite element case study*. Archives of Oral Biology, 2016. **66**: p. 98-107.
91. Toms, S.R., et al., *Quasi-linear viscoelastic behavior of the human periodontal ligament*. Journal of biomechanics, 2002. **35**(10): p. 1411-1415.
92. Cattaneo, P.M., M. Dalstra, and B. Melsen, *The finite element method: a tool to study orthodontic tooth movement*. J Dent Res, 2005. **84**(5): p. 428-33.
93. Hohmann, A., et al., *Correspondences of hydrostatic pressure in periodontal ligament with regions of root resorption: A clinical and a finite element study of the same human teeth*. Computer methods and programs in biomedicine, 2009. **93**(2): p. 155-161.
94. Hohmann, A., et al., *Periodontal ligament hydrostatic pressure with areas of root resorption after application of a continuous torque moment*. Angle Orthod, 2007. **77**(4): p. 653-9.
95. Nakago-Matsuo, C., T. Matsuo, and T. Nakago, *Intracellular calcium response to hydraulic pressure in human periodontal ligament fibroblasts*. Am J Orthod Dentofacial Orthop, 1996. **109**(3): p. 244-8.

## CHAPTER 8: CONCLUSIONS

96. Grove, J., et al., *The Effect Of Mechanical Vibration (50 Hz Applied to Maxillary First Premolars) On Root Resorption Associated With Orthodontic Force*. Manuscript submitted for publication. 2017.
97. Quinn, R. and D. Yoshikawa, *A reassessment of force magnitude in orthodontics*. American journal of orthodontics, 1985. **88**(3): p. 252-260.
98. Reitan, K., *Some factors determining the evaluation of forces in orthodontics*. American Journal of Orthodontics, 1957. **43**(1): p. 32-45.
99. Maeda, Y., et al., *Histomorphometric analysis of overloading on palatal tooth movement into the maxillary sinus*. American Journal of Orthodontics and Dentofacial Orthopedics, 2015. **148**(3): p. 423-430.
100. Rygh, P., *Ultrastructural changes in pressure zones of human periodontium incident to orthodontic tooth movement*. Acta Odontol Scand, 1973. **31**(2): p. 109-22.
101. Yadav, S., et al., *The effect of mechanical vibration on orthodontically induced root resorption*. The Angle Orthodontist, 2016.
102. Nakagami, G., et al., *Effect of vibration on skin blood flow in an in vivo microcirculatory model*. Bioscience trends, 2007. **1**(3): p. 161-166.
103. Matsuda, N., et al., *Proliferation and differentiation of human osteoblastic cells associated with differential activation of MAP kinases in response to epidermal growth factor, hypoxia, and mechanical stress in vitro*. Biochemical and biophysical research communications, 1998. **249**(2): p. 350-354.
104. Yousefian, J., et al., *A new experimental model for studying the response of periodontal ligament cells to hydrostatic pressure*. American Journal of Orthodontics and Dentofacial Orthopedics, 1995. **108**(4): p. 402-409.
105. Zhang, C., et al., *Effects of mechanical vibration on proliferation and osteogenic differentiation of human periodontal ligament stem cells*. Archives of Oral Biology, 2012. **57**(10): p. 1395-1407.
106. Miles, P., et al., *The effects of a vibrational appliance on tooth movement and patient discomfort: a prospective randomised clinical trial*. Australian orthodontic journal, 2012. **28**(2): p. 213-218.
107. Middleton, J., M. Jones, and A. Wilson, *The role of the periodontal ligament in bone modeling: the initial development of a time-dependent finite element model*. American Journal of Orthodontics and Dentofacial Orthopedics, 1996. **109**(2): p. 155-162.
108. Jones, M., et al., *A validated finite element method study of orthodontic tooth movement in the human subject*. Journal of Orthodontics, 2001. **28**(1): p. 29-38.
109. Boester, C.H. and L.E. Johnston, *A clinical investigation of the concepts of differential and optimal force in canine retraction*. The Angle orthodontist, 1974. **44**(2): p. 113-119.
110. Storey, E. and R. Smith, *Force in orthodontics and its relation to tooth movement*. Aust J Dent, 1952. **56**(1): p. 11-8.

## CHAPTER 8: CONCLUSIONS

111. Di Domenico, M., et al., *Cytokines and VEGF induction in orthodontic movement in animal models*. BioMed Research International, 2012. **2012**.
112. Dorow, C. and F.G. Sander, *Development of a model for the simulation of orthodontic load on lower first premolars using the finite element method*. J Orofac Orthop, 2005. **66**(3): p. 208-18.
113. Chen, J., et al., *A periodontal ligament driven remodeling algorithm for orthodontic tooth movement*. J Biomech, 2014. **47**(7): p. 1689-95.
114. Choy, K., et al., *Effect of root and bone morphology on the stress distribution in the periodontal ligament*. American Journal of Orthodontics and Dentofacial Orthopedics, 2000. **117**(1): p. 98-105.
115. Kondo, K., *A study of blood circulation in the periodontal membrane by electrical impedance plethysmography*. Kokubyo Gakkai Zasshi, 1969. **36**(1): p. 20-42.
116. Middleton, J., M.L. Jones, and A.N. Wilson, *Three-dimensional analysis of orthodontic tooth movement*. J Biomed Eng, 1990. **12**(4): p. 319-27.
117. Knox, J., et al., *An evaluation of the stresses generated in a bonded orthodontic attachment by three different load cases using the Finite Element Method of stress analysis*. J Orthod, 2000. **27**(1): p. 39-46.
118. Rungsiyakull, C., et al., *Surface morphology optimization for osseointegration of coated implants*. Biomaterials, 2010. **31**(27): p. 7196-204.
119. Burstone, C.J., *The biomechanics of tooth movement*, ed. B.S. Kraus and A. Ripamonti. 1982, Philadelphia: Lea and Febinger.
120. Provatidis, C.G., *Numerical estimation of the centres of rotation and resistance in orthodontic tooth movement*. Computer methods in biomechanics and biomedical engineering, 1999. **2**(2): p. 149-156.
121. Vollmer, D., et al., *Determination of the centre of resistance in an upper human canine and idealized tooth model*. Eur J Orthod, 1999. **21**(6): p. 633-48.
122. Lindauer, S.J. *The basics of orthodontic mechanics*. in *Seminars in Orthodontics*. 2001. Elsevier.
123. Sarrafpour, B., et al., *Tooth eruption results from bone remodelling driven by bite forces sensed by soft tissue dental follicles: a finite element analysis*. PloS one, 2013. **8**(3): p. e58803.
124. Li, W., et al., *Towards automated 3D finite element modeling of direct fiber reinforced composite dental bridge*. Journal of Biomedical Materials Research Part B: Applied Biomaterials, 2005. **74**(1): p. 520-528.
125. Malkin, A.I.A., A.Y. Malkin, and A.I. Isayev, *Rheology: concepts, methods, and applications*. 2006, ChemTec Publishing.
126. Drolshagen, M., et al., *Development of a novel intraoral measurement device to determine the biomechanical characteristics of the human periodontal ligament*. Journal of Biomechanics, 2011. **44**(11): p. 2136-2143.



## CHAPTER 8: CONCLUSIONS

127. Sawada, A., et al., *Viscoelasticity of Human Oral Mucosa: Implications for Masticatory Biomechanics*. Journal of Dental Research, 2011. **90**(5): p. 590-595.
128. Ogden, R. *Large deformation isotropic elasticity-on the correlation of theory and experiment for incompressible rubberlike solids*. in *Proceedings of the Royal Society of London A: Mathematical, Physical and Engineering Sciences*. 1972. The Royal Society.
129. Burstone, C.J. and R.J. Pryputniewicz, *Holographic determination of centers of rotation produced by orthodontic forces*. American journal of orthodontics, 1980. **77**(4): p. 396-409.
130. Nägerl, H., et al., *Centers of rotation with transverse forces: an experimental study*. American Journal of Orthodontics and Dentofacial Orthopedics, 1991. **99**(4): p. 337-345.
131. Pedersen, E., K. Andersen, and P. Gjessing, *Electronic determination of centres of rotation produced by orthodontic force systems*. The European Journal of Orthodontics, 1990. **12**(3): p. 272-280.
132. Tanne, K., et al., *Patterns of initial tooth displacements associated with various root lengths and alveolar bone heights*. American Journal of Orthodontics and Dentofacial Orthopedics, 1991. **100**(1): p. 66-71.
133. Nyashin, Y., et al., *Centre of resistance and centre of rotation of a tooth: experimental determination, computer simulation and the effect of tissue nonlinearity*. Computer methods in biomechanics and biomedical engineering, 2015(ahead-of-print): p. 1-11.
134. Cattaneo, P.M., M. Dalstra, and B. Melsen, *Moment-to-force ratio, center of rotation, and force level: a finite element study predicting their interdependency for simulated orthodontic loading regimens*. American Journal of orthodontics and dentofacial orthopedics, 2008. **133**(5): p. 681-689.
135. Quinn, R.S. and D.K. Yoshikawa, *A reassessment of force magnitude in orthodontics*. American journal of orthodontics, 1985. **88**(3): p. 252-260.
136. Brudvik, P. and P. Rygh, *The initial phase of orthodontic root resorption incident to local compression of the periodontal ligament*. The European Journal of Orthodontics, 1993. **15**(4): p. 249-263.
137. Lee, B.W., *Relationship between tooth-movement rate and estimated pressure applied*. Journal of dental research, 1965. **44**(5): p. 1053-1053.
138. Iwasaki, L.R., et al., *Human tooth movement in response to continuous stress of low magnitude*. American Journal of Orthodontics and Dentofacial Orthopedics, 2000. **117**(2): p. 175-183.
139. Ren, Y., et al., *Optimum force magnitude for orthodontic tooth movement: a mathematic model*. American journal of orthodontics and dentofacial orthopedics, 2004. **125**(1): p. 71-77.
140. Lee, B.W., *The force requirements for tooth movement, Part I: Tipping and bodily movement*. Aust Orthod J, 1995. **13**(4): p. 238-48.

## CHAPTER 8: CONCLUSIONS

141. Andreasen, G. and P. Johnson, *Experimental Findings on Tooth Movements Under Two Conditions of Applied Force*. The Angle Orthodontist, 1967. **37**(1): p. 9-12.
142. Andreasen, G.F. and D. Zwanziger, *A clinical evaluation of the differential force concept as applied to the edgewise bracket*. Am J Orthod, 1980. **78**(1): p. 25-40.
143. Palmer, R.M., et al., *A prospective clinical trial of single Astra Tech 4.0 or 5.0 diameter implants used to support two - unit cantilever bridges: results after 3 years*. Clinical oral implants research, 2012. **23**(1): p. 35-40.
144. Zurdo, J., C. Romao, and J.L. Wennström, *Survival and complication rates of implant - supported fixed partial dentures with cantilevers: a systematic review*. Clinical oral implants research, 2009. **20**(s4): p. 59-66.
145. Wennström, J.L., et al., *Oral rehabilitation with implant - supported fixed partial dentures in periodontitis - susceptible subjects*. Journal of clinical periodontology, 2004. **31**(9): p. 713-724.
146. Kim, P., et al., *The impact of cantilevers on biological and technical success outcomes of implant-supported fixed partial dentures. A retrospective cohort study*. Clinical Oral Implants Research, 2014. **25**(2): p. 175-184.
147. Qian, J., A. Wennerberg, and T. Albrektsson, *Reasons for Marginal Bone Loss around Oral Implants*. Clinical Implant Dentistry and Related Research, 2012. **14**(6): p. 792-807.
148. Li, I., et al., *A mathematical model for simulating the bone remodeling process under mechanical stimulus*. Dental Materials, 2007. **23**(9): p. 1073-1078.
149. Lin, D., et al., *Dental implant induced bone remodeling and associated algorithms*. Journal of the Mechanical Behavior of Biomedical Materials, 2009. **2**(5): p. 410-432.
150. Stegaroiu, R., et al., *Influence of restoration type on stress distribution in bone around implants: A three-dimensional finite element analysis*. International Journal of Oral & Maxillofacial Implants, 1998. **13**(1): p. 82-90.
151. Yokoyama, S., et al., *The influence of implant location and length on stress distribution for three-unit implant-supported posterior cantilever fixed partial dentures*. The Journal of prosthetic dentistry, 2004. **91**(3): p. 234-240.
152. Baggi, L., et al., *Implant-Bone Load Transfer Mechanisms in Complete-Arch Prostheses Supported by Four Implants: A Three-Dimensional Finite Element Approach*. Journal of Prosthetic Dentistry, 2013. **109**(1): p. 9-21.
153. Rungsiyakull, C., et al., *Bone's responses to different designs of implant-supported fixed partial dentures*. Biomechanics and Modeling in Mechanobiology, 2015. **14**(2): p. 403-411.
154. Chen, S. and I. Darby, *Dental implants: Maintenance, care and treatment of peri - implant infection*. Australian dental journal, 2003. **48**(4): p. 212-220.

## CHAPTER 8: CONCLUSIONS

155. Yoda, N., et al., *In Vivo Load Measurement for Evaluating the Splinting Effects of Implant-Supported Superstructures: A Pilot Study*. International Journal of Prosthodontics, 2013. **26**(2): p. 143-146.
156. Kawata, T., et al., *Behaviours of three-dimensional compressive and tensile forces exerted on a tooth during function*. Journal of Oral Rehabilitation, 2007. **34**(4): p. 259-266.
157. Kobari, H., et al., *An in vivo study on loading distribution in different implant configurations for supporting fixed partial denture*. In press. International journal of oral & maxillofacial implants, 2016.
158. Chen, J., et al., *Multiscale design of surface morphological gradient for osseointegration*. Journal of the mechanical behavior of biomedical materials, 2013. **20**: p. 387-397.
159. Bonnet, A.S., M. Postaire, and P. Lipinski, *Biomechanical study of mandible bone supporting a four-implant retained bridge Finite element analysis of the influence of bone anisotropy and foodstuff position*. Medical Engineering & Physics, 2009. **31**(7): p. 806-815.
160. Ishigaki, S., et al., *Biomechanical stress in bone surrounding an implant under simulated chewing*. Clinical Oral Implants Research, 2003. **14**(1): p. 97-102.
161. Shigemitsu, R., et al., *Biological-data-based finite-element stress analysis of mandibular bone with implant-supported overdenture*. Computers in Biology and Medicine, 2014. **54**: p. 44-52.
162. Cruz, M., et al., *Three-dimensional finite element stress analysis of a cuneiform-geometry implant*. Int J Oral Maxillofac Implants, 2003. **18**(5): p. 675-84.
163. Ichim, I., J.A. Kieser, and M.V. Swain, *Functional significance of strain distribution in the human mandible under masticatory load: Numerical predictions*. Archives of Oral Biology, 2007. **52**(5): p. 465-473.
164. Field, C., et al., *Influence of tooth removal on mandibular bone response to mastication*. Archives of Oral Biology, 2008. **53**(12): p. 1129-1137.
165. Halldin, A., et al., *The effect of static bone strain on implant stability and bone remodeling*. Bone, 2011. **49**(4): p. 783-789.
166. Pjetursson, B.E., et al., *A systematic review of the survival and complication rates of implant - supported fixed dental prostheses (FDPs) after a mean observation period of at least 5 years*. Clinical Oral Implants Research, 2012. **23**(s6): p. 22-38.
167. Hälg, G.A., J. Schmid, and C.H. Hammerle, *Bone level changes at implants supporting crowns or fixed partial dentures with or without cantilevers*. Clinical oral implants research, 2008. **19**(10): p. 983-990.
168. Brägger, U., et al., *Technical and biological complications/failures with single crowns and fixed partial dentures on implants: a 10 - year prospective cohort study*. Clinical Oral Implants Research, 2005. **16**(3): p. 326-334.

## CHAPTER 8: CONCLUSIONS

169. Walls, A.W., *Cantilever FPDs have lower success rates than end abutted FPDs after 10-years of follow-up*. Journal of Evidence Based Dental Practice, 2010. **10**(1): p. 41-43.
170. Romeo, E. and S. Storelli, *Systematic review of the survival rate and the biological, technical, and aesthetic complications of fixed dental prostheses with cantilevers on implants reported in longitudinal studies with a mean of 5 years follow - up*. Clinical oral implants research, 2012. **23**(s6): p. 39-49.
171. Aglietta, M., et al., *A systematic review of the survival and complication rates of implant supported fixed dental prostheses with cantilever extensions after an observation period of at least 5 years*. Clinical oral implants research, 2009. **20**(5): p. 441-451.
172. Wennstrom, J., et al., *Bone level change at implant-supported fixed partial dentures with and without cantilever extension after 5 years in function*. J Clin Periodontol, 2004. **31**(12): p. 1077-83.
173. Barao, V., et al., *Comparison of different designs of implant-retained overdentures and fixed full-arch implant-supported prosthesis on stress distribution in edentulous mandible—A computed tomography-based three-dimensional finite element analysis*. Journal of biomechanics, 2013. **46**(7): p. 1312-1320.
174. Bodic, F., et al., *Bone loss and teeth*. Joint Bone Spine, 2005. **72**(3): p. 215-221.
175. Wang, C., et al., *Simulated bone remodeling around tilted dental implants in the anterior maxilla*. Biomechanics and modeling in mechanobiology, 2015: p. 1-12.
176. Eskitascioglu, G., et al., *The influence of occlusal loading location on stresses transferred to implant-supported prostheses and supporting bone: a three-dimensional finite element study*. The Journal of prosthetic dentistry, 2004. **91**(2): p. 144-150.
177. Schwartz - Dabney, C. and P. Dechow, *Variations in cortical material properties throughout the human dentate mandible*. American journal of physical anthropology, 2003. **120**(3): p. 252-277.
178. Hazelwood, S.J., et al., *A mechanistic model for internal bone remodeling exhibits different dynamic responses in disuse and overload*. Journal of Biomechanics, 2001. **34**(3): p. 299-308.
179. Wolff, J., *Das gesetz der transformation der knochen*. DMW-Deutsche Medizinische Wochenschrift, 1893. **19**(47): p. 1222-1224.
180. Huijkes, R., et al., *Adaptive bone-remodeling theory applied to prosthetic-design analysis*. Journal of biomechanics, 1987. **20**(11-12): p. 1135-1150.
181. Liao, Z., et al., *Simulation of multi-stage nonlinear bone remodeling induced by fixed partial dentures of different configurations: a comparative clinical and numerical study*. Biomechanics and Modeling in Mechanobiology, 2016: p. 1-13.
182. Lanyon, L.E., *Functional Strain as a Determinant for Bone Remodeling*. Calcified Tissue International, 1984. **36**: p. S56-S61.

## CHAPTER 8: CONCLUSIONS

183. Carter, D.R. and W.C. Hayes, *The compressive behavior of bone as a two-phase porous structure*. The Journal of Bone & Joint Surgery, 1977. **59**(7): p. 954-962.
184. Mengoni, M. and J.-P. Ponthot, *An enhanced version of a bone-remodelling model based on the continuum damage mechanics theory*. Computer methods in biomechanics and biomedical engineering, 2015. **18**(12): p. 1367-1376.
185. Huiskes, R., et al., *Effects of mechanical forces on maintenance and adaptation of form in trabecular bone*. Nature, 2000. **405**(6787): p. 704-706.
186. Chen, J., et al., *A periodontal ligament driven remodeling algorithm for orthodontic tooth movement*. Journal of biomechanics, 2014. **47**(7): p. 1689-1695.
187. Christen, P., et al., *Bone remodelling in humans is load-driven but not lazy*. Nat Commun, 2014. **5**.
188. Huiskes, R., H. Weinans, and M. Dalstra, *Adaptive bone remodeling and biomechanical design considerations for noncemented total hip arthroplasty*. Orthopedics, 1989. **12**(9): p. 1255-1267.
189. Weinans, H., R. Huiskes, and H. Grootenboer, *The behavior of adaptive bone-remodeling simulation models*. Journal of biomechanics, 1992. **25**(12): p. 1425-1441.
190. Chou, H.-Y., J.J. Jagodnik, and S. Müftü, *Predictions of bone remodeling around dental implant systems*. Journal of Biomechanics, 2008. **41**(6): p. 1365-1373.
191. Ay, S., et al., *Assessment of mandibular bone mineral density in patients with type 2 diabetes mellitus*. Dentomaxillofacial Radiology, 2005. **34**(6): p. 327-331.
192. Schwartz-Dabney, C. and P. Dechow, *Edentulation alters material properties of cortical bone in the human mandible*. Journal of Dental Research, 2002. **81**(9): p. 613-617.
193. Dechow, P.C. and W.L. Hylander, *Elastic properties and masticatory bone stress in the macaque mandible*. American journal of physical anthropology, 2000. **112**(4): p. 553-574.
194. Hellmich, C., C. Kober, and B. Erdmann, *Micromechanics-based conversion of CT data into anisotropic elasticity tensors, applied to FE simulations of a mandible*. Annals of biomedical engineering, 2008. **36**(1): p. 108-122.
195. Misch, C.E., Z. Qu, and M.W. Bidez, *Mechanical properties of trabecular bone in the human mandible: implications for dental implant treatment planning and surgical placement*. Journal of oral and maxillofacial surgery, 1999. **57**(6): p. 700-706.
196. Cruz, M., et al., *Three-dimensional finite element stress analysis of a cuneiform-geometry implant*. International Journal of Oral & Maxillofacial Implants, 2003. **18**(5): p. 675-684.
197. Hart, R.T., et al., *Modeling the biomechanics of the mandible: a three-dimensional finite element study*. Journal of biomechanics, 1992. **25**(3): p. 261-286.

## CHAPTER 8: CONCLUSIONS

198. Wong, R.C., et al., *The modular endoprosthesis for mandibular body replacement. Part 2: Finite element analysis of endoprosthesis reconstruction of the mandible*. Journal of Cranio-Maxillofacial Surgery, 2012. **40**(8): p. e487-e497.
199. Li, J., et al., *A mathematical model for simulating the bone remodeling process under mechanical stimulus*. Dental Materials, 2007. **23**(9): p. 1073-1078.
200. Vahdati, A., et al., *Role of subject-specific musculoskeletal loading on the prediction of bone density distribution in the proximal femur*. Journal of the mechanical behavior of biomedical materials, 2014. **30**: p. 244-252.
201. Norman, R.G. and L.D. Streiner, *Biostatistics: the bare essentials*. 3 ed. 2008, Hamilton, Ontario, Canada: BC Decker Inc.
202. Carter, D.R., *Mechanical loading histories and cortical bone remodeling*. Calcified tissue international, 1984. **36**(1): p. S19-S24.
203. Wang, C., et al., *Numerical simulation of dental bone remodeling induced by implant - supported fixed partial denture with or without cantilever extension*. International journal for numerical methods in biomedical engineering, 2013. **29**(10): p. 1134-1147.
204. Prendergast, P. and D. Taylor, *Prediction of bone adaptation using damage accumulation*. Journal of biomechanics, 1994. **27**(8): p. 1067-1076.
205. Yoda, N., et al., *Effect of Configurations of Implants supporting a Four-unit Fixed Partial Denture on Loading Distribution*. In press. International Journal of Prosthodontics. , 2016.
206. Aglietta, M., et al., *Clinical and radiographic changes at implants supporting single - unit crowns (SCs) and fixed dental prostheses (FDPs) with one cantilever extension. A retrospective study*. Clinical oral implants research, 2012. **23**(5): p. 550-555.
207. Käyser, A., *Shortened dental arches and oral function*. Journal of oral rehabilitation, 1981. **8**(5): p. 457-462.
208. Ramakrishaniah, R., et al., *A comparative finite elemental analysis of glass abutment supported and unsupported cantilever fixed partial denture*. Dental Materials, 2015. **31**(5): p. 514-521.
209. Pepato, A.O., et al., *Analysis of masticatory efficiency by electromyographic activity of masticatory muscles after surgical treatment of zygomatic-orbital complex fractures*. International journal of stomatology & occlusion medicine, 2013. **6**(3): p. 85-90.
210. Renaud, M., P. Mercier, and A. Vinet, *Mastication after surgical reconstruction of the mandibular residual ridge*. Journal of oral rehabilitation, 1984. **11**(1): p. 79-84.
211. Marunick, M., et al., *Occlusal force after partial mandibular resection*. J Prosthet Dent, 1992. **67**(6): p. 835-8.
212. Endo, N., *Studies on masticatory functions in patients with surgical mandibular reconstruction*. Oral Surgery, Oral Medicine, Oral Pathology, 1972. **34**(3): p. 390-407.

## CHAPTER 8: CONCLUSIONS

213. Namaki, S., et al., *Masticatory efficiency before and after surgery in oral cancer patients: comparative study of glossectomy, marginal mandibulectomy and segmental mandibulectomy*. Journal of oral science, 2004. **46**(2): p. 113-117.
214. Van Ruijven, L. and W. Weijs, *A new model for calculating muscle forces from electromyograms*. European journal of applied physiology and occupational physiology, 1990. **61**(5-6): p. 479-485.
215. Fukunaga, T., et al., *In vivo behaviour of human muscle tendon during walking*. Proceedings of the Royal Society of London B: Biological Sciences, 2001. **268**(1464): p. 229-233.
216. Hattori, Y., et al., *Occlusal and TMJ loads in subjects with experimentally shortened dental arches*. J Dent Res, 2003. **82**(7): p. 532-6.
217. Schindler, H., et al., *Jaw clenching: muscle and joint forces, optimization strategies*. Journal of dental research, 2007. **86**(9): p. 843-847.
218. Chou, H.-Y., et al., *Influence of mastication and edentulism on mandibular bone density*. Computer methods in biomechanics and biomedical engineering, 2015. **18**(3): p. 269-281.
219. Pedotti, A., V. Krishnan, and L. Stark, *Optimization of muscle-force sequencing in human locomotion*. Mathematical Biosciences, 1978. **38**(1): p. 57-76.
220. Osborn, J. and F. Baragar, *Predicted pattern of human muscle activity during clenching derived from a computer assisted model: symmetric vertical bite forces*. Journal of biomechanics, 1985. **18**(8): p. 599-612.
221. Nubar, Y. and R. Contini, *A minimal principle in biomechanics*. The bulletin of mathematical biophysics, 1961. **23**(4): p. 377-391.
222. Rues, S., et al., *Forces and motor control mechanisms during biting in a realistically balanced experimental occlusion*. Archives of oral biology, 2008. **53**(12): p. 1119-1128.
223. Seireg, A. and R. Arvikar, *A mathematical model for evaluation of forces in lower extremities of the musculo-skeletal system*. Journal of biomechanics, 1973. **6**(3): p. 313IN19323-322IN20326.
224. Loeb, G.E., *Optimal isn't good enough*. Biological cybernetics, 2012. **106**(11-12): p. 757-765.
225. Conley, K.E. and S.L. Lindstedt, *Energy-saving mechanisms in muscle: the minimization strategy*. Journal of experimental biology, 2002. **205**(15): p. 2175-2181.
226. Hidaka, O., et al., *Influence of clenching intensity on bite force balance, occlusal contact area, and average bite pressure*. J Dent Res, 1999. **78**(7): p. 1336-44.
227. Peck, C.C., G.E. Langenbach, and A.G. Hannam, *Dynamic simulation of muscle and articular properties during human wide jaw opening*. Arch Oral Biol, 2000. **45**(11): p. 963-82.

## CHAPTER 8: CONCLUSIONS

228. Pruijm, G.J., H.J. Dejongh, and J.J. Tenbosch, *Forces Acting on the Mandible during Bilateral Static Bite at Different Bite Force Levels*. Journal of Biomechanics, 1980. **13**(9): p. 755-763.
229. Weijjs, W.A. and B. Hillen, *Physiological Cross-Section of the Human Jaw Muscles*. Acta Anatomica, 1985. **121**(1): p. 31-35.
230. Weijjs, W.A. and B. Hillen, *Relationships between Masticatory Muscle Cross-Section and Skull Shape*. Journal of Dental Research, 1984. **63**(9): p. 1154-1157.
231. Chen, J., et al., *Biomechanics of oral mucosa*. Journal of The Royal Society Interface, 2015. **12**(109): p. 20150325.
232. Koriath, T.W., D.P. Romilly, and A.G. Hannam, *Three - dimensional finite element stress analysis of the dentate human mandible*. American Journal of Physical Anthropology, 1992. **88**(1): p. 69-96.
233. Gonda, T., et al., *Biomechanical factors associated with mandibular cantilevers: analysis with three-dimensional finite element models*. International Journal of Oral & Maxillofacial Implants, 2014. **29**(6).
234. Al-Ahmari, A., et al., *A comparative study on the customized design of mandibular reconstruction plates using finite element method*. Advances in Mechanical Engineering, 2015. **7**(7): p. 1687814015593890.
235. Faulkner, M., D. Hatcher, and A. Hay, *A three-dimensional investigation of temporomandibular joint loading*. Journal of biomechanics, 1987. **20**(10): p. 997-1002.
236. Hunter, L., E. Hendrix, and J. Dean, *The cost of walking downhill: is the preferred gait energetically optimal?* Journal of biomechanics, 2010. **43**(10): p. 1910-1915.
237. Kistemaker, D.A., J.D. Wong, and P.L. Gribble, *The central nervous system does not minimize energy cost in arm movements*. Journal of neurophysiology, 2010. **104**(6): p. 2985-2994.
238. Miller, R.H., et al., *Evaluation of the minimum energy hypothesis and other potential optimality criteria for human running*. Proceedings of the Royal Society of London B: Biological Sciences, 2011: p. rspb20112015.
239. Morgan, D., et al., *Effect of step length optimization on the aerobic demand of running*. Journal of Applied Physiology, 1994. **77**(1): p. 245-251.
240. De Rugy, A., G.E. Loeb, and T.J. Carroll, *Muscle coordination is habitual rather than optimal*. The Journal of Neuroscience, 2012. **32**(21): p. 7384-7391.
241. Katsumata, A., et al., *3D CT evaluation of masseter muscle morphology after setback osteotomy for mandibular prognathism*. Oral Surgery, Oral Medicine, Oral Pathology, Oral Radiology, and Endodontology, 2004. **98**(4): p. 461-470.
242. Shibuya, Y., et al., *Evaluating the masticatory function after mandibulectomy with colour - changing chewing gum*. Journal of oral rehabilitation, 2013. **40**(7): p. 484-490.
243. Shiga, H., et al., *Gender difference in masticatory performance in dentate adults*. Journal of prosthodontic research, 2012. **56**(3): p. 166-169.



## CHAPTER 8: CONCLUSIONS

244. Sato, Y., et al., *An evaluation of chewing function of complete denture wearers*. The Journal of prosthetic dentistry, 1989. **62**(1): p. 50-53.
245. Okiyama, S., K. Ikebe, and T. Nokubi, *Association between masticatory performance and maximal occlusal force in young men*. Journal of oral rehabilitation, 2003. **30**(3): p. 278-282.
246. Dicker, G., et al., *Adaptation of jaw closing muscles after surgical mandibular advancement procedures in different vertical craniofacial types: a magnetic resonance imaging study*. Oral Surgery, Oral Medicine, Oral Pathology, Oral Radiology, and Endodontology, 2007. **103**(4): p. 475-482.
247. Sieg, P., et al., *Defect-related variations in mandibular reconstruction using fibula grafts.: A review of 96 cases*. British Journal of Oral and Maxillofacial Surgery, 2002. **40**(4): p. 322-329.
248. López-Arcas, J.M., et al., *The fibula osteomyocutaneous flap for mandible reconstruction: a 15-year experience*. Journal of Oral and Maxillofacial Surgery, 2010. **68**(10): p. 2377-2384.
249. Conley, J. and P.J. Gullane, *The sternocleidomastoid muscle flap*. Head & neck surgery, 1980. **2**(4): p. 308-311.
250. Nakata, Y., et al., *Changes in stomatognathic function induced by orthognathic surgery in patients with mandibular prognathism*. Journal of Oral and Maxillofacial Surgery, 2007. **65**(3): p. 444-451.
251. Alghazzawi, T.F., *Advancements in CAD/CAM technology: Options for practical implementation*. Journal of prosthodontic research, 2016. **60**(2): p. 72-84.
252. Chen, J., et al., *Shape Optimization for Additive Manufacturing of Removable Partial Dentures-A New Paradigm for Prosthetic CAD/CAM*. PloS one, 2015. **10**(7): p. e0132552.